Laser-Induced Material Ejection from Model Molecular Solids and Liquids: Mechanisms, Implications, and Applications

Savas Georgiou* and Antonis Koubenakis#

Institute of Electronic Structure and Laser, Foundation for Research and Technology-Hellas, P.O. Box 1527, 71110 Heraklion, Crete, Greece

Received July 24, 2002

Contents

I. Introduction

Upon irradiation of condensed phases with laser pulses at high laser irradiances, massive material ejection is observed. This phenomenon has been named "ablation". A plot of the quantity of the removed material as a function of laser fluence usually has a sigmoidal dependence, as in Figure 1, though the exact shape may differ considerably depending on system properties and irradiation parameters. Despite its apparent violent nature, this efficient material removal method has provided the basis for a wide spectrum of highly successful applications, ranging from analytical chemistry[1−4] to microelectronics,[5−9] medicine,[1,7] restoration of painted artwork,[10] etc. In some of these applications, UV ablation is used to effect ejection of material in the gas phase for its analysis or subsequent deposition.[2−4,9] In the other applications, UV ablation is employed to effect the appropriate shaping or processing of the substrate via the removal[1,5−8,10,11] of unwanted material. In either case, ablation offers the crucial advantage of micrometer precision in the removed depth, with little thermal or other degradation to the ejected or remaining material. Further advantages include a high degree of reproducibility, the capability of interfacing with a variety of laser-based techniques for on-line monitoring of the process, etc.

Despite the widespread and highly successful applications, several aspects of laser ablation of molecular substrates induced with nanosecond or shorter pulses remain poorly understood. The first and foremost problem to be elucidated remains the issue of fundamental mechanisms responsible for the material ejection, i.e., how the absorbed light energy results eventually in material ejection. Generally, the phenomenon is described phenomenologically from the dependence of the etching depth (or of the amount of the removed material) on laser fluence (laser pulse energy per unit irradiated area, i.e., F_{laser}). Usually, the fluence at which the sharp increase in the etching depth is observed, or the F_{laser} intercept of the extrapolation of the rising section of the curve, is considered to be the threshold for ablation. However, despite their predominant use, such curves do not yield much physical insight, especially since they differ quantitatively and even qualitatively according to irradiation and system parameters. Even the existence of a threshold is very difficult to ascertain from examination of these curves. Clearly, the question raised is if ablation can be identified with specific physical characteristics that distinguish it from processes at lower fluences or if it is adequately specified only in terms of the amount of material removed. Unfortunately, for several applications, only the amount of removed material is of concern, and as a result, this issue has been emphasized over that of the involved physical processes.

* To whom correspondence should be addressed. Phone: +30 81 0391121. Fax: +30 81 0391318. E-mail: sgeorgiu@iesl.forth.gr.
# Present address: Department of Chemistry, Swiss Federal Institute of Technology (ETH), Hönggerberg HCI, CH-8093 Zurich, Switzerland.

10.1021/cr010429o CCC: $44.00
Published on Web 02/12/2003

Savas Georgiou received his B.Sc. in chemistry and mathematics from Knox College, Illinois (1983), and his Ph.D. in physical chemistry (on the study of photodissociation dynamics of organometallic compounds) from the University of Utah (1988). He subsequently performed postdoctoral work on Raman spectroscopy of biomolecules at Princeton University. After a two-year military service in the Greek Army, in 1993 he joined the Institute of Electronic Structure and Laser of Foundation for Research and Technology—Hellas, where he is now a Senior Researcher. He has also held positions as a Visiting Assistant Professor at the Chemistry Department of the University of Crete and as an Assistant Professor at the Physics Department of the University of Ioannina, Greece. He has received various awards and has participated in several European Union research projects. His current interests focus on studies of laser ablation, laser photochemistry and biophysics, and laser material processing schemes.

Antonis Koubenakis was born in 1973 in Heraklion, Crete, Greece. He received his B.Sc. degree in physics in 1996 and his M.Sc. degree in atomic and molecular physics in 1997 from the University of Crete. He subsequently performed work on the mechanisms of laser desorption/ablation of van der Waals solids at the Foundation for Research and Technology—Hellas (F.O.R.T.H.) and received his Ph.D. from the University of Crete in March 2002. For this work, he received a prize from the Gordon Conference of Laser Interactions with Materials (June 2000). He is currently a postdoctoral fellow in the research group of Prof. Renato Zenobi at the Swiss Federal Institute of Technology in Zurich (ETH). A. Koubenakis has coauthored 15 articles in international journals. His research interests include the study of laser desorption processes, mass spectroscopy, and near-field optical analytical techniques.

The difficulties encountered in trying to establish the fundamental physical processes underlying the phenomenon can be easily appreciated by considering a schematic of the various steps leading to material ejection. In the first step, energy must be coupled into the system via absorption. Typically, fluences of ~100 mJ/cm^2 (3 MW/cm^2) or higher are required experimentally to effect material ejection by nanosecond laser pulses. Given a typical cross section of ~10^{-18}-

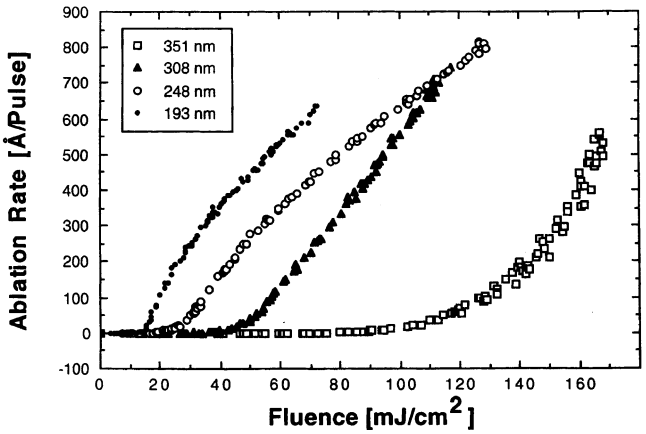

Figure 1. Etching curves typical of the ones determined in the UV ablation (nanosecond pulses) of molecular systems (the particular ones concerning irradiation of polyimide at the indicated wavelengths). Absorption coefficients: $\alpha(193\text{ nm}) = 4.25 \times 10^5\text{ cm}^{-1}$; $\alpha(248\text{ nm}) = 3.1 \times 10^5\text{ cm}^{-1}$; $\alpha(308\text{ nm}) = 10^5\text{ cm}^{-1}$; $\alpha(351\text{ nm}) = 0.32 \times 10^5\text{ cm}^{-1}$. The measurements rely on mass-loss measurements using a quartz crystal microbalance. Changes in the features of the curves depending on laser wavelength are clearly noted. The curves exhibit the so-called "Arrhenius tails" that have been a matter of controversy. At high fluences, the curves tend to saturate (observed for the curves at the shorter, more strongly absorbed wavelegenths). This is often ascribed to the increasing absorption/scattering of the incident light by the material ejected during the laser pulse. Reprinted with permission from Küper, S.; Brannon, J.; Brannon, K. *Appl. Phys. A* **1993**, *56*, 33. Copyright 1993 Springer-Verlag.

cm^2/molecule, multiphoton processes and other nonlinearities in the absorption process, such as annihilation of electronically excited states, saturation effects, etc., become highly likely. Establishing the absorbed energy experimentally is no easy task, since the extensive material ejection during the laser pulse results in significant scattering and absorption of the incident light by the ejecta. In fact, the extensive material ejection severely limits the use of any spectroscopic technique in probing processes in the substrate (at least up to microsecond time scales after the nanosecond laser pulse). Following light absorption, material ejection can be envisaged to be induced in at least four different ways. At least for nanosecond pulses, a good percentage of the absorbed energy can be expected to decay into thermal energy, since typical radiationless decay constants for organic molecules are ~10^{-12}–10^{-9} s. In view of the low thermal conductivity of molecular systems, high surface temperature changes may be attained, and desorption/evaporation rates can be substantial (thermal mechanism). However, given the very short time scale of irradiation, phase transformations under nonequilibrium conditions may occur (explosive boiling/phase explosion), resulting in quantitative and even qualitative differences from "simple" thermal processes. Unfortunately, the dynamic optical, thermophysical, etc. properties under these conditions can be distinct from those of a uniformly heated system, which further complicates the quantitative analysis and even the interpretation of the results. The fast change in temperature implies also a volume change and thus a high-amplitude pressure generation, which

can result in material ejection via essentially "mechanical" rupture (spallation) of the upper layers of the substrate. To complicate things even further, upon UV excitation, most organic molecules photodissociate with rather significant quantum efficiency. The formation of a high number of gaseous photoproducts that exert a high pressure upon expansion and/or the high amount of energy that is liberated by exothermic reactions can contribute to material ejection (photochemical mechanism).

These processes necessarily occur in parallel; thus, the question is raised of which one is responsible for material ejection. Clearly, the different processes will result in different features/effects, and thus the specification of their contribution is intimately related to the question of the nature of ablation. The relative importance of the processes can be approximately assessed via some simple criteria. Assuming a "thermal energy pulse" and photoinert systems, the relative importance of thermal versus mechanical processes depends on the ratio of pulse duration to thermal and stress relaxation times. These times are given, respectively, by $t_{thermal} = l_{abs}^2/D$ and $t_{acoustic} = l_{abs}/c_S$, where l_{abs} is the optical penetration depth (assumed to be much smaller than the laser beam radius, so that a one-dimensional analysis applies), D is the thermal diffusivity, and c_S is the speed of sound. The two terms represent, respectively, the time for heat diffusion ("thermal equilibration") and the time for acoustic wave (and thus mechanical relaxation) within the optical penetration depth. Typically, for molecular solids, l_{abs} in UV is in the range from 100 nm to 5 μm, and $D \approx 10^{-7}$ m^2/s, so $t_{thermal} \approx 1$ μs and $t_{acoustic} < 1$ ns. Of course, in the case of UV excitation, the previous delineation assumes that the time scale of electronic energy deactivation, $\tau_{elec-deact}$, is fast enough compared to the previous times. The $\tau_{elec-deact} \leq t_{thermal}$ condition is expected to be fulfilled for most molecular systems, but the $\tau_{elec-deact} \leq t_{acoustic}$ condition may not be (sections II.B.4 and II.B.5). Neglecting for the moment this issue, the following delineation can be drawn:

(a) For laser pulse durations shorter than $t_{thermal}$ (thermal confinement regime), the temperature profile is determined by the laser light distribution, i.e.,

$$\Delta T(z) = \frac{\alpha F_{laser}}{\rho C_P} e^{-\alpha z} \quad (1)$$

where $\Delta T(z)$ is the temperature "jump" induced at depth z from the surface, α is the absorption coefficient, ρ the mass density, F_{laser} the laser fluence, and C_P the heat capacity, light reflection and scattering being neglected. Since the maximum possible temperature is attained in the target volume, thermal desorption/evaporation rates can be significant and can account for the high material removal rates observed at high laser fluences. Furthermore, under this condition, the extent of thermal dissipation and damage adjacent to the irradiated area is limited. This has been one of the key factors in the success of nanosecond UV laser processing of molecular substrates.

(b) The previous argument, however, does not explain some of the unique features of the phenomenon that have been crucial for its widespread implementation, e.g., how fragile molecules are ejected with minimal fragmentation. It now appears that, at least for simple systems (photoinert and low cohesive energy) and nanosecond pulses, these unique features may be associated with "nonequilibrium" phase transformation, namely explosive boiling. In this case, an extra criterion may be introduced to establish whether material ejection is due to simple thermal desorption or to ablation, namely the rate of homogeneous bubble formation being competitive with evaporative cooling rates (section II.B.2) or with the rate of energy consumed for bubble formation in the presence of nuclei promoting heterogeneous nucleation (section III.A).

(c) For even shorter laser pulses, such that $\tau_{pulse} < t_{acoustic}$ (stress-confinement regime), heating is effected under nearly isochoric conditions, leading to the most efficient possible generation of a thermoelastic wave. In the presence of an interface with a lower acoustic impedance medium (e.g., air), this wave contains, due to reflection at the interface, both compressive and tensile stresses. Such a high-amplitude bipolar stress wave can lead to the ejection of material via essentially mechanical rupture of the upper layers (spallation) (sections II.B.5 and III.B.1).

Despite their appealing simplicity, the above criteria clearly serve only as approximate guidelines. In most cases, there is a competition or synergy between the various processes, and which one dominates will depend sensitively on the characteristics of the substrate (in particular, cohesive energy).

Evidently, it is very difficult to specify or control experimentally all the different aspects involved in the phenomenon. For the theoretical description, analytical treatments similarly have to resort to considering the individual processes, but unfortunately, this simplification in mathematical formalism may miss essential aspects of the phenomenon. Several interesting features of material ejection in the irradiation of molecular solids at high laser fluences have been indicated by molecular dynamics (MD) simulations based on the breathing sphere model. However, even here, because of the enormous computing power required to simulate the laser/matter interaction, several simplifications are made in the representation of the molecules and irradiation conditions. In view of these difficulties, it is easily understandable that a wide range of uncertainties and controversies exist concerning the mechanisms of ablation.

These problems aside, the previous discussion directly indicates that the study of UV ablation is highly interdisciplinary, encompassing questions from the fields of thermodynamics, photophysics/chemistry, hydrodynamics, etc. As a result of this interdisciplinarity, the study of UV ablation can be expected to result in new information about molecular photophysics/chemistry. This is clearly underscored by the fact that the wide range and high success of the applications of the phenomenon would not have been expected by conventional photochemistry. To the contrary, by any conventional photophysical/chemical criterion, the employed high irradiances would be

expected to result in ill-defined effects. The fact that this is not the case suggests the need to introduce new concepts that may be of far-reaching scientific impact. Indeed, important issues concerning nonequilibrium phase transformations, electronic excitation and deactivation processes, material dynamics, etc. have already been raised and studied in the field.

Though the "power" of UV ablation is illustrated in the processing of the complex polymers, biopolymers, tissues, painted artwork, etc.,[1−11] the study of the processes underlying the phenomenon in realistic systems raises significant difficulties. Studies on simple molecular systems may provide a useful starting point by enabling detailed probing and elucidation of the processes. Simple compounds at ambient conditions are usually liquids or gases. Laser-induced material ejection from liquids has been extensively studied in its own right. It has also provided a basis for understanding processes in complex systems, in particular tissues. On the other hand, to simulate the solid state of the substrates commonly encountered in practice, while retaining the advantage of molecular simplicity, a number of studies have been performed on films/solids of simple compounds condensed at low temperatures, namely cryogenic or van der Waals films.

In the following, the work on cryogenic films is presented first, and subsequently that on liquids. Certainly, laser-induced material ejection processes in these systems are expected to be closely related. The first reason for adopting this separate presentation is that no fully satisfactory general model(s) for the dependence of the phenomenon on the phase/state of the substrate has thus far been developed. In retrospect, it is clear that in both cases, similar problems/questions/mechanisms have been addressed all along, but this has been recognized only in recent studies. Furthermore, even if the same basic mechanisms are largely involved in both phases, there are significant differences in terms of their energy content, tensile strength, efficiency to propagate stress waves, species diffusivity and reactivity, etc. that may affect various aspects of the phenomenon. Some of these differences will be noted. The second and main reason for the separate presentation is that different experimental techniques have been employed in the case of solids versus liquids. As a result, different aspects of the phenomenon have been largely emphasized in the corresponding studies.

II. Studies on Cryogenic (van der Waals) Molecular Solids

A. Delineation of Photodesorption Processes

In the past decade, there has been considerable work on photodesorption processes from cryogenic or van der Waals films. In these studies, the van der Waals films serve as model systems for examining molecular dynamics in condensed phases and for comparing to corresponding processes in the gas phase. The studies exploit the fact that these films can be prepared in a vacuum, thereby enabling powerful techniques developed previously in the realm of molecular dynamics and surface science to be applied to probe the photoinduced processes. These techniques will not be described here, since they have been reviewed in detail in the literature.[12] By far, the most usual one has been[12] quadrupole mass spectroscopy (QMS) in a time-of-flight (TOF) arrangement to establish the nature and the intensity as well as the translational distributions of the ejected species.

In the framework of these studies, it was early demonstrated that the processes induced in the irradiation of cryogenic films at high enough fluences exhibit distinct differences from those observed at low laser fluences.[14,18,24] At very low fluences (≤1−5 mJ/cm^2, depending on adsorbate absorptivity), only photofragments or a few parent molecules are observed to eject in the gas phase[12,13] (Figure 2). The

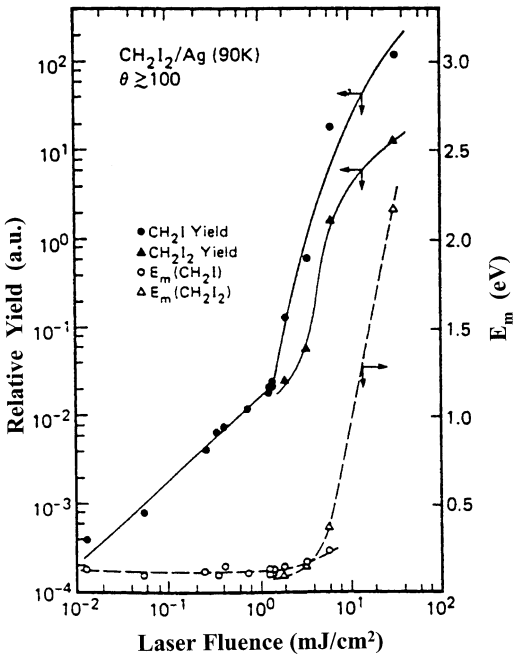

Figure 2. Intensities and most probable translational energies (E_m values) of the gas-phase ejected CH_2I and CH_2I_2 species as a function of laser fluence in the irradiation of CH_2I_2 multilayer film (where θ is the number of monolayers) at $\lambda = 308$ nm. Up to ~2 mJ/cm^2, only CH_2I is ejected in the gas phase. Its intensity scales linearly with the laser fluence, and its most probable translational energy is constant. This corresponds to electronically mediated photodesorption. At higher fluences, ejection of the parent molecule CH_2I_2 becomes increasingly signicant. In this fluence range, the translational energies of both parent and fragment scale sharply with laser fluence. Reprinted with permission from ref 15. Copyright 1989 American Institute of Physics.

desorption signal originates exclusively from absorbing molecules, thus establishing the existence of molecular selectivity in the ejection process. Only excited molecules or fragments from the topmost few layers of the film contribute to the signal. Ejection is generally[13,14,18,23] ascribed to electronically mediated processes, e.g., to the repulsion between fragments during photolysis or to the repulsion developed between the electronically excited molecules and their neighboring molecules. Generally, the photodesorption yield is observed to increase linearly with F_{laser} (Figures 2 and 3a). Furthermore, at these fluences, the translational distribution (e.g., shape

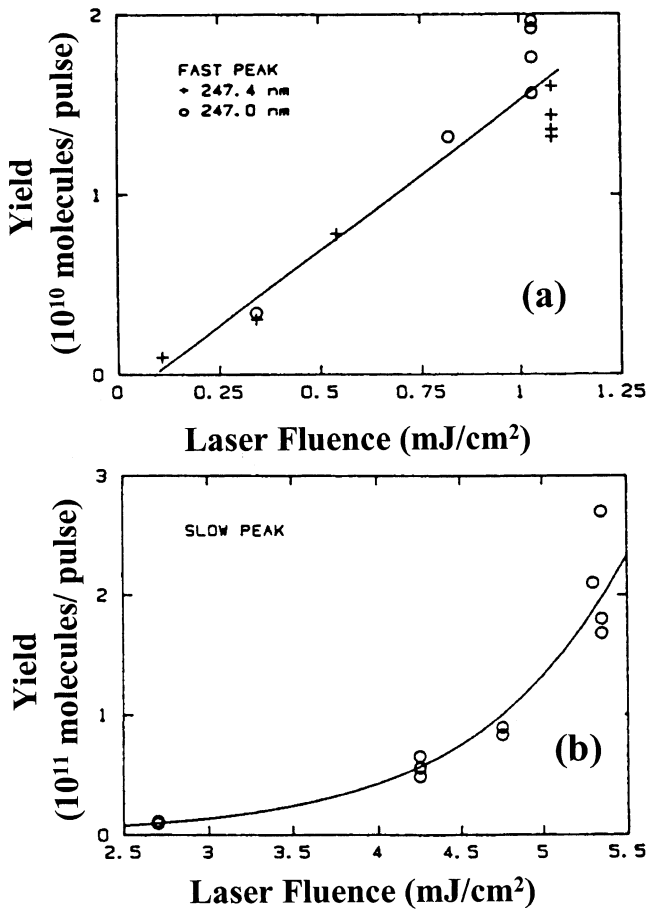

Figure 3. NO desorption signal vs laser fluence in the UV irradiation of condensed NO films (250 ML thick). (a) Fast peak due to electronically mediated desorption (λ = 247 nm). (b) Slow peak ascribable to laser-induced thermal desorption (λ = 273.7 nm). Reprinted with permission from ref 18. Copyright 1988 American Institute of Physics.

and $\langle E_{trans} \rangle$) of the photodesorbed molecules/fragments is independent of the laser fluence (F_{laser}) and can be related to the energy dissipation during the desorption process (Figure 2).

In contrast, at higher fluences and for thicker solids [$F_{laser} \geq 10$ mJ/cm^2 for $\Theta \geq 30$ monolayers (ML); Figures 2 and 3b], ejection of as much as a few monolayers per pulse is generally observed. Accordingly, the term "explosive photodesorption" was coined for this phenomenon.[15] The fluence necessary for its observation decreases with increasing surface coverage, apparently because of the increased rate and density of energy deposition in the film. No selectivity is indicated in this fluence range, and even constituents that do not absorb at the irradiation wavelength are observed to desorb. For example, in the irradiation of CH_2I_2/NH_3 mixture at λ = 308 nm, significant desorption of NH_3 is observed, despite the fact that NH_3 does not absorb at this wavelength.[14] In contrast, at lower fluences, only CH_2I or I fragments are detected in the gas phase, while NH_3 desorption is negligible. The translational energies are generally found to scale with incident laser fluence (Figure 2), which sharply contrasts with the invariance of the translational distributions observed for surface-mediated processes. Domen and Chuang[13] first noted that these features of "explosive photodesorption" are very similar to those observed in the photoablation of polymers. Due to the lack of selectivity and the supralinear (nearly exponential) (Figures 2 and 3b) dependence of desorption intensity on laser fluence, the process has been considered to be "thermal" in nature.

This "explosive" regime has been observed for a wide number of systems (adsorbates) on surfaces, such as CH_3I,[17] NO,[18,21,22] Cl_2,[19,20] CH_3Br,[24] CH_2I_2,[13−16] C_6H_6,[25,26,37] C_6H_5Cl,[37,38] $C_6H_5CH_3$,[38−41] etc. [In the earliest studies, there is some ambiguity about the exact regime in which desorption is effected, e.g., the contradictory explanations advanced[23,24] for the photoejection from H_2O and NH_3 films at 248 and 193 nm]. However, surface scientists largely neglected the phenomenon, evidently because of its "apparent" unselective nature. Nevertheless, even in the first studies, evidence was provided[18] that explosive desorption cannot be considered a "simple" thermal process. In the UV irradiation (λ = 220−270 nm) of condensed NO films at low laser fluences, electronically mediated photodesorption is observed[18] (Figure 3a). At higher fluences, the desorbing NO signal exhibits an additional translational component with velocities corresponding closely to the estimated film surface temperature (Figure 4). In agreement with the presumed thermal nature of the process, the intensity of this component shows a nearly exponential dependence on laser fluence (Figure 3b). Most interestingly, at even higher fluences, the characteristics of this translational component change (Figure 4b). This change was ascribed exclusively to the adiabatic-like expansion of the ejected material, as a result of its high quantity (section II.C). No other significance was ascribed to this difference, though in retrospect, the change may have direct mechanistic implications (section II.C).

B. The Phenomenon of Explosive Desorption

1. Cluster Ejection

At present, in the whole field of ablation of molecular substrates, well-defined physical criteria for describing the phenomenon remain to be established. Several different features have been associated with it, but thus far, none has proven to be general enough. As indicated in the preceding article in this issue, molecular dynamics simulations based on the breathing-sphere model[28−30] suggest that there is a well-defined fluence threshold, above which massive ejection of material occurs largely in the form of clusters. In contrast, at lower laser fluences, ejection of material occurs exclusively in the form of monomers and (distinctly different from the electronically-mediated process discussed in section II.A) is ascribed to thermal surface vaporization. The change from monomer to cluster ejection is suggested to reflect a change in the mechanism of material ejection, i.e. different processes may be delineated within the "explosive desorption regime". In fact, cluster ejection has often been implicated[11,28] to be a particular, if not an inherent, feature of the processes induced at high laser fluences. However, the current evidence as well as the MD simulations indicates that cluster

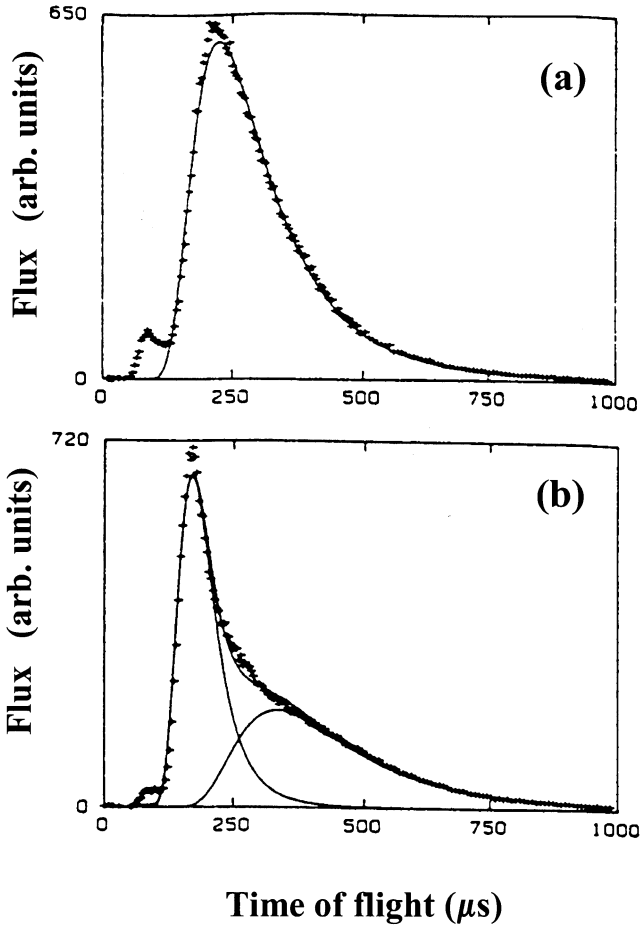

Figure 4. "Evolution" of the desorbate translational distributions with increasing laser fluence in the UV irradiation of condensed NO films (>400 ML thick) at $\lambda =$ 273.7 nm in the "explosive photodesorption" regime. (a) Onset of collisional regime ($F_{laser} \approx 4.5$ mJ/cm^2). Fit of the slow peak to a Maxwellian distribution at 300 K. The total yield is about 1.7×10^{13} molecules/shot. (b) Supersonic expansion. The fit consists of a Maxwellian at 135 K and a shifted Maxwellian at 150 K with a 620 m/s stream velocity. Note that the fast peak (maximum at ~80 μs) that is ascribed to electronically mediated desorption is distinct from the supersonic peak. Reprinted with permission from ref 18. Copyright 1988 American Institute of Physics.

ejection is due to different mechanisms according to the laser pulse width. For this reason, the discussion herein is limited only to the irradiation with typical nanosecond pulses, whereas the influence of the laser pulse width is discussed in section II.B.5. The plausible limitations resulting from the neglect of the electronic degrees of freedom in the MD simulations are addressed in sections II.B.4, II.B.5, and III.C.

Experimentally, the suggested intense cluster ejection is not documented in most cases. For the majority of systems mentioned in section II.A to have been studied in the explosive regime, signal for even dimers of the parent molecules accounts for ≈5% or less of the total signal.[18,20−22] Evidence for cluster ejection deriving from changes in the translational distributions with successive laser pulses[28] is inconclusive, as these may be ascribed to film structural changes. However, the failure to detect clusters may be partly due to the limitations of the employed ionization techniques. In most cases, ionization of the neutral desorbates is effected with high electron-impact energies ($E_{electron} > 50$ eV) or high laser intensities. These conditions may result in extensive fragmentation of the clusters.[33]

Nevertheless, $(HBr)_n$ clusters ($n \leq 4$) have been detected[27] in the irradiation of HBr multilayers at 193 nm with 0.3−5 MW/cm^2 irradiances ($\tau_{pulse} \approx 30$ ns). Though the study did not recognize it, the irradiation condition clearly corresponds to "explosive desorption" (ejection yield of 100 langmuirs per pulse). The relative intensities of the clusters (1.00:0.01:0.001:0.001, for cluster size n from 1 to 4) were noted to be inconsistent with their formation in adiabatic expansion of a gas. Thus, the clusters were suggested to eject directly from the surface. The possibility of cluster ejection in the irradiation at high fluences was recognized by Knutzer et al.[17] in the irradiation of condensed CH_3I films at 266 nm. The resonant multiphoton ionization spectra of the desorbates were noted to become broad and featureless in the "explosive photodesorption" regime. These spectral features are strongly indicative of cluster ionization. Evidence for cluster ejection in the irradiation of 2,5-dihydroxybenzoic acid and poly(ethylene glycol) films ($F_{laser} = 4-12$ mJ/cm^2 at $\lambda = 337$ nm) has been obtained by trapping the ejected material on a plate and examining the morphology of the deposited material by atomic force microscopy (AFM).[34] The study has carefully avoided the caveats of the trapping method. At low fluences, the collected films are smooth, indicating molecular deposition. In contrast, at higher fluences (>4 mJ/cm^2), the films are rough and composed of particles (~200 nm diameter), indicating the deposition of material in the form of clusters or droplets. Cluster contribution is indicated to decrease at higher laser fluences, in good agreement with the results of simulations.[30] Cluster formation has been reported occasionally for other systems but has not been studied in detail.[42]

Haskin and John[32] have examined the desorbate time-of-flight spectra as a function of the delay time and position of the focused postdesorption ionization laser beam in the 266-nm irradiation ($I = 15$ MW/cm^2) of films of chrysene-d_{12} (Figure 5). When the ionization beam is focused ~100 μm away from the surface, a well-defined parent ion peak of high resolution is observed. In sharp contrast, when ionization is effected close to the surface (~50 μm), the recorded parent ion signals are found to be broad and of very low resolution (Figure 5). These changes in the mass spectra resolution can be attributed to the fact that, close to the surface, clusters are ionized, whereas at larger distances, the ejected molecular clusters have disintegrated into their monomers. Disintegration may be due to the high internal energy excitation of the ejected clusters, thus resulting in significant evaporation (section II.B.2), and/or due to the numerous collisions that the clusters suffer in the plume (section II.C). At any rate, according to the previous result, a second reason for the failure of most studies to detect clusters may be related to the fact that desorbate detection is effected at relatively large distances (>10^{-1} m) from the substrate. The time scale of cluster ejection was also

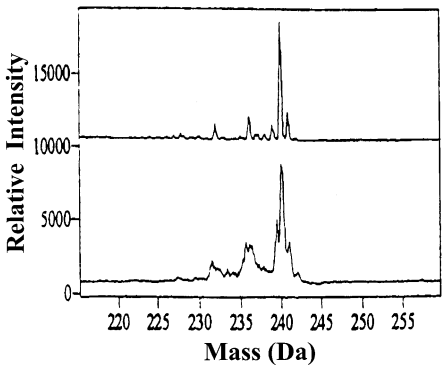

Figure 5. Mass spectra of laser-ejected chrysene-d_{12} recorded by postdesorption laser ionization with the focused ionizing beam 100 μm (upper graph) and 50 μm (lower graph) from the surface. The desorption wavelength is 266 nm, and the delay between desorption and ionization laser pulses is fixed at 0.4 μs. The parent ion envelope consists of the molecular ion (m/z = 240), the ^{13}C isotopomer (m/z = 241), and satellite [M - nD] peaks associated with the loss of 1−4 deuterium atoms from the parent chrysene-d_{12}. Reprinted with permission from ref 32. Copyright 1999 American Chemical Society.

examined. At relatively low laser fluences, cluster ejection is indicated to last for 0.5−0.8 μs, after which desorption is largely in the form of monomers, whereas at high fluences, cluster ejection continues up to ~1.5 μs. The temporal evolution of the ejection processes will be considered further in the next section.

Cluster observation has been common in the irradiation of frozen aqueous solutions of salts. In the 266-nm irradiation of frozen $CeCl_3/H_2O$ solutions (absorption is ascribed to electronic excitation of the hydrated metal[35]) at 3 × 10^8 W/cm^2 ($\tau_{pulse} \approx 8$ ns), $CeO(D_2O)_x^+$ ($x \leq 5$) and $D_3O^+(D_2O)_n$ (n = 1−3) complexes are detected.[35] Fragmentation of larger laser-ejected clusters and/or condensation processes in the plume are implicated. $(H_3O)^+(H_2O)_n$ and $Na^+(H_2O)_n$ (n = 1−30) ionic clusters series have also recently been reported[43] in the IR ablation of frozen aqueous solutions of a protein, but the mechanism of cluster formation in this case remains to be fully elucidated. In the irradiation of frozen aqueous solutions of $XMnO_4$ (X = Na, K) salts at 532 nm,[36] neutral cluster ejection, established via photoionization at 322 nm, is observed upon irradiation at $I \approx 6 \times 10^7$ W/cm^2, while direct ejection of ions is observed at 2.5 times higher irradiances. Peaks corresponding to $M(H_2O)_n^+$ (M = Na, K) clusters, with n values as high as ~16, have been detected. Interestingly, though the cluster size distribution resembles that obtained in supersonic jets, the estimated Mach number for the plume expansion in the laser process is too small (section II.C.). Thus, as in the irradiation of HBr films,[27] the observed cluster series is indicated to represent or derive largely from clusters directly ejected from the film. Probably, in the case of these systems, the strong interaction of the metallic ion with the solvent molecules prevents the clusters from being completely fragmented/evaporated to their monomers. Other factors, such as degree of internal excitation, differences in the collisional rates in the plume, etc., may also affect the stability of the ejected clusters in the various systems, but at present such considerations are highly speculative. The importance of the strength of the intermolecular interactions for the common observation of adduct peaks in MALDI has often been indicated.[44,45]

In all, cluster ejection in the irradiation at high irradiances is by now demonstrated for a number of molecular solids. In contrast, at lower fluences, it is a rather rare observation and is largely accounted for by system-specific (substrate-mediated) mechanisms.[14] Certainly, the generality of the statement is far from being proven, but elucidation of the factors that contribute to the evolution and survival rate of the clusters in the plume will help in addressing this issue further. Yet, even if established, cluster ejection does not provide a mechanistic understanding of the phenomenon.

2. Ejection Mechanisms

In a different approach, the operation of two different, competing mechanisms in the UV irradiation of van der Waals solids at high irradiances has been shown through the comparative examination of the ejection efficiencies of *nonabsorbing* dopants (alkanes such as c-C_3H_6, c-C_6H_{12}, $C_{10}H_{22}$, and ethers/alcohols $(CH_3)_2(CH_2)_nO$, D_2O) of varying binding energies to the matrix.[39−41] $C_6H_5CH_3$ is employed as a matrix because of its minimal fragmentation,[46] thereby avoiding complications due to any photoreactivity. Since the dopants do not absorb at the irradiation wavelength (λ = 248 nm),[46] their relative ejection efficiencies provide information on the nature of the energy dissipation in the film and of the mechanisms by which it results in material ejection. Essentially, in the comparison of these systems, the particularities of the excitation step(s) remain the same, so the nature of the ejection process can be examined independently of the photoabsorption.

The desorption efficiencies are probed as a function of laser fluence via time-of-flight quadrupole mass spectrometry (i.e., neutral desorbates are detected via electron impact). Interestingly, a fluence range (1 × 10^5−3 × 10^6 W/cm^2, $\tau_{pulse} \approx 30$ ns) can be delineated in which the desorption signal as a function of laser fluence (Figure 6) clearly follows an exponential (Arrhenius-type) dependence, or more strictly,

$$S \propto \sqrt{\frac{1}{2\pi m k_B T}} \exp\left(-\frac{\Delta E_{des}}{k_B F_{laser}}\right) \qquad (2)$$

The activation energies (ΔE_{des}) for the laser-induced ejection of the various dopants are found to be in rather good correspondence with their binding energies to the matrix, as these are determined by conventional thermal desorption spectroscopy (TDS) (Table 1).[47] As a result, at these fluences, only dopants that are weakly bound to the matrix are observed in the gas phase.[40] Thus, it is strongly suggested that desorption at these fluences is consistent with surface thermal vaporization. Other mechanisms of ejection are shown to be unimportant. It is noted that for weakly bound dopants, the desorption signal can be very high, a point whose importance will be underlined in section II.B.3.

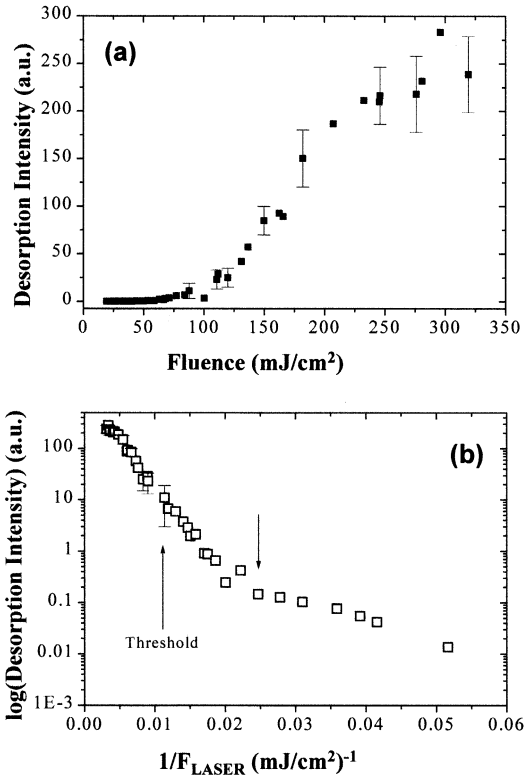

Figure 6. (a) Desorption intensity of neutral toluene ($C_6H_5CH_3$) recorded from freshly deposited films as a function of the incident laser fluence at 248 nm. (b) Semilogarithmic plot of the desorption yield as a function of $1/F_{laser}$. Reprinted with permission from ref 47. Copyright 2002 University of Crete.

Table 1. Comparison of Desorption Energies Determined by Thermal Desorption Spectroscopy and Activation Energies for the Laser-Induced Desorption below the Ablation Threshold (Reprinted with permission from ref 47. Copyright 2002 University of Crete.)

system[a]	compound	E_{TDS} (kJ/mol)[b]	E_{des} (kJ/mol)[c]
neat $C_6H_5CH_3$	$C_6H_5CH_3$	41 ± 2	30 ± 3
$(CH_3)_2O/C_6H_5CH_3$	$(CH_3)_2O$	16 ± 3	17 ± 3
	$C_6H_5CH_3$	35 ± 3	25 ± 3
c-$C_3H_6/C_6H_5CH_3$	c-C_3H_6	15 ± 3	14 ± 3
	$C_6H_5CH_3$	35 ± 3	
$C_6H_{12}/C_6H_5CH_3$	C_6H_{12}	33 ± 4	22 ± 6
	$C_6H_5CH_3$	39 ± 3	25 ± 3
$C_{10}H_{22}/C_6H_5CH_3$	$C_{10}H_{22}$	*d*	77
	$C_6H_5CH_3$	45 ± 5	31 ± 2

[a] Mixtures of the indicated compounds with a 1:5 molar ratio of the dopant vs $C_6H_5CH_3$. [b] Binding energy of the compounds as determined by thermal desorption spectroscopy. The binding energy of $C_6H_5CH_3$ differs in the different systems, due to the influence of the relatively high concentration of the dopants. [c] Activation energies determined from conventional semilogrithmic plots of the laser-induced desorption signals vs $1/F_{laser}$. [d] $C_{10}H_{22}$ desorbs thermally at temperatures well above that at which all $C_6H_5CH_3$ has desorbed.

In contrast, in the irradiation at higher laser irradiances ($I > 3.3 \times 10^6$ W/cm^2), the ejection intensities of the various dopants show no correlation with their binding energies to the matrix.[39,40] Even dopants that are strongly bound to the matrix (such as $C_{10}H_{22}$, with a binding energy to the matrix of ~0.8 eV) are found to be ejected efficiently. Furthermore, the dopant-to-matrix signal ratios reach values close to the initial film stoichiometry (but, note that deviations are usually observed in the case of the strongly bound dopants) (Figure 7a). It is demonstrated that there is no change in the light absorption process. Thus, these changes in ejection efficiencies, as compared to the observations at lower fluences, signify a change in the mechanism.

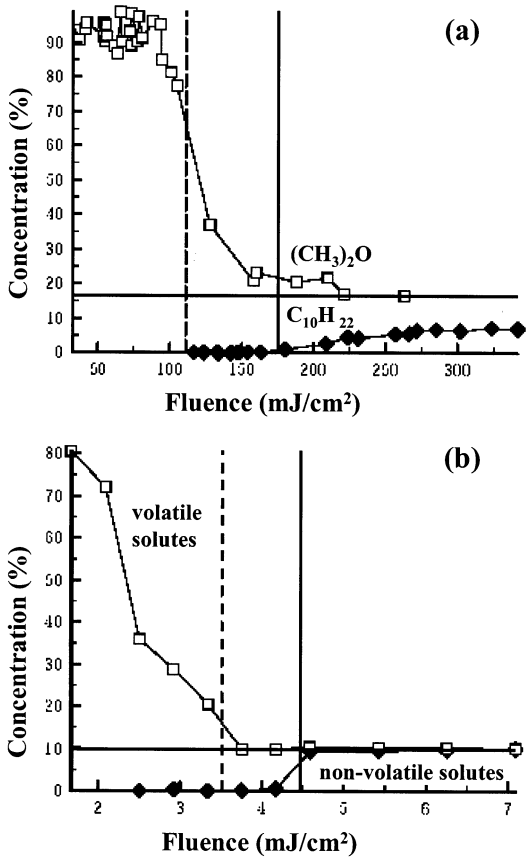

Figure 7. Concentration [i.e., $I_{dopant}/(I_{dopant} + I_{toluene})$] of $(CH_3)_2O$ and $C_{10}H_{22}$ dopants in the plume as function of the laser fluence (F_{laser}) in the irradiation of frozen mixtures of these dopants with $C_6H_5CH_3$. (a) Mass spectrometric measurements (λ = 248 nm) and (b) molecular dynamics simulations. The horizontal lines indicate the initial concentration of dopants in the sample. The solid and dashed vertical lines mark the ablation thresholds for the corresponding systems (different due to the different heat capacities and cohesive energies of the two systems). Reprinted with permission from ref 40. Copyright 2001 American Institute of Physics.

For the strongly bound dopants, the ejection signal relative to that of $C_6H_5CH_3$ remains nearly constant with successive laser pulses. Furthermore, the F_{laser} correspondence of their ejection efficiency closely corresponds to that of the matrix.[40,41,47] Both features indicate the unselective ejection of a film thickness according to

$$l_{ejected} = \frac{1}{\alpha} \ln\left(\frac{F_{laser}}{F_{thr}}\right) \quad (3)$$

where α represents the (effective) absorption coefficient. The dependences of both toluene and dopant signals are well described by the same threshold fluence, F_{thr}. These features establish that *ablation*

entails the nearly nonselective expulsion of a volume of material. Thus, UV ablation is qualitatively a different phenomenon from thermal desorption (usually presumed for explosive photodesorption), and it can be experimentally identified through the ejection of strongly bound species. *In other words, in the "explosive desorption" regime, two different fluence ranges can be distinguished where qualitatively different mechanisms operate.*

The previous conclusion corresponds well to the delineation drawn by the MD simulations (for nanosecond pulses) for the operation of different mechanisms above versus below a well-defined, specific laser fluence (the threshold). Indeed, simulations[40] on the $(CH_3)_2O/C_6H_5CH_3$ and $C_{10}H_{22}/C_6H_5CH_3$ systems yield results that are in very good correspondence with the experimental observations (Figure 7b). Interestingly, the simulations show that the strongly bound dopants are ejected exclusively within clusters of the matrix, whereas the weakly bound ones are ejected largely in the form of monomers. Survival of a percentage of the clusters at the detection volume will affect the ionization process[31] and may account, at least partly, for the fact that the mass-spectroscopically determined ratio of dopant and matrix intensities appears to be lower than the film stoichiometry (Figure 7a). Thus, though still not fully proven experimentally, the previously defined criterion for the ejection of dopants that are strongly bound to the matrix appears to be intimately correlated with the criterion advanced by the simulations for the onset of cluster ejection.

The change in the mechanism of material ejection at a specific fluence suggests the operation of a process that is competitive with the thermal surface evaporation and which becomes dominant above the threshold. The nature of this process is indicated by the abrupt change in the slope of Figure 6b at a fluence ($\sim$40 mJ/cm^2) well below the determined ablation threshold. At this fluence, the surface film temperature is estimated to correspond to the melting point of the matrix.[41] In support of this correspondence, above this fluence, the mobility of weakly bound dopants within the $C_6H_5CH_3$ matrix is indicated to become quite high (diffusion constant indicated to be $\geq 10^{-12}$ m^2/s). In parallel, as established by optical examination, structural changes are induced to the film (neat $C_6H_5CH_3$ films) (Figure 8a).[47] Changes in the substrate have been monitored by the transient transmission and reflection of a HeNe beam incident on the film. A sharp decrease in the transmitted signal (Figure 8b) is observed 100−200 ns after the UV laser pulse. By means of gated imaging techniques, the transmission decrease is established to be due to light scattering and not absorption. The time scale of the light scattering is consistent with that of the formation of bubbles in liquids overheated above their boiling point (section III.A.). For fluences below the threshold, the bubbles finally collapse, and the morphology of the film is permanently modified. With increasing laser fluences, the bubbles grow in size and number, as indicated by the exponentially increasing scattered light intensity (Figure 8b). At a specific laser fluence,

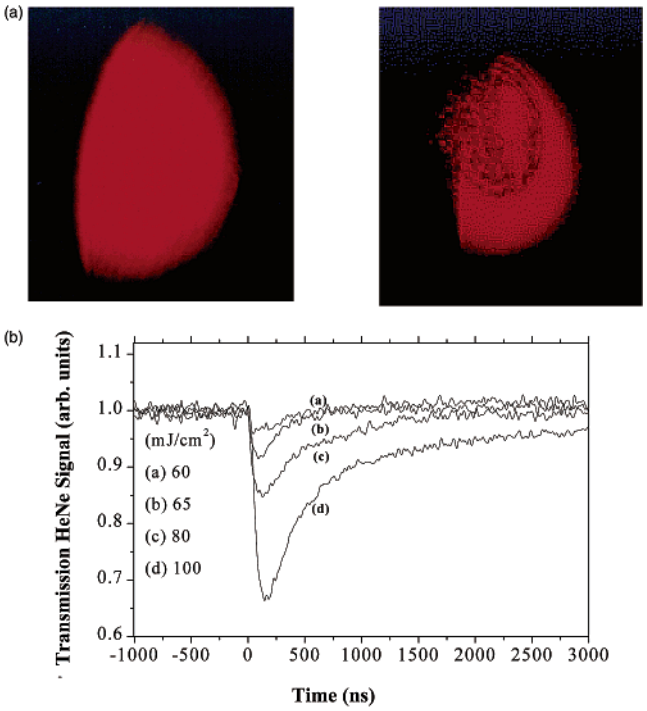

Figure 8. (a) Transmission images of HeNe beam on $C_6H_5CH_3$ films following irradiation with (left) $\sim$2000 pulses at $\sim$30 mJ/cm^2 and (right) 50 pulses at $\sim$55 mJ/cm^2 (i.e., below the ablation threshold, but at a fluence at which melting should occur). (b) Time-resolved transmission at λ = 633 nm upon irradiation of condensed $C_6H_5CH_3$ films with one UV pulse (λ = 248 nm) at the indicated fluences. The signal has been normalized to the transmitted intensity before the UV pulses. Reprinted with permission from ref 47. Copyright 2002 University of Crete.

their growth becomes high enough to result in material ejection.

For organic molecules, the optical penetration depth (l_{abs}), at least at λ < 300−350 nm, is in the 100 nm−10 μm range (e.g., for the $C_6H_5CH_3$ films, $l_{abs} \approx 4$ μm). The thermal relaxation time, $t_{thermal} = \rho C_P l_{abs}^2/4D \approx 10$ μs (where ρ is the density, C the heat capacity, and D the thermal conductivity), is much longer than the typical nanosecond excimer laser pulses. Thus, energy remains confined (thermal confinement regime) and can result in melting and, at higher fluences, in the strong overheating of the liquid. Liquids heated above the temperature corresponding to the external pressure at their saturation temperature are thermodynamically metastable (Figure 9a), since their chemical potential μ_L is higher than that of the vapor, μ_V[48−60] (in the present case, the external pressure is specified by the recoil momentum of the evaporating gas). However, the transformation (boiling) requires bubble formation, which is limited by the work necessary for the formation of a new interface within the liquid (i.e., the surface tension, σ).[52,53] According to thermodynamics, the free energy for bubble formation is given by

$$\Delta G = N[\mu_V(P_V) - \mu_L(P_L)] - (P_V - P_L)V_V + A\sigma$$

$$= \frac{4\pi R_{bubble}^3}{3}(p_{sat} - P_L)(1 - \frac{\nu_L}{\nu_V}) + 4\pi R_{bubble}^2\sigma \quad (4)$$

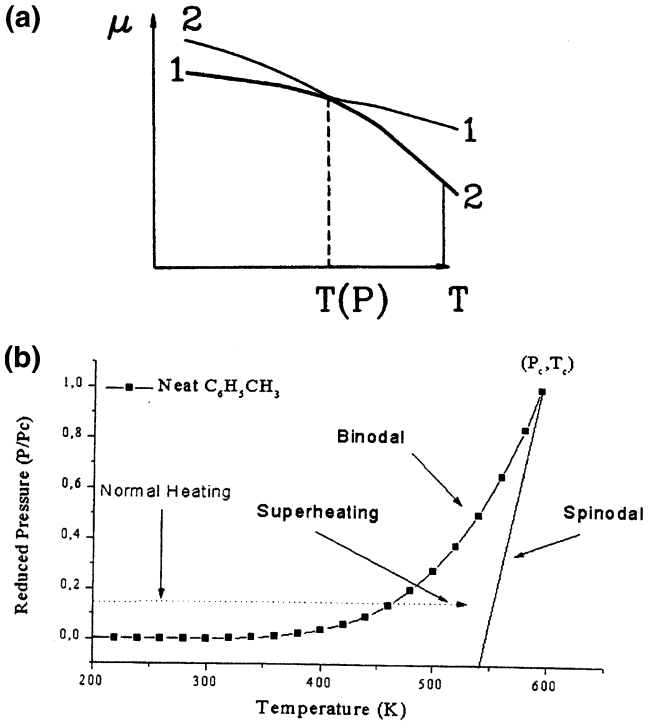

Figure 9. (a) Schematic of the temperature dependence (at constant pressure) of the chemical potential of the liquid (1) and of the gas phase (2) of a one-component system. The crossing corresponds to the equilibrium point (i.e., projection of the binodal for the given pressure). (b) The binodal and spinodal curves and the region of metastability for toluene. *C* is the critical point, and $T_c = 593$ K and $P_c = 41$ bar are respectively the temperature and the pressure of the compound at the critical point. Reprinted with permission from ref 47. Copyright 2002 University of Crete.

P_V and P_L are respectively the pressure inside the bubble and the ambient pressure of the liquid, μ is the chemical potential of the corresponding states, *A* is the surface area of the bubble, *N* is the number of molecules within the bubble, and ν_V and ν_L are, respectively, the specific volume of the vapor and of the liquid. In the first equation, the second term represents the work directed against the pressure forces and the third the work for the bubble interface formation. The second equation derives under the assumption of constant P and T and relatively low degree of superheating.[53] For bubbles exceeding a critical value, $R_{cr} = 2\sigma/(P_V - P_L)$, given by the requirement of mechanical stability of the bubble, $\Delta G < 0$ and subsequent growth is thermodynamically unavoidable. However, for smaller R_{bubble}, the surface tension term dominates and $\Delta G > 0$. Consequently, the number of homogeneously nucleated bubbles formed via thermal fluctuations is given by

$$N_n^{hom} = N_o \exp\left[-\frac{\Delta G(R_{bubble})}{k_B T}\right] \qquad (5a)$$

where N_o is the number density of the molecules in the liquid. The corresponding rate *J* (number per volume and time) for the spontaneous formation of bubbles with the critical size R_{cr} is

$$J = k_f N_o \exp\left[-\frac{\Delta G(R_{cr})}{k_B T}\right] = k_f N_o \exp\left[-\frac{16\pi\sigma^3}{3k_B T_L(\eta p_{sat} - P_L)^2}\right]$$

$$\eta \equiv \exp\left[\frac{\nu_L}{R T_L}(P_L - p_{sat}(T_L))\right] \qquad (5b)$$

Here, k_f denotes the molecular evaporation rate (which obtains somewhat different values depending on the derivation), η relates the pressure within the critical bubble with the saturation pressure $p_{sat}(T)$ at the corresponding temperature, and ν_L is the specific volume of the liquid (assumed to be incompressible). The mean time of formation of a critical nucleus in a volume *V* is $\tau = (JV)^{-1}$ and determines the lifetime of the metastable state. Both σ [approximated usually by $\sigma = \sigma_o(1 - T/T_C)^x$, where T_C is the critical temperature of the compound][52,53] and $P_V - P_L$ factors depend sensitively on temperature. Thus, bubble growth and the lifetime τ depend critically on the maximum attained film temperature and its subsequent temporal evolution.

The surface film temperature drops rapidly after the end of the laser pulse as a result of the evaporative cooling. For small overheating, the work provided by the evaporating gas (i.e., the first term in eq 4) is insufficient to compensate for the surface tension limitation, and thus bubble growth eventually halts. However, at higher fluences, the surface temperature reaches high enough values for bubble growth to become significant. In other words, the higher the attained temperature, the deeper the excursion of the liquid into the "metastability region" indicated in Figure 9b. Due to the sharp decrease of σ and the increase of $(P_V - P_L)^2$ factors with temperature, *J* increases sharply (by orders of magnitude) over a small temperature range, which accounts for the "threshold-like" behavior of laser ablation. Furthermore, since σ and P_V are related to the cohesive energy of the system,[48−53] the threshold for material ejection can be expressed as

$$F_{thr} = L_p(E_{cr} - CT_o) \qquad (6)$$

where L_p represents the optical penetration depth, E_{cr} the critical energy density (J/cm^3), and CT_o (*C*, heat capacity; T_o, initial temperature) the initial energy content. The increase of the threshold with increasing system cohesive energy has been reproduced by both MD simulations[40] and experimental study[39] (Figure 7). However, these qualitative aspects aside, the quantitative analysis of the dynamics of explosive boiling on the nanosecond time scale does not appear to be well established. For instance, the degree of overheating necessary for material ejection is found both experimentally[40,41,47] and by the MD simulations[28−30] to be lower than that suggested by conventional thermodynamic considerations.[49−51,58,59] The latter usually consider that volume ejection occurs at the spinodal decomposition limit. At this limit, the stability criteria are violated (e.g., $(\partial P/\partial V)_T = 0$, $(\partial T/\partial S)_P = 0$, which is physically unacceptable)

and the liquid phase becomes unstable, decomposing spontaneously (i.e., in an activationless process) into a gaseous and liquid droplet mixture. The fact that the massive ejection associated with ablation is observed at much lower temperatures indicates the process to be under kinetic rather than thermodynamic constraints. [It is noted that recent density functional analysis[61] and biased Monte Carlo simulations[62] on superheated liquids have indicated several shortcomings of the classical nucleation theory. In fact, even the assumption of a spherical form for the critical bubbles is indicated to be a simplification (at least for large overheatings).]

According to the above, there is essentially a competition between surface and volume vaporization, with the latter becoming dominant above a specific fluence. A similar delineation has also been considered by Wu et al.[64] in the irradiation of frozen glycerol at 193 nm, largely on the basis of the observed desorbate translational distributions (section II.C.). High enough temperatures (~550 K), suggestive of "phase explosion", are also estimated in the irradiation of frozen aqueous solutions of salts.[36] As will be discussed in the next section, explosive boiling directly accounts for the indicated unique features associated with material ejection at high laser fluences (for nanosecond pulses). Thus, in addition to the usual criterion of thermal confinement, *the criterion of the rate of homogeneous bubble formation being faster than the rate of evaporative cooling must be employed to establish whether material ejection represents really a volume ejection (ablation) process or simply a surface thermal evaporation process.*

3. Implications for Relevant Applications (MALDI, MAPLE)

There are a number of immediate implications of the suggested delineation and, in particular, of the identification of nanosecond-induced laser ablation with explosive boiling. If the upper layers of the substrate are superheated, the underlying material should also melt. This is illustrated for dopants that are weakly bound to the matrix by the contribution through diffusion and thermal desorption from the underlying (nonejected) layers.[38,41] The contribution of the prolonged ("postablation") thermal evaporation to the total ejection signal in UV ablation has often been noted.[1,11,14,32,36] This may result in discrepancies from the previously suggested ejection of a well-defined volume of material (e.g., for the previously noted deviations for the strongly bound dopants). Furthermore, the consequent segregation effects within the melt must be carefully considered when multipulse irradiation protocols are employed, since they can be severe and can seriously complicate interpretation of the results.[41] These effects on the structural integrity of films and their implication for practical applications[63] have been noted.

The most important result of the studies on simple systems appears to be the finding that dopants/analytes that are strongly bound to the substrate/matrix can be ejected only in the ablative regime. Therefore, in MALDI and MAPLE techniques, the observation of the biopolymers in the gas phase only at high fluences appears to be due to the existence of an actual, physically significant threshold. In contrast, the matrix can be detected at lower fluences, due to the fact that it can desorb thermally. Accordingly, the desorption/evaporation terms in the MALDI and MAPLE acronyms are misnomers. In MALDI studies, there is still controversy about this issue[65,66] on the basis that the detection limit is dependent on the employed spectroscopic technique. We note that this does not affect the validity of the argument for the presence of a threshold, but it rather is related to the question of the specification of its exact value.

Along the same lines, the previous delineation suggests that terms such as "thermal ablation" may be misleading.[1] The term "thermal ablation" is employed to describe extensive desorption, largely consistent with thermodynamic properties (e.g., ΔH_{subl}, ΔH_{vap}, etc.), whereas the "nonthermal" term is used to describe deviations from this behavior. However, it is clear that the amount of material removed, even if extensive, does not define a new phenomenon, and instead the term "ablation" should be reserved for the unique characteristics/features that are observed above a specific fluence.

With all caution, it is interesting to note that a distinction relevant to the thermal surface desorption versus volume material ejection delineation is often drawn, even in the case of polymers, between a low laser fluence range in which mass loss occurs due to the depletion of light volatile species (photoproducts) and the fluence range in which actual etching (ablation) is effected.[1,11] This similarity suggests that common features become evident for a variety of molecular systems, thus providing the basis for the development of more "universal" laser -material-removal models. On the other hand, as the studies in section II.A show, the yield due to direct electronically mediated processes is quite low, indicating that such processes (invoked within a so-called "photophysical" model of ablation) cannot be relevant for the extensive material ejection observed at high fluences.

Another implication concerns the physical significance of the activation energies determined from the semilogarithmic plots of ejection signals versus $1/F_{laser}$ (Figure 6b). It is clear that the value determined in the ablative regime must be related to the activation energy of the process (related to the bubble nucleation energy within the "explosive boiling model") and cannot be related with the binding energy of specific molecules. In fact, even the values determined below the threshold are related to ΔE_{des} from superheated liquids and may differ from the tabulated ΔH_{evap} under ambient pressure. This discussion illustrates plausible pitfalls in the interpretation of Arrhenius-type fittings to the ejection efficiencies of analytes in UV ablation (a usual approach in the study of more complex systems). This aspect has been well emphasized by Zhigilei and Garrison.[28−30]

The explosive boiling model can also explain the suggestion of the MD simulations for the ejection of material in the ablative regime mainly in the form

of clusters. Since the sensible heat ($C_P\Delta T$) that has been "stored" in the metastable liquid suffices for the vaporization of only a fraction of the liquid,[57,58] a large percentage of the material is ejected in the form of droplets, exactly as observed in the molecular dynamics simulations for the longer laser pulses (150 ps). (Thermodynamically, this results from the fact that explosive boiling occurs under nonconstant P_L and T.[52]) As a result of the ejection of material largely in droplets/clusters, the requisite energy may be quite lower than ΔH_{evap}. The explosive boiling model can also account for the ejection of the weakly bound dopants mainly as monomers and the ejection of the strongly bound analytes within clusters of the matrix.[40] During homogeneous bubble formation, the desorption rate of the strongly bound dopants into the bubbles is very slow, and as a result, these species are ejected only within the liquid droplets formed during the process. Explosive boiling of mixtures has been considered previously.[52,53] A plausible implication is that the fast "exploitation" of the excess energy for the vaporization of the volatile component (in the case MALDI, of the matrix itself) into bubbles may result in the rapid cooling of the material, thereby limiting thermal degradation of any labile dopants and also heat conduction (and consequently thermal degradation) to the substrate. This possibility is under examination.

Several implications of the suggested cluster ejection in relationship with protein stabilization and ionization processes are discussed in the other articles of this issue. The discussion therein further highlights the importance of considering cluster ejection in ablation. Herein, we note only that if a large number of clusters survive at the detection volume, their presence may seriously affect the detection efficiency of the cluster-embedded species.[34,52] Calibrating the spectroscopic techniques for their relative sensitivity toward clusters versus monomers is practically impossible, especially since the distribution of cluster size is not known. Because of this, quantitative gas-phase measurements may tend to be "artifactual", and discrepancies between studies may appear according to the employed detection technique.

4. Energy Dissipation Processes

Despite their neglect in the previous discussion, the nature of the initial electronic excitation and subsequent deactivation step(s) is expected to be of direct relevance to the material ejection process. Though these processes are usually implicated in the ablation of photolabile systems (section III.B.2.), their consideration is nevertheless important, even for photoinert systems. In fact, it has led to the prediction of the ablation threshold on a basis quite different from that assumed in the MD simulations. Fain and Lin[67] have argued that the initial population of highly excited phonons increases further the rate of the electronic relaxation, thereby introducing a mechanism of positive feedback. The rate of energy transfer from the electronically excited molecules to the phonons of the molecular crystal increases with decreasing energy separation (ΔE_{dif}). Consequently, electronic energy decay will accelerate as higher and higher phonons are populated (Figure 10). When energy flow into the

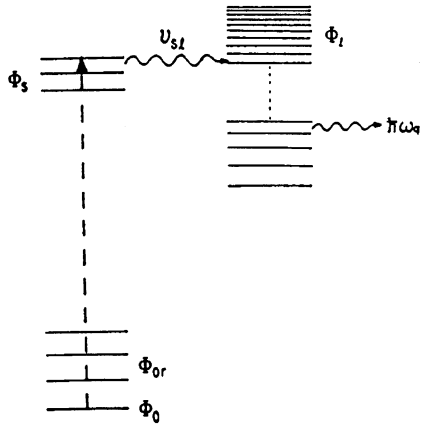

Figure 10. Representation of the de-excitation processes according to Fain and Lin. Optical excitation occurs from the vibronic levels of the ground electronic state, ϕ_o, to the excited electronic state, ϕ_s. Isoenergetic with ϕ_s is a set of vibronic levels, ϕ_l, belonging either to another electronic state or to the ground state, ϕ_o. A set of excited states, ϕ_l, interacts with phonons, giving rise to the stimulated emission of phonons, $\hbar\omega_q$. Reprinted with permission from ref 67. Copyright 1989 American Institute of Physics.

phonons exceeds their decay rate, their number begins to increase exponentially, i.e., an "avalanche" phenomenon, thus resulting in explosive-like vaporization. It was later argued[68] that the avalanche phenomenon may alternatively be due to the interaction of the electronic excited states with localized vibrational excitons (vibrons), which should decay much slower than phonons, thereby making "hot spot" formation more likely.

The model successfully accounts for the observed[13−15] dependence of the threshold on film thickness. Further experimental support for the model derives from the study[68] of the dependence of the luminescence decay of films of Cl_2 on laser fluence ($\lambda = 308$ nm). As the ablation threshold is approached, the decay is found to exhibit distinctly nonexponential temporal behavior. The deviation from the exponential decay is demonstrated to be due to the accelerated internal conversion of the assessed S_1 state of Cl_2, rather than to energy transfer or other plausible decay mechanisms. (However, the possibility that the formation of a metastable liquid may also affect the electronic energy decay process was not recognized.) Similar quenching of the luminescence close to the threshold is also reported for 2,5-dihydroxybenzoic acid and ferrulic acid.[69,70] The plausible importance of exciton pooling mechanisms for ionization in MALDI has often been underlined.[70−73] As discussed in section III.C, similar processes are indicated to be important in the ablation of liquids and also of polymers.

Quite early, Levine and Vertes[74−77] argued that the rates of vibrational energy transfer between analytes and matrix may be one of the key factors in MALDI. In the initial studies, the limitation in the rate of energy transfer was invoked mainly to account for the stability of the ejected proteins within an essentially simple thermal desorption mechanism (section II.D.2). The importance of the energy-transfer

processes has been ramified recently by molecular dynamics simulation[78] of the vibrational-to-translational energy-transfer processes in the irradiation of a solid O_2 system. For irradiation at low laser fluences, this rate is rather slow because the crystal thermally expands and, as a result, the coupling efficiency of the vibrational-to-phonon modes decreases. However, at much higher excitation rates, the sample melts, and diffusion of the vibrationally excited species occurs. The interaction of excited species results in very fast energy transfer to translational modes. This results in a pressure pulse (the simulation is performed for 30-ps pulses, closely corresponding to the stress-confinement regime), which causes rapid material expansion and eventually ejection in the form of clusters. The importance of the interaction of vibrationally excited molecules for the energy-transfer rates has been demonstrated experimentally in picosecond studies in liquids.[79]

In all, despite the limited experimental evidence, novel aspects of energy decay/dissipation processes are indicated that are of direct relevance to the material ejection process. These aspects have not been considered in the "explosive boiling" model discussed previously. Yet, the models may not be contradictory to each other, and it is plausible that they have just captured different aspects of the phenomenon. The studies in the present section may well describe the initial stage of energy dissipation into vibrational/phonon modes, which is, in any case, the starting point of the MD simulations based on the "breathing-sphere" model.[28−30] The good agreement of the MD simulations with experiments is probably due to the fact that, for nanosecond irradiation, electronic decay is faster than or at most comparable with the laser pulse width. Thus, material ejection is mainly determined by the energy distribution following electronic state deactivation (note also that the processes considered in refs 67 and 78 suggest an *acceleration* of the electronic energy decay and dissipation). In fact, optical properties of superheated liquids are indicated to differ greatly from those at equilibrium conditions (section III.C), and the same can be expected for the electronic deexcitation rates. Thus, even if the explosive boiling model is in principle correct, the quantitative analysis of the experiments must eventually take into account these effects. To this end, it is important in future studies to examine energy decay processes in parallel with the formation of the metastable liquid phase. Substrate-mediated laser superheating of liquids (section III.A) can provide a most convenient method to study photophysical properties under metastable conditions. Furthermore, more elaborate theoretical work and simulations including the electronic degrees of freedom are evidently required.

The importance of electronic processes may be at least partly elucidated via the study of the wavelength dependence of the ejection processes. For the "phase explosion" mechanism, material ejection should be wavelength independent, aside from any (effective) absorption coefficient corrections. Some early studies on IR ablation have been reported,[80] but no system has been studied systematically enough in both UV and IR to enable a meaningful comparison. Similarly, very little has been reported on the comparison at different UV wavelengths. A study on the comparative examination of benzyl derivatives at 193 and 248 nm was of a preliminary nature.[37] Examination of wavelength dependence is also important in assessing the relative contribution of photochemical versus thermal processes to material ejection.[1,11]

5. Laser Pulse Dependence

The previous results hold for irradiation with UV nanosecond pulses (typically excimer laser). In the irradiation with shorter pulses, material ejection is considered to be in the stress-confined regime and to be due to the "mechanical" rupture (spallation) of a surface layer under the action of the tensile component of the generated stress, as described in detail in section III.B and in the contribution by Paltauf and Dyer in this issue. MD simulations provide further support for this model.[30] In comparison with thermal evaporation or explosive boiling, photomechanical ablation requires less energy per unit volume for material removal, since only the bonds at the interface between the ejected layer and the underlying one need to be broken without extensive volatilization. Therefore, ablation can be effected at lower substrate temperatures and thus lower incident laser fluences. For this reason, extensive attention has been given to the exploitation of this "cold ablation" mechanism. A number of additional advantages are expected for this mechanism, e.g., minimization of the segregation/diffusion effects described for nanosecond pulses (section II.B.3), reduced photolysis (due to the lower fluences required), and reduced recombination product formation (section II.D) in the case of photolabile systems, etc.

In the few reports thus far on the pico- and femtosecond ablation of molecular solids, the threshold is sometimes,[47,82] though not in all cases,[81,83,84] found to decrease as compared with nanosecond irradiation. For laser pulses that are not short enough (e.g., ~50−100 ps), the invariability of the threshold[84] is understood, since the change in the pulse duration is insufficient to effect a switch from the thermal to the stres-confinement regime. However, the invariability for femtosecond pulses observed in few studies remains difficult to account for. On the other hand, neither the decrease observed in the other studies can be unequivocally ascribed to the suggested mechanistic change. In femtosecond irradiation, electronic multiphoton processes can be expected to become highly likely and may be partly responsible for the decrease. Indeed, nitrogen films can be ablated efficiently with picosecond pulses (λ = 263 nm, τ_{pulse} = 8 ps, 5 J/cm^2)[89,90] and frozen acetone and methanol with femtosecond pulses (λ = 790 nm, τ_{pulse} = 130 fs, at 4 × 10^{15} W/cm^2),[91] athough these compounds are transparent at the irradiation wavelengths (however, these studies were performed at very high irradiances, well above the threshold). The increasing importance of multiphoton processes is indicated in the ablation of polymers[1,92,93] as well as in surface science (desorption induced by multiple electronic transitions, DIMET).[88]

Even in the absence of multiphoton processes, electronic energy processes, which are neglected in the thermal versus stress-confinement delineation, will be of determining importance in the irradiation with femtosecond pulses. For instance, the rate of electronic energy decay (usually ≥10 ps) will determine the degree of effected stress-confinement. Furthermore, energy de-excitation processes may differ greatly from the nanosecond case, with significant implications for the material ejection process. The importance of electronic processes appears to be also indicated by the observation of enhanced desorbate fragmentation in the first few femtosecond studies.[47,83] This result is incompatible with the photomechanical model, since this model suggests material to eject largely in the form of cold, "large" chunks. On the basis of the discussion in section II.D.1, this should result in reduced fragmentation, at variance with the experimental results. It is also noted that, in the case of polymers, a most dinstinct difference in the photoproducts that remain in the substrate has been observed[85,86] between nanosecond and femtosecond ablation. It appears that the examination of the chemical products may be most informative about the mechanisms in the irradiation with short laser pulses.

A most interesting indication on the interplay of the various factors that become important with decreasing laser pulses has been reported in the case of copper−phthalocyanine films.[94] The ablation threshold is found to decrease with decreasing laser pulse width (35 mJ/cm^2 for 170-fs pulses; 80 mJ/cm^2 for 250-ps pulses; 140mJ/cm^2 for 100-ns pulses; in all cases, λ = 780 nm). Multiphoton processes are indicated to occur. Interestingly, the etching depth in the femtosecond and picosecond cases remains nearly constant with increasing F_{laser} above the threshold, which differs distinctly from the usual gradual increase observed for the nanosecond case (e.g., the one in Figure 1 or 6a). The difference suggests a mechanistic change. A pressure-driven material ejection is suggested for the femtosecond or picosecond case.

6. Substrate-Mediated Ejection/Confined Ablation

The previous discussion has focused on processes induced in the irradiation of the "free" surface of absorbing films. In several experiments, material ejection is effected via irradiation through the transparent substrate that supports the condensed film or, in other cases, via light absorption by the substrate itself. This mode of irradiation presents a number of experimental advantages, in particular if ablation of cryogenic films is to be employed for the production of molecular beams for use in kinetic studies or for surface experiments.[19−22] However, it is now understood that the mechanisms of material ejection may differ from those described above for the irradiation of the free surface of the substrates. A number of different terms, such as confined ablation, backward irradiation ejection (or even the apparently contradictory term "transmission irradiation mode"), and laser-induced forward transfer, have been employed to describe the laser-induced material ejection effected in these cases.

Substrate-mediated laser-induced desorption has been extensively studied for (sub)monolayers, mainly with a view toward analytical applications.[95−97] The interest derives from the fact that, for small or weakly bound molecules, laser-induced substrate-mediated desorption can be effected with minimal decomposition. Thus, combined with gas-phase diagnostic methods, it provides a powerful tool for the trace analysis of adsorbates on a variety of surfaces. This process will not be discussed further, since a general consensus[96,97] on its purely thermal equilibrium mechanism appears to have been reached. Instead, the discussion will focus on the UV-induced ejection observed in the irradiation of multilayers.

For transparent multilayer films on an absorbing substrate, heat conduction from the substrate (in competition with conduction into the substrate, the ratio of energy conducted to the film versus the substrate being $\sqrt{D_f/D_s}$) can result in the heating of the overlying layer. Assuming that the interface temperature rise is instantaneous, the temperature profile in the film can be approximated by[98]

$$\Delta T = \frac{(1-R)F_{laser}}{\rho_f c_{p,f}\sqrt{D_f} + \rho_s c_{p,s}\sqrt{D_s}} \frac{1}{\sqrt{\pi t}} e^{-\frac{z^2}{4D_f t}} \qquad (7)$$

where z represents the distance from the interface, R the surface reflection, ρ the density, and C_p the heat capacity, and the subscripts f and s refer to film and substrate, respectively. Analytical solutions of the temporal and spatial (depth) temperature evolution in films of N_2 and H_2O condensed on an absorbing metallic substrate have been presented.[100,101] If the film heat conductivity is high enough, the surface temperature of the condensed film will rise sufficiently to result in material loss via thermal vaporization. At even higher fluences, the interface temperature increase may result in local melting and subsequent (heterogeneous) vaporization of the material adjacent to the substrate in a process similar to that considered in section III.A. For moderate energy input, the vapor formation may be insufficient to overcome the film adhesion and to provide the necessary kinetic energy for the ejection of the overlying layer. In this case, only deformation of the film may occur. However, at higher energy absorption rates, extensive bubble growth will occur, resulting in the detachment of the film and the development of a high pressure, leading to spallation of the whole matrix.[34,37] The importance of the induced pressure has also been indicated by MD simulations.[102,103] A detailed analytical description has been reported[109] but for different type of films.

The previous features have been been recently visualized by novel ultra-high-speed optical microscopy in the irradiation of viscous *liquid* α-terpineol doped with highly absorbing $BaTiO_3$ nanoparticles (because of the liquid state, the dynamics differs somewhat from that of solids).[104,105] The film thickness is 10−15 μm, and absorption is limited to 1 μm at the support−film interface. At low fluences (∼20 mJ/cm^2), deformation of the film can be detected, but no material ejection occurs. At somewhat higher fluences, however, the vigorous bubble formation

close to the interface results subsequently in material ejection. Material removal is initiated at ~500 ns, well after the laser pulse ($\tau_{pulse} \approx 150$ ns).[105] The delay is acribed to the slow formation of the bubbles due to the high viscocity of the medium. Most interestingly, two distinct regimes[104] could be identified in relation with the dynamics of the plume ejection, likely due to the different degree of bubble growth and impulse strength provided for material ejection. For intermediate laser fluences, the plume collapses into a jet ("jetting regime") after 1 μs. In contrast, at higher fluences, a dense plume consisting of vapor and micrometer-sized particles/droplets is ejected.

The ejection of large, micrometer-sized particles in the irradiation at high fluences has also been demonstrated[34] in the irradiation ($\lambda = 10.6$ μm, 2 J/cm^2) of 2,5-dihydroxybenzoic acid/poly(ethylene glycol) films on silica substrate by AFM characterization of the trapped ejected material. The indicated volume ejection should result in the ejection in the gas phase of embedded dopants/analytes independently of their binding energy. Indeed, efficient ejection of biopolymers[106−108] via substrate-mediated absorption/heating has been demonstrated. Advantage is taken of this irradiation mode for the deposition of polymers and biomolecules in the so-called laser-induced forward transfer deposition described in the article by Chrisey et al. in this issue. However, difficulties in the reproducibility of the signals, at least in the analytical applications, have been noted. Likely, this is due to the high sensitivity of the ejection process to film thickness,[19,22,103] a dependence that is not so critical for irradiation of the free surface of the films.

Several other studies have been performed under confined ablation conditions and will be mentioned in the appropriate sections. Interest presents the attempt[110] to use surface plasmon resonance spectroscopy (i.e., probing the surface plasmon frequencies of the metal substrate on which the films are condensed) to monitor with nanosecond time resolution the laser-induced ($\lambda = 248$ nm, $\tau_{pulse} = 30$ ns, 8−26 mJ/cm^2) material ejection process from condensed films (2-propanol, acetone, and tetrafluoromethane). Differences in the time delay of the ejection onset from a few monolayers (thickness of ~50 Å) were observed according to the nature of the adsorbates. Unfortunately, the observed differences are difficult to analyze, because of the combined effect of substrate heating and absorption by the film. Despite its indicated potential, the technique has not been pursued further in the case of frozen films.

Finally, a first intriguing report[87] on femtosecond-induced substrate-mediated material ejection has been published. Near-infrared ($\lambda = 800$ nm, $\tau_{pulse} \approx 150$ fs, $I \approx 5 \times 10^{11}$ W/cm^2) laser desorption of multilayer benzene films on Pt results in a hyperthermal translational component. Ejection was ascribed[87] to impulse transferring from the metallic surface to the topmost desorbate layers via elastic collisions of the molecules, though a pressure-induced material ejection process also seems likely. In other studies,[99] ejection upon femtosecond laser irradiation is indicated to be highly forward peaked, much more so than in the corresponding nanosecond case. This high forward peaking has been taken advantage of for the deposition of submicrometer structures of biopolymers.[99]

In all, for nanosecond pulses and at least for photoinert systems, through the parallel contribution of experiments, analytical considerations, and simulations, a unifying understanding of the processes leading to the laser-induced material ejection seems to be attained. Certainly, several aspects remain to be addressed for a fully satisfactory model to be established. Furthermore, it will be important to examine how these processes evolve with increasing molecular size and cohesive energy of the system from these model solids to more complex ones. Nevertheless, it is clear that new directions of fundamental importance, e.g., in thermodynamics, molecular photophysics, and molecular structural rearrangements, have opened up. As for the material ejection induced by ultrafast irradiation, though detailed molecular dynamics and analytical work has already been performed, very little can be assumed at present, as clearly experimental work has been very limited.

C. Desorbate Translational Distributions

In principle, detailed information on the mechanisms of material ejection would be expected from the examination of the desorbate translational, angular, and internal energy distributions. Typically, ionization of the desorbates with an electron beam or with a second laser pulse is employed to establish their velocity distribution from the time of their flight from the substrate to the detection volume. The corrections necessary for the proper analysis of these spectra are well described in the literature[111] (though in the case of ablation, arguments for its modification have appeared[114]). Internal energy distributions can be conveniently probed via state-selective ionization of the desorbates, usually via resonantly enhanced multiphoton ionization (REMPI). Determination of the angular distributions is quite demanding on the vacuum system design if detection is based on mass spectrometric techniques, but more straightforward approaches employing optical imaging have been developed.[152]

Characterization of the desorbate distributions has proven to be a most powerful approach in the study of surface-mediated photodesorption, yielding detailed information about energy distribution/dissipation in the desorption process.[111] However, in ablation, due to the large amount of ejected material, numerous collisions occur between the desorbates, resulting in significant modification of their initial distributions. Thus, the translational distributions recorded in laser ablation are expected to represent a convolution of the initial "impulse" given during ejection and the subsequent postdesorption dynamics in the plume. However, at present, the relative contribution of these processes is not clear, so models and explanations usually deal with the one or the other extreme.

Elucidation of the factors affecting translational distributions is of major importance, because they are one of the main experimental results available in

ablation studies. Furthermore, the energy transfer between the various degrees of freedom that is effected by the postdesorption collisions may be crucial for the various features of ablation (e.g., for the stability of ejected analytes in MALDI, for the resolution of the mass spectra in laser ablation mass spectroscopy and MALDI, for the structural quality of films deposited by MAPLE, etc.). In the case of realistic substrates, interpretation of the translational distributions is hampered by the formation of plasma. In contrast, in the case of van der Waals films, due to their low cohesive energies (and the large ionization potential of the molecules), material ejection can be effected at fluences at which plasma formation is minimal. Thus, comparison of experimental data and theoretical models is more straightforward. [In this section, no distiction is made between IR- and UV-induced processes, since the relevant information is very scarce. Yet, this is a most important question that needs to be addressed in the future.]

Illustrative examples of the change in the desorbate translational distributions with increasing laser fluence are provided in the UV irradiation of condensed NO films[18] and of frozen glycerol films.[64] At intermediate laser fluences (i.e., corresponding to thermal desorption), the spectra are usually well described by Maxwell−Boltzman distribution with a temperature close to the estimated film temperature. In contrast, at high laser fluences, the desorbate translational distributions (Figure 4) can generally be described by "shifted" Boltzman distributions (though several exceptions are also noted[26,139,158,166]):

$$dN(\vec{v},T,v_{drift}) = N\left(\frac{m}{2\pi k_B T}\right)^{3/2} \exp\left\{-\frac{m}{2k_B T}[v_x^2 + v_y^2 + (v_z - v_{drift})^2]\right\} d^3v \quad (8)$$

The drift velocity v_{drift} can be related to the models described below. In several cases, the description of the distributions requires two shifted Maxwellians,[20−22] but the physical significance of the two components is not clear. The change of the translational distributions to shifted-Boltzmann distributions is often ascribed to an adiabatic-like expansion of the material due to the high ejected quantity.[18−22,64,112−114] With increasing laser fluence, the average ($\langle E_{trans} \rangle$) and the most probable translational energies (E_{trans}^{mp}) shift to higher values (Figures 2 and 11), consistent with the idea that the higher amount of ejected material results in a "tighter" adiabatic expansion. A forward-peaked angular distribution of the desorbates is often observed, described usually by a $\cos^p \vartheta$ (with p as high as 25) dependence,[111] where ϑ is the angle from the perpendicular to the surface.

State-specific ionization of the desorbates has been used to probe the internal energy distributions, thus complementing translational distribution studies. In the 193-nm ablation of condensed NO films[22] (under "confined ablation" conditions), the average rotational energy is found to be more than ~10-fold smaller

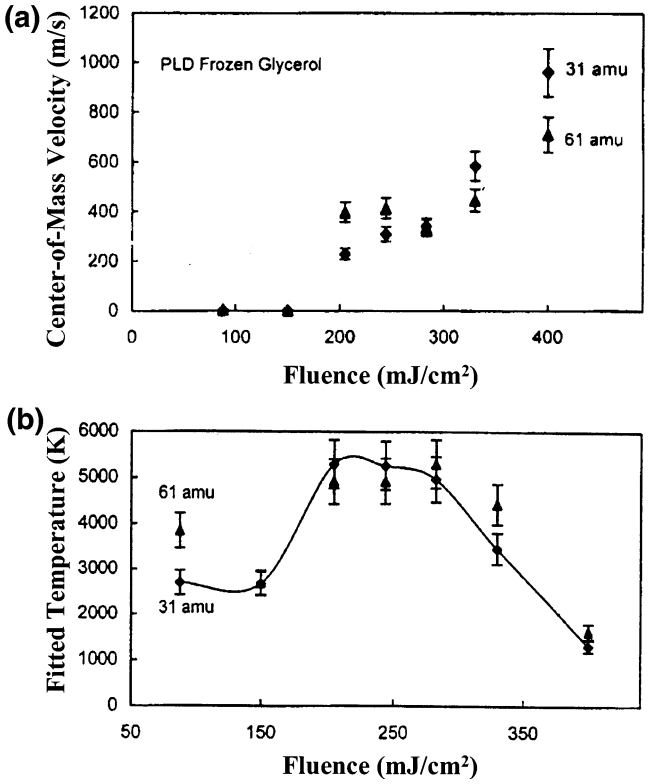

Figure 11. (a) Fluence dependence of the fitted center-of-mass velocities of the TOF spectra of the $HOCH_2CHOH$ (61 amu) and CH_2OH (31 amu) peaks detected in the UV irradiation (λ = 193 nm) of frozen glycerol films (the two peaks are considered to derive, respectively, from the parent glycerol and photofragment $HOCH_2CHOH$ via electron impact dissociation in the mass spectrometer ionizer). The data show an onset of the center-of-mass velocity at F_{laser} = 200 mJ/cm^2 for both peaks. The center-of-mass velocity becomes supersonic above 300 mJ/cm^2. (b) Temperature fitted from TOF spectra as a function of fluence for the two peaks. Trend lines are added as a visual aid and have no scientific significance. Reprinted with permission from ref 64. Copyright 2001 American Institute of Physics.

than $\langle E_{trans} \rangle$ for both $v = 0$ and $v = 1$ (Table 2). Additionally, the vibrational energy is low, e.g., for molecules with E_{trans} = 0.6 eV, the $v = 1/v = 0$ vibrational distribution was 3 ± 1%. The observation of translationally fast but rotovibrationally cold distributions is strongly indicative of the development of a supersonic expansion. The cooling effect as a result of the expansion of the material has also been demonstrated in the "laser evaporation" of aniline from a cryogenic CO_2 matrix on an absorbing substrate[115] (acting as a heat source) as well as in the CO_2 laser-induced ejection of benzimidazole dissolved in a glycerol/water matrix.[116] A significant decrease in the vibrational temperature is demonstrated as a function of the time delay or position between the ablating and ionizing laser beams. The degree of cooling is indicated to depend on the matrix, with matrix molecules of fewer internal degrees of freedom providing more effective cooling.[116]

Analytical descriptions and computer simulations of the postdesorption dynamics provide further information on the extent of the collisional perturbation. Usually, a 1D geometry (planar front of the

Table 2. Average Values of the Desorbate Translational and Internal Energy Distributions in the 193-nm Laser Vaporization of NO Multilayer Films ($F_{laser} \approx 20-25$ mJ/cm^2) (Reprinted with permission from ref 22. Copyright 1989 The American Physical Society.)

probe delay[a,b] (μs) ($\pm 3\mu$s)	$\langle E_T \rangle$ (eV)	$\langle E_R \rangle$[c] (eV)	T_{rot}[d] (K)	$\langle F_2/F_1 \rangle$[e]	$\langle v = 1/v = 0 \rangle$
85	0.71	0.024 ± 0.006	220 ± 20	$1.1 \pm {}^{0.5}_{0.4}$	
100	0.56	0.017 ± 0.004	180 ± 20	$0.70 \pm {}^{0.4}_{0.3}$	
100 ($v = 1$)	0.56		130 ± 30		0.03 ± 0.01
135	0.31	0.009 ± 0.002	108 ± 15	$0.50 \pm {}^{0.3}_{0.2}$	
160	0.22	0.011 ± 0.003	120 ± 15	$0.20 \pm {}^{0.2}_{0.1}$	
210	0.14	0.014 ± 0.003	160 ± 20	$0.35 \pm {}^{0.2}_{0.1}$	

[a] The energy distributions are determined via state-selective multiphoton ionization of the NO desorbates. The probe delay represents the delay between the desorption/ablating and the ionizing laser pulses. [b] All results are for $v = 0$ except where noted. Reported errors represent 2σ. [c] Average rotational energy calculated from analyzed rotational populations. [d] Rotational best-fit temperature for low J. [e] Average spin−orbit ratios ($\Pi_{3/2}/\Pi_{1/2}$) for $E_{int} < 600$ cm^{-1}.

ejected material) is assumed, since the laser spot width on the substrate is large compared with all other relevant lengths of the flow. The approximation loses validity with increasing distance from the surface and increasing dimensions of the plume.

Analytical models rely on the concept of the Knudsen layer.[120−128] For moderate densities of desorbed particles (e.g., 0.5 monolayer in a 10-ns desorption period), a Knudsen layer is assumed to form close to the target surface, in which the velocity distribution evolves from "half-range" Maxwellian (all desorbing particles streaming away from the surface, i.e., $v_x > 0$) to a "full-range" distribution (i.e., $-\infty < v_x < \infty$) in a center-of-mass coordinate system. The width of the Knudsen layer is indicated to be ~15−20 free mean paths.[122] Based on mass, momentum, and energy conservation across the layer, the following conditions are derived between parameters at the boundary of the Knudsen layer (denoted by the subscript KL) and those at the film surface (denoted by the subscript s):

$$\frac{T_{KL}}{T_s} = \left[\sqrt{1 + \pi\left(\frac{\gamma-1}{\gamma+1}\frac{\alpha}{2}\right)^2} - \sqrt{\pi}\,\frac{\gamma-1}{\gamma+1}\frac{\alpha}{2}\right]^2 \quad (9a)$$

$$\frac{\rho_{KL}}{\rho_s} = \sqrt{\frac{T_s}{T_{KL}}}\left[\left(\alpha^2 + \frac{1}{2}\right)e^{\alpha^2}\,\mathrm{erfc}(\alpha) - \frac{\alpha}{\sqrt{\pi}}\right] + \frac{1}{2}\frac{T_s}{T_{KL}}\left[1 - \sqrt{\pi}\,\alpha\, e^{\alpha^2}\,\mathrm{erfc}(\alpha)\right] \quad (9b)$$

$$\frac{p_{KL}}{p_s} = \frac{\rho_{KL} T_{KL}}{\rho_s T_s} \quad (9c)$$

where $\alpha = (\gamma/2)^{1/2} M$ [M is the Mach number, $M = u_{KL}/(\gamma R T_{KL})^{1/2}$], erfc is the complementary error function [$\mathrm{erfc}(\alpha) = (2/\sqrt{\pi})\int_\alpha^\infty e^{-s}\,ds$], T denotes temperature, P pressure, and ρ number density, and $\gamma = C_P/C_V = (j+5)/(j+3)$, where j is the number of accessible internal degrees of freedom. M is sometimes considered to be a variable (≤ 1 for one-dimensional flow) but to a good approximation can be set equal to 1, so that the flow velocity equals the sound speed α: $u_{KL} = \alpha = \sqrt{\gamma k_B T_{KL}/m}$ (m is particle mass). In this case, the relation $k_B T_s = E^{mp}_{trans}/2$ is replaced by $k_B T_s = E^{mp}_{trans}/\eta_K$, with $\eta_K = (\gamma/8)[1 + (1 + 16/\gamma)^{1/2}]^2$ (ranging from 2.52 for a monatomic particle to 3.28 for a polyatomic molecule). Thus, even for few gas-phase collisions (as low as three per particle), a significant percentage of the initial thermal energy may be transformed into forward-directed kinetic energy, and the temperature of the vapor will be indicated to be quite lower than the initial temperature in the film. In parallel, the collisions are predicted to result in partial sharpening of the angular distribution to $\cos^4\vartheta$,[121] and in the partial backscattering of desorbed particles (~18% for monatomic gases up to ~25% for polyatomic gases).

At even higher quantities of ejected material, the Knudsen layer is assumed to be followed by an unsteady adiabatic expansion. Plume dynamics is described by the conservation equations for mass (continuity equation), momentum (Euler equation), and energy:

$$\frac{\partial \rho}{\partial t} + \nabla(\rho \cdot V) = 0 \quad (10a)$$

$$\frac{\partial V}{\partial t} + (V\cdot\nabla)V + \frac{1}{\rho}\nabla P = 0 \quad (10b)$$

$$\frac{\partial E}{\partial t} + (V\cdot\nabla)E + \frac{P}{\rho}(\nabla\cdot V) = \nabla\Phi \quad (10c)$$

where ρ represents density, V the velocity vector, P pressure, and E the energy). Φ is the external heat input into the gas and is assumed to be zero in the adiabatic approximation. The expansion results in the further decrease of the vapor temperature and the parallel increase of the Mach number (M). Kelly[121] assumes an analogy to a firing gun (i.e., the material is held initially within a reservoir of a specific depth and then at $t = 0$, the gate at $x = 0$ is removed and the material expands adiabatically) in order to derive

$$u_M = M\alpha_M = M(\gamma k_B T_M/m)^{1/2}; \quad T_M = T_{KL}\left[\frac{\gamma+1}{2 + (\gamma-1)M}\right]^2 \quad (11)$$

for the resulting flow velocity and the temperature. In parallel, the angular distribution narrows even further, to $\cos^p\vartheta$, where $p = (1 + M)^2$ (for $j = 0$). Detailed mathematical treatment of gas expansion within the Knudsen layer model has been presented.[120−128]

Table 3. Results of the Monte Carlo Simulation on the Distributions of Rapidly Desorbed Particles from a Surface[a] (Reprinted with permission from ref 132. Copyright 1991 The American Physical Society.)

system	Θ (ML)	Z	N_{coll}	$\langle\cos\theta\rangle$	T_{xy} (K)	T_z (K)	v_{drift} (10^4 cm/s)	T_{int} (K)	η_K
Xe	0.1	0	2.18	0.7355	283 ± 1	946 ± 66	1.47 ± 0.10		2.53
	1.0	0	12.17	0.8927	53 ± 1	1273 ± 44	1.57 ± 0.06		2.53
NO	0.1	2	1.86	0.7158	337 ± 3	997 ± 46	3.00 ± 0.07	426 ± 3	2.80
	1.0	2	1.84	0.8560	113 ± 1	2063 ± 149	2.27 ± 0.29	153 ± 1	2.80
valine	0.1	3	2.50	0.7319	322 ± 3	1171 ± 108	1.45 ± 0.16	414 ± 3	2.88
	1.0	3	16.53	0.8634	120 ± 3	2291 ± 168	1.34 ± 0.20	168 ± 3	2.88
valine	0.1	13	2.54	0.7002	253 ± 3	1237 ± 105	1.47 ± 0.16	468 ± 2	3.12
	1.0	13	18.47	0.8393	151 ± 2	3186 ± 265	1.54 ± 0.28	326 ± 1	3.12
(NO, He)	0.1		8.41	0.8669	119 ± 3	1022 ± 88	5.81 ± 0.22	87 ± 2	
	0.9		10.63	0.8428					
(NO, Ar)	0.1		9.13	0.8762	69 ± 2	1512 ± 107	2.51 ± 0.26	95 ± 2	
	0.9		9.34	0.8452					
(NO, Xe)	0.1		10.00	0.8551	87 ± 7	1449 ± 210	2.23 ± 0.61	121 ± 4	
	0.9		10.28	0.8453					
(valine, He)	0.1		14.95	0.9026	138 ± 6	954 ± 79	4.01 ± 0.10	46 ± 3	
	0.9		16.87	0.8645					
(valine,[b] He)	0.1		15.57	0.8733	181 ± 7	1200 ± 101	3.89 ± 0.14	114 ± 3	
	0.9		18.80	0.8390					
	initial distribution						0.6667		

[a] Θ, number of monolayers assumed to desorb. In the case of the neat films (upper section of the table), the numbers represent the total amount desorbed. In the case of mixtures (lower section of the table), the total desorbing amount is, in all cases, one monolayer and the values 0.1 and 0.9 represent the surface coverage by the molecules only. Z, number of internal degrees of freedom assumed to participate in collisions. $\bar{n}$, average number of collisions experienced by a molecule. $\langle\cos\theta\rangle$, average angular distribution of the desorbates. T_{xy}, T_z, T_{int}, and v_{drift}, parameters obtained by fitting the simulated velocity distributions of the desorbed particles to elliptical translational distributions. η_K, the values that are obtained by fitting the simulation results to the equation $E_{trans}^{mp} = n_K k_B T_s$ based on Knudsen layer formation. [b] Simulations performed with $Z = 13$.

Computer simulations have been employed in parallel to examine the validity of the analytical solutions. Sibold and Urbassek have employed the Monte Carlo method to simulate the one-dimensional (1D)[122] and the three-dimensional (3D)[123] single-component pulsed-gas expansion of atoms in the vacuum *under the assumption of constant flux*. The 3D problem is shown to be uniquely specified by the number of ejected monolayers per square meter per second (Θ) and by the aspect ratio of the desorbed plume ($b = r_o/v\tau_{pulse}$, where r_o is the laser spot width). As either Θ or b increases, the average number of collisions experienced per particle (N_{coll}) increases, with a significant increase of the translational energy along the axis of desorption. In a different approach by NoorBatcha et al.,[130−132] particles are considered to desorb according to *a time-dependent flux*, $\phi(t) \propto \exp(-t/\tau_f)$. It is shown that the number of collisions increases sharply when $\tau_f < 10^{-8}$ s (Table 3). According to both models, the distributions are best described by two temperatures, T_z (temperature along the axis perpendicular to the surface) and T_{xy} (temperature along the radial axes), resulting in the so-called "elliptical distributions", though the physical significance of these parameters has been questioned:[120,121,127,138]

$$I(v,\theta) \propto v^3 \exp\left[-\frac{m}{2k_B}\left[\frac{(v\cos\theta - v_{drift})^2}{T_z}\right] + \frac{v^2\sin^2\theta}{T_{xy}}\right] \quad (12)$$

Both v_{drift} and T_z are predicted to increase, while T_{xy} decreases with increasing N_{coll}. Due to the kinematics of the collisions, fast molecules focus in the center of the jet, whereas slow ones focus at large angles. For given Θ, $\langle E_{trans}\rangle$ and N_{coll} increase and the angular distribution broadens with the number of internal modes because of the higher internal energy that can be "dumped" into the translational motions (Table 3). These simulations are in qualitative agreement with the predictions of the Knudsen layer model, i.e., that the translational distributions of the desorbates for different systems but with the same number of internal degrees of freedom can be well described by a single parameter (η_K in the Knudsen model). However, with increasing desorbing amount, deviations are observed between the Knudsen model and the simulations, indicating that the description of the transaltional distributions must incorporate the influence of the surface coverage.

The previous theoretical studies appear to provide a quantitative understanding of the experimental results mentioned at the beginning of this section. The changes in the translational distributions with increasing laser fluence are often considered[18,64,112,113,134] to illustrate the evolution from vaporization to Knudsen layer formation and finally to the unsteady adiabatic expansion. For instance, in the 193 nm irradiation of frozen glycerol films (Figure 11), the nonzero v_{drift} value observed at fluences above ~200 mJ/cm^2 is ascribed to the enhanced contribution of collisions, and the supersonic center-of-mass velocities observed at even higher fluences (300 mJ/cm^2) are ascribed to adiabatic expansion (however, note the very high parallel increase of the time-of-flight T_z between 200 and 300 mJ/cm^2 in Figure 11b). A number of experimental studies rely on the Knudsen layer concept to estimate surface temperatures, consistent with estimated absorbed laser density. Furthermore, the indicated very efficient energy "removal" from the internal degrees of freedom may result in the stabilization of

the ejected thermally labile molecules. In fact, this is the basic idea of the "cooling plume model" for rationalizing the reduced thermal degradation of biopolymers in MALDI. A hydrodynamic analysis was employed[75,136,137] to examine this point for typical MALDI conditions (in combination with the bottleneck model advanced by the same team). The "cooling plume model" has been invoked in a number of cases, as will be discussed in detail below.

Yet, despite the evidence from the previous studies, it is not clear how far the analogy to the adiabatic expansion can be extended. In the previous theoretical studies, the desorbates are assumed to originate from the surface with a thermal Maxwellian velocity distribution. However, as shown in section II.A, the nature of the ejection process in ablation is indicated to be much more complex (prolonged ejection of material in the form of clusters and monomers from a superheated liquid). Chen et al.[142−145] have noted that the prolonged vaporization of material provides a source of mass and energy inflow to the plume, which makes the unsteady expansion nonadiabatic. This contribution was modeled by adding an appropriate mass and energy source in the hydrodynamic equations (eqs 10a and 10c). It is shown that the consequent increase of entropy results in translational energies 2−3 times higher than those expected from the previous models. Furthermore, the acceleration by this "dynamic" source in a direction perpendicular to the surface may result in the more forward-peaked expansion of the plume. In some analogy to the previous suggestion, the simulations by the Garrison[30,138] and Vertes[45] groups indicate that the velocity of the ejecta correlates with their initial depth within the film. Surface molecules are ejected with higher velocities due to the "push" they get from the molecules below. The axial velocity distribution is shown[30,138] to be well described by a modified Maxwell−Boltzmann (MB) distribution with a range of stream velocities, whereas a simple MB distribution with the same temperature can well describe the radial distribution. An important point of this suggestion is that, in contrast to other models, a single temperature can consistently describe the differences between the axial and radial translational distributions without resorting to the adoption of "elliptical" parameters.

The difficulties in accounting consistently for all features of the experimental translational distributions have been detailed in a number of studies. It should be cautioned, however, that a number of "trivial" factors may affect the experimental translational distributions and may account for some of the observed discrepancies from theoretical models. A nonhomogeneous laser profile or even the use of a Gaussian beam, ill-defined amorphous structure of the deposited films, etc. will result in desorbates with a convolution of different translational and angular distributions. Furthermore, a sensitive dependence of the translational distributions on number of pulses, angle of laser incidence, etc. has been noted.[25] In particular, there has been an inexcusable lack of attention to the mode of irradiation (i.e., confined ablation or ejection effected by a combination of direct adsorbate absorption and surface-mediated heating employed in several experiments), though it is clear that this parameter may critically affect the desorbate observables. However, the major limitation in the evaluation of the theoretical models derives from the fact that a complete set of translational, angular, and internal energy distributions as a function of *number of ejected particles* is needed. Aside from the evident immense undertaking that such measurements represent, the usual direct way to vary experimentally the number of ejected particles is through a change of the laser fluence. However, a change in the fluence affects both the quantity of ejected material and the initial temperature, thereby complicating the comparison of experimental results with theoretical models.

In the UV irradiation of indole films[139] ($\lambda = 266$ nm, $\tau_{pulse} = 10$ ns) under conditions resulting in the ejection of 2.0 monolayers per shot, the neutral molecule is characterized by a high translational temperature (3400 K), while the vibrational temperature is only 210 K, and the angular distribution is forward-peaked, with the major component being proportional to $\cos^7 \theta$. These features would appear to suggest an adiabatic-like expansion. However, the vibrational temperature is similar for different velocities. Furthermore, both "cold" and "hot" molecules are found to be described by the same angular distribution. These features are inconsistent with a "jet-like" expansion, since molecules in the densest region of a jet are expected to experience more collisions than the average and thus should be cooled to lower vibrational temperatures. The number of collisions is estimated to be only 2−7, and collisional perturbation is indicated to account only for 10% of the vibrational cooling. These discrepancies were suggested to be due to the non-Boltzmann nature of the initial desorbate translational distribution. Similarly, in various studies,[36,141] the estimated Mach number is much lower (∼2) than that expected for adiabatic expansion (≥5). It has been suggested[36] that the discrepancy can be ascribed to the fact that ejection lasts for microseconds, and thus it should be considered to be of the "steady" expansion type, i.e., $T_M = T_{KL}(\gamma + 1)/[2 + (\gamma - 1)M^2]$ instead[121] of eq 11. Similar difficulties are recognized in accounting for the angular distributions,[139] which are often bimodal, at variance with the predicted simple $\cos^p \vartheta$ dependence. The bimodality has been ascribed to the contribution of different desorbate populations (e.g., "ablative" versus "postablative" ejection)[140] and/or to the reduced number of collisions (thus less forward-peaked expansion) of the particles ejected from the periphery of the irradiated spot.[127]

In the IR ablation of neat C_6H_6 films (on nonabsorbing substrates), Braun and Hess[25] have found that the desorbate's most probable translational energy, E_{trans}^{mp}, does not increase monotonically with laser fluence, but most interestingly it shows a "phase transition"-like dependence (Figure 12). The characteristic "plateau" of the diagram appears at fluences suggestive of film temperatures close to the melting point of the compound. In view of the similarity of the E_{trans} vs F_{laser} diagram to a P, T thermodynamic

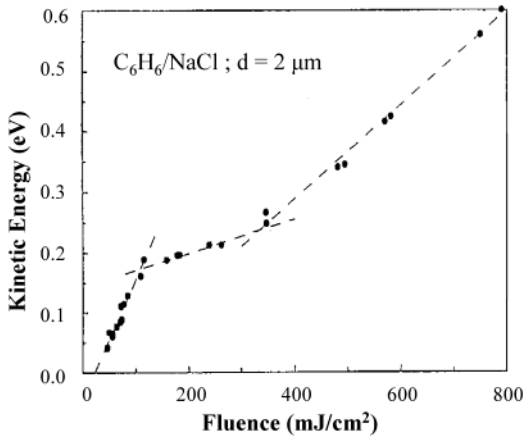

Figure 12. Most probable translational energy as a function of the incident laser fluence in the IR laser (λ = 1033.48 cm^{-1}) ablation of 2-μm-thick benzene films condensed on a NaCl window. The dashed straight lines indicate the separation of the measured data into three regions with different slopes. Reprinted with permission from ref 25. Copyright 1993 American Institute of Physics.

diagram (but not necessarily a valid correspondence), ablation, at least in IR, was claimed to be photothermal in nature. Evidently, the implicit assumption is that the most probable desorbate velocities are mainly determined by the film temperature changes. However, the fitting of the time-of-flight spectra requires nonzero and rather large v_{drift} values, which would appear to indicate substantial gas-phase collisions. It should also be noted that the exact dependence of Figure 12 has not thus far been reported for any other system.

In an approach similar to that described above, in the 248-nm irradiation of neat $C_6H_5CH_3$,[41,47] CH_3I,[190] and C_6H_5Cl films,[38,141] at low fluences, the most probable velocity (v_{mp}) of the desorbates shows a very weak dependence on F_{laser}, but above the threshold, the slope changes abruptly (Figure 13a). It is clear that v_{mp} does not scale smoothly as a function of the desorbing signal (Figure 13b), and thus the abrupt change cannot be ascribed exclusively to enhanced collisional effects in the plume. Similarly, the parallel high increase of both center-of-mass v_{drift} and T_z in Figure 11 does not appear to be fully compatible with gas-phase collisional models. In view of these results, the change from MB distributions to shifted MB distributions that is observed[18,64] as the ablative regime is approached indicates an extra "component" of the desorbate velocities, besides the collisional perturbation. The extra component may be related to the "explosive boiling" process or the dynamic "impulse" effect.[143]

In all, even for simple one-component systems, the experimental desorbate distributions do not appear to be fully accounted for by existing models. The interplay of a number of plausible factors has already been underlined. Furthermore, if we accept the tenet that ejection occurs largely in the form of clusters, which subsequently disintegrate, then the accurate theoretical description of the desorbate distributions will depend critically on the elucidation of the factors that affect cluster evolution in the plume. It is

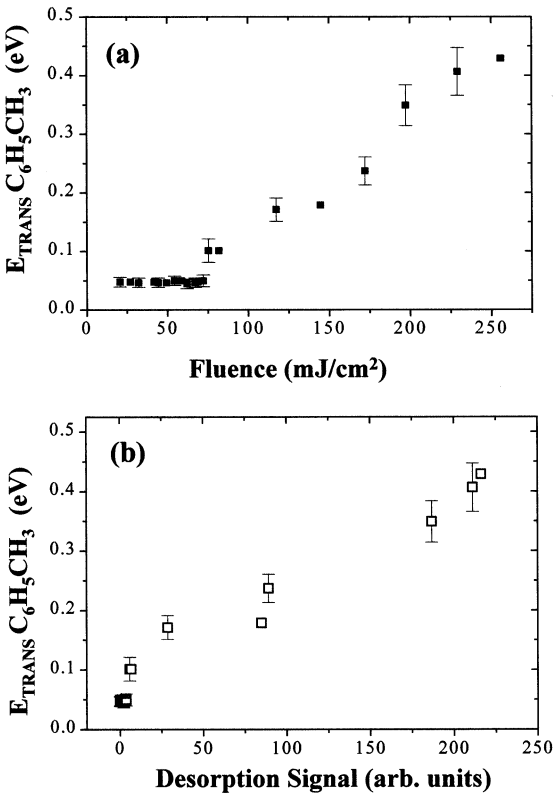

Figure 13. (a) F_{laser} dependence of the most probable translational energies, E_{trans}, of the neutral parent molecules detected in the irradiation of thick $C_6H_5CH_3$ films at 248 nm ($\tau_{pulse} \approx 30$ ns). (b) The same data as a function of the desorbing material. Reprinted with permission from ref 47. Copyright 2002 University of Crete.

interesting to note that, in the laser-induced ejection from HBr multilayers,[27] distinctly different angular distributions have been observed for the different cluster sizes. Though the exact regime of irradiation in this study is unclear, their result, nevertheless, underlines the complexity of the cluster ejection process and of their subsequent dynamics in the plume. Thus far, very little theoretical attention has been paid to the cluster ejection/translational distributions correlation.

For bicomponent systems, additional features relating to the characteristics of the two components (masses, collisional cross sections, relative concentrations, etc.) become crucial. Once more, the various models suggest different degrees of desorbate distribution pertubations. For Knudsen layer formation, the sputtered material tends to move together (i.e., in a single gas cloud), independently of the mass (i.e., different species develop a similar flow velocity),[129] in close analogy to the case of supersonic beams. The light component is characterized by a low TOF temperature and the heavy one by a high one.[129] In Monte Carlo simulations, the influences of the relative concentration, the number of internal degrees (Table 3),[132] and the different masses[133] or desorption energies[135] of the two ejected compounds have been studied for *thermal desorption* from binary mixtures. Because of the difference in the initial velocity of the two components, segregation effects in the ejected plume are demonstrated, with its front (outer) part being composed preferentially of the "lighter" spe-

cies.[133] As a result of the collisional energy transfer, the average translational energy of the light species becomes lower than that of the heavy species (Figure 14). Furthermore, depending on the degree of inter-

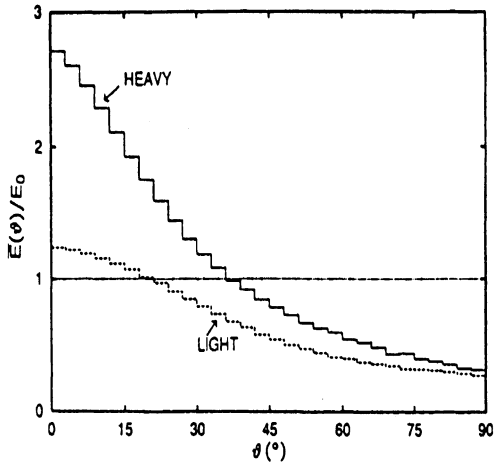

Figure 14. Mean energy $\bar{E}\vartheta$ of particles arriving at an angle ϑ with respect to the surface normal as calculated by Monte Carlo simulation in the thermal desorption of a system composed of two particles with a 1:5 mass ratio. Solid line, heavy particles; dashed line, light particles; dotted line, mean energy for the collision-free flow, $\bar{E}\vartheta = E_o$ as a reference. Reprinted with permission from ref 133. Copyright 1993 The American Physical Society.

mixing of the two components in the plume, the translational distributions may be a convolution of populations that have suffered different degrees of collisional perturbations and, as a result, become bimodal. On the other hand, in the molecular dynamics simulations, the translational distributions of the analytes have been correlated with their initial position in the film.[30,45,138] "Heavy" analytes are shown[30,45,138] to be ejected with a translational distribution nearly identical with that of the matrix (major component of the mixture). Time-of-flight spectra of the analytes are suggested to be sharpest at the threshold, deteriorating at high fluences. The deterioration with increasing fluence is ascribed to the release of the analytes from a higher film thickness, resulting in a higher variation of the velocity distribution, and to the higher attained surface temperatures. A more detailed discussion is presented by Zhigilei et al. in the preceding article in this issue.

Experimentally, differences between the two components ejected in the irradiation of mixtures may be due to the nonuniform mixing/segregation effects in the film.[112] However, differences are also documented in cases where there is no evidence for segregation. In the 248-nm irradiation of $C_6H_5CH_3$/C_nH_{2n} mixtures *below the threshold*,[47] the E_{trans}^{mp} of the dopants weakly bound to the matrix (e.g., $(CH_3)_2O$ and C_3H_6) are lower than that of $C_6H_5CH_3$, despite the fact that at these fluences desorption is thermal (section II.B), and both the dopant and the matrix should desorb with equal E_{trans}^{mp}. Clearly, there is collisional energy transfer in the plume from the "light" dopant to the matrix molecules, which are thus accelerated to velocities higher than those attained in the irradiation of the neat $C_6H_5CH_3$ film. This result appears to be in qualitative correspondence to the Monte Carlo simulations,[133] but quantitative comparison requires further examination.

Different translational features are observed in the ablative regime.[141] As clearly indicated by Figure 15,

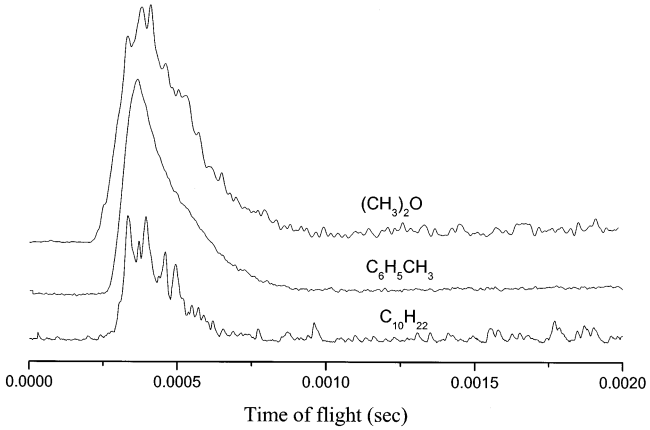

Figure 15. Time-of-flight curves recorded in the ablation of $C_{10}H_{22}/C_6H_5CH_3$ and $(CH_3)_2O/C_6H_5CH_3$ (in both cases, 1:5 molar ratio) solids ($\lambda = 248$ nm, $\tau_{pulse} \approx 30$ ns, in each case, at a fluence ~1.5 above the corresponding threshold). Reprinted with permission from ref 47. Copyright 2002 University of Crete.

well-defined differences are observed between the strongly and the weakly bound dopants in terms of their translational distributions.[39,47] The indicated features are observed for all fluences above the ablation threshold. Similar differences are also observed between amino acids and phenol desorbates in the CO_2 laser-induced ejection from their frozen solution within an ethanol/glycerol matrix.[185] The rather broad distributions of the weakly bound dopants ($(CH_3)_2O$, phenol) may be ascribed to collisional effects in the plume. Alternatively, the distribution broadness may reflect the extensive contribution of "postablation" thermal desorption that occurs for these compounds (section II.B.3). On the other hand, for the strongly bound dopants (decane, amino acids), which are supposed to be ejected within clusters of the matrix molecules, the time-of-flight spectra are nearly superimposable with those of the matrix.[39] This closely corresponds to the findings in MALDI that proteins are ejected with the same velocity as the matrix independently of their masses,[147−152] and to the prediction of the molecular dynamics simulations.[30,45,138]

In the very few reported examples, the angular distributions of the "heavy" analytes are indicated to be even more forward-peaked than those of the matrix molecules. Puretzky et al.[153] managed to monitor the time evolution of the angular distributions of DNA and of the matrix in UV MALDI ($\lambda = 248$ nm, $F_{laser} = 50$ mJ/cm^2) via laser-induced fluorescence imaging of the plume. To this end, DNA was tagged with a fluorophore. A sharpening of the angular distribution of DNA as compared with that of the matrix has been observed. It has been well accounted for by a hydrodynamic description of the flow.

The same mechanisms as those described above have also been invoked to account for the transla-

tional distributions of the products ejected in the ablation of photoreactive compounds. For instance, for products that are strongly bound to the matrix, the translational distributions in the ablative regime are[38,39,141] nearly identical with those of the parent molecule, exactly as observed for strongly bound dopants discussed above. On the other hand, the velocities of the "light" fragments or photoproducts[38,64,141] have been usually correlated with the picture indicated by 3D Monte Carlo simulations.[133] It is understandable that, due to the massive material ejection, photoproduct translational distributions in ablation are mainly determined by the plume dynamics, and there is minimal influence of the initial fragmentation or reactivity process (in contrast to electronically mediated photodesorption processes). Yet, in a few cases, photofragments may be observed with very high velocities and translational distributions deviating considerably from the previous models. It is likely that these are formed by photofragmentation in the gas phase (plume),[38,64,176] resulting in additional energy deposition on the fragment. The effect of chemical reactions (atom recombination and molecule dissociation) that may occur in the plume on the desorbate distributions has also been examined by Monte Carlo simulations. It is shown that chemical reactions in the plume result in significant spread of the angular and translational distributions.[154]

Summarizing previous studies, it is clear that some general trends have by now been established for a number of simple molecular solids/films. The trends appear to be extrapolable to more complex systems, at least MALDI. However, the interpretation of the observed trends and features in terms of gas phase (i.e., plume) and primary processes (i.e., film) of the ejection remains to be fully elucidated. It is noted that even the description of distributions for desorption from a metastable liquid (i.e., below the threshold) calls for additional theoretical work. This is an aspect that has been largely overlooked in the literature. Studies on solids of very simple (monatomic and diatomic) molecules may be most useful and provide the most stringent test of the various models, since, understandably, their extension to polyatomic molecules presents a number of additional complexities.

It has been usual in studies on complex systems such as polymers to base rather detailed and strong mechanistic statements (e.g., temperatures attained in the film, thermal versus nonthermal nature of ejection, etc.) on translational distribution fittings. However, in view of the interpretational uncertainties discussed above and of the sensitive dependence of the translational distributions on a number of experimental parameters, caution should be exerted in trying to extract mechanistic conclusions from such fittings. Additionally, the interpretation of the translational distributions in the irradiation of these systems is further complicated by the formation of a plasma, extensive secondary fragmentation and reactivity in the plume, etc.

D. Chemical Processes and Effects

The issue of chemical processes and effects in the ablation of molecular substrates is closely related to the question of the mechanism(s) of the phenomenon (sections II.A and II.B), since photochemical processes have been suggested[1,11,155] to contribute to, or even dominate, material ejection in the irradiation of photolabile systems. In fact, the issue of photochemical versus thermal mechanisms has been the most hotly debated topic in the field of ablation of molecular substrates. However, even in the case of a thermal mechanism (e.g., explosive boiling), the energy released by the induced exothermic reactions can be substantial, thus affecting quantitatively the features of the material ejection process[157] (e.g., threshold, ejection efficiencies, etc.).

Studies dedicated to addressing the issue of photochemical-induced material ejection have been detailed in the case of liquids (section III.B.2). In this section, we take a more general view of the chemical processes in the UV ablation of molecular substrates. Specifically, independently of the specific mechanisms responsible for material ejection, how can chemical processes in UV ablation be described? Conventional photochemistry considers bond breaking and formation in a well-defined environment under well-defined conditions. In contrast, in UV ablation, a large number of electronically excited molecules are formed, high temperatures are attained, high-amplitude stress waves are induced, and, as described above, the "physical" condition of the substrate is rather unusual—all these within a time-varying framework. Therefore, the real challenge raised in UV ablation of molecular substrates is the development of appropriate models with predictive power to describe chemical processes under the above conditions.

The issue of the nature and the extent of chemical modifications is also crucial for the optimization of the various applications of UV ablation. The processed molecular substrates (polymers, tissues, etc.) generally include a wide variety of chromophores, which upon photoexcitation may dissociate into highly reactive fragments. Additional species may be formed by the thermal or stress-induced breakage of weak bonds. In material-processing schemes, it is important to minimize accumulation of these species in the substrate, since they may form in the short- or long-term byproducts (e.g., oxidation products) with detrimental effects on the integrity of the substrate. In analytical diagnostics of laser-ejected material, it is important that fragmentation does not compromise parent molecule signal intensity. On the other hand, control of the fragmentation may be useful for the group analysis/characterization of the compounds.

In the following sections, we consider first the qualitative (product patterns) and quantitative aspects (extent of photolysis and product yields) in the irradiation of photolabile/photodissociable systems, whereas section II.D.2 considers the issue of thermal degradation in the ablation of molecular solids. As clearly indicated by the previous discussion, this division is somewhat formalistic (since a high degree of coupling between the thermal and (photo)chemical processes is expected), and the reason for adapting it is for simplicity of presentation.

1. Photochemical Processes and Effects

The studies on van der Waals films have indicated a number of unexpected features about chemical processes and effects in the irradiation of molecular solids with high-intensity laser fields. A most interesting result in the study by Domen and Chuang[13−16] was the observation of intense parent peak in the "explosive desorption" from CH_2I_2 films ($\lambda = 308$ nm) (Figure 2). In the ablation of Cl_2 films at 355 and 193 nm, the Cl signal comprises less than 7−10% of the total desorption signal[20] (Table 4). These findings are

Table 4. Relative Yields of Species Detected in the Ablation of Photolabile Systems[a] (Reprinted with permission from ref 161. Copyright 1996 American Chemical Society.)

parent molecule	species	neutral ratio[b,c]
Cl_2 ($\lambda = 355$ nm)	Cl_2	1
	Cl	0.10 ± 0.03
ICl ($\lambda = 532$ and 266 nm)	ICl	1
	I	<0.18
	Cl	<0.84
	I_2	0.19
	Cl_2	0.60
XeF_2 ($\lambda = 266$ nm)	XeF_2	1
	XeF	0
	Xe	9.11
	F	4.31
	F_2	1.154

[a] The study corresponds to "confined ablation". [b] The reported ratios have been corrected for the relative detection efficiencies of the various species/fragments in the mass spectrometer. [c] Parent peak normalized to 1.

most surprising given that, upon excitation at the corresponding wavelengths, the studied molecules dissociate in the gas phase with near-unity quantum yield. No evidence for fragmentation has been obtained in the irradiation of NO_2 films[158] ($\lambda = 248$ nm under a "confined ablation" scheme) and of H_2O films ($\lambda = 193$ nm).[176] These results bear directly on the feature of ablation of molecular substrates that has been crucial for its use for analytical purposes, e.g., in MALDI. Stability of dopants (e.g., no decomposition or reaction with the surrounding polymer) is also observed in the UV ablation of doped polymers, at least for photoinert dopants (e.g., naphthalene, phenanthrene, etc.).[159]

It can be suggested that the observed parent peak represents molecules that are ejected without having absorbed a photon themselves. Since photodissociation occurs only for molecules that have absorbed a photon, whereas even molecules that do not themselves absorb are ejected, an "apparent" fragmentation yield is expected, given by

$$\frac{N_{\text{fragment}}}{N_{\text{parent}}} = \frac{qF_{\text{laser}}(1 - \exp(-\alpha l_{\text{ejected}}))}{h\nu\rho l_{\text{ejected}} N_a/\text{MW}} \quad (13)$$

where α is the absorption coefficient, F_{laser} is the incident fluence, ρ, N_α, and MW are the density, the Avogadro number, and the molecular weight, respectively, and l_{ejected} is the ejected layer thickness. For typical values as for the systems studied above, this ratio ranges from 10^{-2} to 10^{-1}, thus accounting at least semiquantitatively for the reduced apparent fragmentation yield. [In some of the previous studies,[20,158−161] the employed mode of irradiation corresponds to "confined ablation". As discussed in section II.B.2, in confined ablation, material may largely be ejected intact. So, in these experiments, the apparent degree of desorbate photofragmentation may be greatly reduced from that in the irradiation of the free surface of the substrates.] Another important implication becomes apparent by comparison with eq 3. It is clear that l_{ejected} is energy-density dependent, whereas the photodissociation/product number is photon flux dependent. Thus, differences in the apparent fragmentation yield with irradiation wavelength alone do not constitute sufficient evidence for a change in mechanism, as sometimes argued in polymer studies. Furthermore, assuming all factors being the same, the apparent percentage of photolysis of a photolabile chromophore can be reduced by mixing it with another strongly absorbing (photoinert) chromophore. This is, of course, one of the evident factors underlying the success of MALDI. On the other hand, concerning the extent of photofragmentation in the *remaining* substrate, eq 3 suggests it to be constant with laser fluence (since the nonejected layers are subject to the same F_{thr}). However, as discussed below, both eq 13 and the previous implication neglect the possibility of "postablation desorption" of fragments and/or photoproducts that are formed below the etched depth (section II.B.3).

Though eq 13 provides a basis for understanding the extent of desorbate photolysis in UV ablation, it does not appear sufficient to account for all observations concerning chemical effects. Important experimental information in this direction was provided by the examination of the product patterns in the ablation of neat films of ICl and XeF_2.[160,161] Upon electronic excitation to a dissociative state, efficient formation of Cl_2 and I_2 (as well as Cl and I fragments) is observed in the ablation of ICl films ($\lambda = 532$ or 266 nm), and formation of F_2 in the case of XeF_2 ($\lambda = 266$ nm) (Table 4). Clearly, the fragments produced by the photolysis of the parent molecules react extensively with each other (though in the case of ICl, the observed products may partly derive from direct, concerted reactions of the excited parent molecule). It is thus likely that the reduced fragmentation in ablation is due, at least partly, to the operation of efficient recombination processes; i.e., a percentage of the fragments recombines with reformation of the parent molecule. This possibility was stressed already in the first studies by Domen and Chuang.[14,15]

The question is raised, however, about the factors responsible for the efficient operation of the recombination processes/cage effects. Initially, material ejection was generally considered to occur largely during the laser pulse,[17−24] in which case the efficiency of the recombination processes is difficult to account for. Furthermore, in this case, secondary absorption in the gas phase would be expected to be significant, thus resulting in further fragmentation. The secondary gas-phase photolysis has been strongly emphasized in polymer studies.[1,6,11] As illustrated by the discussion in the other articles in this issue, the

relative contribution of photolysis and of reactivity in the gas phase (i.e., plume) versus in the film is an issue of high importance in both MALDI and polymer ablation.

The extent of the relative contribution of photolysis in the gas phase versus in the film evidently depends critically on the time scale of plume ejection (this delineation may be somewhat of an oversimplification, since there is not really a defining line in the evolution from the condensed phase to the gas phase). Even for simple thermal evaporation, desorption continues for 100 ns after the laser pulse, until the effected cooling reduces the temperature to low enough values. In the case of explosive boiling (section II.B.2.), at least for fluences close to the ablation threshold, material ejection can be considerably delayed after the end of the nanosecond laser pulse due to the time necessary for the bubbles to grow to a large enough size.[53] A considerable delay in the material ejection onset has similarly been observed in the irradiation of liquids (section III). Since molecular photolysis occurs very fast (usually on picosecond or nanosecond level), the delay in plume ejection and the prolonged material ejection after the laser pulse suggest that the largest percentage of desorbates is photolyzed in the film before it has been ejected in the gas phase. As a result, their photolysis should be subject to the efficient electronic deactivation and radical recombination processes that are characteristic of condensed phases,[181] thereby explaining, at least qualitatively, the operation of "cage effects" advanced by Domen and Chuang. However, in the case of ablation, the quantitative aspects are far from clear, since the condensed phase is presumably a superheated liquid. Ventzek et al.[162] suggest that the degree of fragmentation can be predicted on the basis of the corresponding equilibrium dissociation/recombination constants within the critical fluid (but such constants are largely unavailable).

The issue of photolysis in the film versus in the plume was specifically addressed in the 248-nm ablation of condensed C_6H_5Cl films.[164] Interestingly, the apparent photolysis yield, as determined from the gas-phase [HCl]/[C_6H_5Cl] ratio, exhibits two dinstinct dependences on F_{laser} (Figure 16). The small yield observed at fluences close to the threshold appears to be consistent with the assumption of reduced photolysis efficiency within a condensed phase (but, the validity of the argument of the photolysis efficiency depends critically on the extent of HCl vs C_6H_5Cl "postablation" desorption, see section II.B.3).[38] At any rate, at higher fluences, at which extensive material ejection during the laser pulse is indicated to occur (Figure 8a), the photolysis yield exhibits a sharp and nearly linear increase with F_{laser}. The correlation strongly suggests the increasing importance of secondary gas-phase photolysis of the compound in the plume. Furthermore, at these fluences, free chlorine becomes significant, whereas this species is hardly detected at lower fluences. Most probably, this represents Cl produced by photolysis of the ejected compound in the initial stages of the plume ejection, when the density of C_6H_5Cl is still low. Multiphoton processes and weak plasma formation

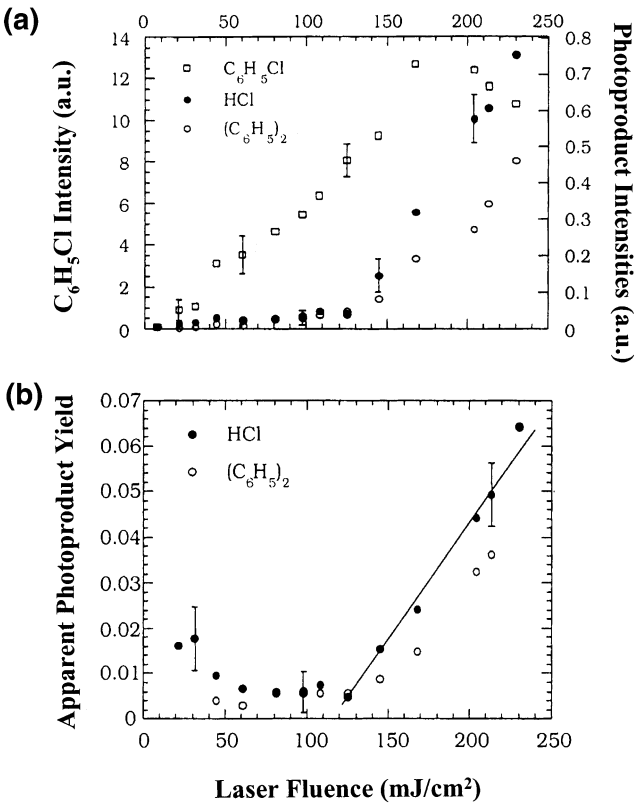

Figure 16. (a) Fluence dependence of the intensities of (neutral) C_6H_5Cl and HCl detected in the UV ($\lambda = 248$ nm, $\tau_{pulse} \approx 30$ ns) irradiation of neat C_6H_5Cl condensed films. The right-hand ordinate refers to C_6H_5Cl and the left-hand one to the intensity of the HCl product. (b) The gas-phase HCl concentration as a function of the incident laser fluence. The change in the dependence of the HCl yield at laser fluences >150 mJ/cm^2 has been ascribed to the increased contribution of secondary photolysis in the ejected plume at these high fluences. Reprinted with permission from ref 164. Copyright 1997 Elsevier Science B.V.

may also become important in determining the extent of desorbate photolysis at higher fluences.

A dependence similar to that shown in Figure 16 is observed for the O_2 photofragment versus parent signal in the irradiation of condensed O_3 films[166] at 248 nm (Table 5). A reduced parent peak at the expense of higher fragment intensity is also found for higher laser fluences in the UV ($\lambda = 266$ and 213 nm)[189] irradiation of polycyclic nitrate films. The degradation of the mass spectra at high fluences, well above the threshold, is a common observation in MALDI, though in this case, enhanced thermal decomposition (section II.D.2) may also be involved. The only case for the opposite trend is reported in the irradiation of frozen glycerol[64] at 193 nm. The $HOCH_2CHOH$ photofragment (Table 5) is found to decrease relative to the ejected parent molecule with increasing laser fluence. The reason for the different behavior observed for this system is not understood.

In the ablation of indole films[139] at 266 nm (at which both solid and vapor indole absorb) at 75 mJ/cm^2 (probably close to the ablation threshold, which however was not determined), the fraction of molecules that interact with the laser light is a percentage of the ejected material, and thus the ionization efficiency is lower than expected. Following ejection,

Table 5. Examples of Photoproducts Observed in the Ablation of Condensed Films of Photolabile Compounds and Reaction Pathways Accounting for Their Formation

system	wavelength (nm)	observed products/fragments	proposed reaction scheme	refs
CH_2I_2	308	CH_2I, I, CH_2	$CH_2I_2 + h\nu \rightarrow CH_2I + I$ $CH_2I_2 + h\nu \rightarrow CH_2 + 2I$	13−15
ICl	532, 266	I, Cl, I_2, Cl_2	$ICl + h\nu \rightarrow I + Cl$ $Cl + Cl \rightarrow Cl_2$ $I + I \rightarrow I_2$	160, 161
Cl_2	355	Cl	$Cl_2 + h\nu \rightarrow Cl + Cl$	19−21
XeF_2	266	XeF, F, F_2	$XeF_2 \rightarrow XeF + F$ $F + F \rightarrow F_2$	161
C_6H_5Cl	248	Cl, C_6H_5, HCl, $C_{12}H_{10}$, (C_6H_6),[a] $C_6H_4Cl_2$, $C_{12}H_9Cl$, $C_{12}H_8Cl_2$	$C_6H_5Cl + h\nu \rightarrow C_6H_5 + Cl$ $C_6H_5Cl + Cl \rightarrow C_6H_4Cl + HCl$ $C_6H_5Cl + C_6H_5 \rightarrow C_6H_4Cl + C_6H_6$ $C_6H_4Cl_2 + C_6H_5 \rightarrow C_6H_4Cl + C_6H_5Cl$ $C_6H_5 + C_6H_5 \rightarrow C_{12}H_{10}$ $C_6H_4Cl + C_6H_4Cl \rightarrow C_{12}H_8Cl_2$[b] $C_6H_4Cl + C_6H_5 \rightarrow C_{12}H_9Cl$[b] $C_6H_4Cl + Cl \rightarrow C_6H_4Cl_2$	38, 47, 156, 157, 164, 167, 172
$CH_2(OH)CH(OH)CH_2OH$ (glycerol)	193	$HOCH_2CH_2OH$, CH_2OH, CH_3	$C_3H_8O_3 + h\nu \rightarrow CH_2OH + HOCH_2CHOH$ (CH_3 is suggested to be formed via protonation in postdesorption collisions)	64
$CHCl_3$	193	$CHCl_2$, HCl, CCl_2, Cl, CCl_3	$CHCl_3 + h\nu \rightarrow CHCl_2 + Cl$[c] $CHCl_3 + h\nu \rightarrow CCl_2 + HCl$ $CHCl_3 + Cl \rightarrow CHCl_2 + HCl$ $Cl + CHCl_3 \rightarrow CCl_3 + HCl$ (a number of additional products may be formed with successive laser pulses)	176, 184
$C_6F_5N_3$ (FPA)	248	C_6F_5N (FPN), N_2, $(C_6F_5N)_2$	$C_6F_5N_3 + h\nu \rightarrow C_6F_5N + N_2$ $C_6F_5N + C_6F_5N \rightarrow (C_6F_5N)_2$	169, 177, 180
O_3	248	O_2, O	$O_3 + h\nu \rightarrow O_2 + O$ (O_2 may also derive from $O + O \rightarrow O_2$ in the film)	166
$Si_3N_3C_6H_{21}$ (hexamethylcyclotrisilazane)	193	H_6C_2SiNH, $Si_2C_4N_2H_{14}$	$Si_3N_3C_6H_{21} + h\nu \rightarrow H_6C_2SiNH + (Si_2C_4N_2H_{14})$ $H_6C_2SiNH + h\nu \rightarrow H_3C-SiH_2-NCH_2$	265

[a] C_6H_6 could not be ascertained experimentally. [b] These products may also be formed, respectively, by the direct reaction of Cl and C_6H_5 with the parent molecule via the so-called "ipso subsitution. [c] The Cl time-of-flight spectrum differs significantly from those of $CHCl_3$ and $CHCl_2$ both in width and peak arrival time. (A similar observation has been also reported in the irradiation of C_6H_5Cl films.) The E_{trans} is comparable to that determined in the gas-phase photolysis of the compound, thereby suggesting that it has undergone very few collisions. It appears likely that it is produced via photolysis of the ejected $CHCl_3$ in the plume, similar to the suggestion advanced in the studies of C_6H_5Cl[38] and indole film.[139] Additional support for this suggestion is related to the high reactivity of the chlorine atom, which suggests that any Cl formed in the film will react before it is ejected.

16% of the desorbates absorb one ablating laser photon and subsequently fluoresce back to higher vibrational levels of the ground electronic state (with the vapor heated from $T_i = 173$ to 233 K), whereas 10^{-5} molecules absorb two photons and ionize. In contrast, in the irradiation at $\lambda = 290$ nm, which is strongly absorbed by the solid but not by the vapor, only 0.1% of the molecules are heated by the ablating laser, and the ionized fraction is reduced from 10^{-5} to 10^{-7}.

In all, the studies thus far have provided strong evidence for the importance of recombination processes in the ablation of moleculer photosensitive films. However, the extent of their influence on the desorbate photofragmentation extent is expected to depend greatly on the specific reactivity of the produced radicals, i.e., to be system-specific. On the other hand, the detrimental effects of secondary absorption in the plume for the apparent photostability of the molecules have been clearly illustrated by the previous studies. This contribution may, in fact, be partly responsible for differences, such as for the enhanced fragmentation and a higher percentage of "internally hot" molecules observed in the "front" part of the plume versus in the main part.[140,152,153] These differences have alternatively been related to the degree of thermal degradation of the corresponding populations,[156,157] but the gas-phase contribution appears to be an equally likely factor in the case of UV ablation. Finally, it is stressed that the previous discussion of film versus plume contribution pertains only to photolysis. The degree of reactivity in the film versus in the plume is a much more involved aspect, which has been a particular consideration in the case of MALDI, as described in the article by Zenobi and Knochenmuss in this issue.

Besides the question of the extent of photofragmentation, another most important question concerns whether product patterns in UV ablation differ from those in conventional photochemistry.

In the few systematic studies of photoproduct formation as a function of laser fluence, different species have been detected *in the gas phase* above versus below the threshold. In the irradiation of condensed fluorophenyl azide[169,177,180] (F_5PhN_3) at 248 nm, F_5PhN and N_2 are detected above the ablation threshold (the smaller detected fragments may be largely due to the cracking at the ionization source). In contrast, below the threshold, only N_2 is detected in the gas phase. Similarly, in the 248-nm irradiation

of neat C_6H_5Cl films[38,172] above the ablation threshold, a number of different products are detected in the gas phase (Table 5), whereas at lower fluences, only HCl is observed from freshly deposited films. It would be tempting to suggest that the observation of the various products above the threshold reflects the reduced reaction selectivity in ablation. However, in both cases, the examination of the irradiated films clearly shows additional photoproducts formed in the substrate below the threshold. In the F_5PhN_3 system, the formation of the dimer, fluoroazobenzene ($F_5PhN{=}NPhF_5$), in the irradiated film[169] is established by FTIR and absorption measurements. The product is formed quantitatively in the film, and all precursor is chemically modified after a sufficient number of pulses. In the C_6H_5Cl system, formation of the phenyl derivatives in the film at fluences below threshold has been established by transmission measurements,[38,172] pump−probe[172] studies, and thermal desorption spectroscopy.[182] *Thus, the detection of a higher variety/number of different products in the gas phase above versus below the threshold must be related mainly to the different material ejection mechanisms in the corresponding fluence ranges* (section II.B.2). Below the threshold, only the volatile products (i.e., N_2, HCl, etc.) desorb, whereas the ones that are strongly bound to the matrix are ejected only in the ablative regime. This delineation must be taken into careful consideration in studies on complex substrates (e.g., polymers) that rely largely on the examination of gas-phase ejected species to extract mechanistic information.

The difference in ejection mechanisms may have important implications for the extent of photoproduct formation in the corresponding fluence ranges. Clearly, in the irradiation below the threshold with successive laser pulses, there is accumulation in the substrate of "heavy" radicals that may result in side reactions and extensive "polymeric" formation. This possibility is indicated in the examination of the C_6H_5Cl[38,182] and halocarbon films.[184] The deleterious effects of accumulating chemical modifications to the integrity of the substrate and/or efficiency of material ejection have been noted in MADLI[173] and in the irradiation of polymers[11,86,174,178] (usually observed for irradiation close to the threshold). In contrast, these side effects may be reduced in extent in the ablative regime, due to the efficient removal of even the larger, strongly bound species. Indeed, subsequent irradiation at higher fluences removes the modified layers, with restoration of the ejection signal. As indicated above, eq 3 suggests the extent of photofragmentation and photoproduct formation in the remaining substrate to be constant with laser fluence. However, this neglects the possibility that fragments and/or photofragments that are formed below the etched depth and are weakly bound to the matrix may diffuse to the surface and thermally desorb ("postablation" desorption; section II.B.3). This effect may be a crucial factor for the success of the various laser material-processing schemes, since it indicates that small (usually the most reactive) species formed even below the etched depth may be efficiently removed. Thus, we have stressed[178,179] that the importance of high substrate absorptivity for successful laser material processing may be related, besides the well-known criterion for efficient material removal and good surface morphology, to the optimal effected etching rate versus depth of product accumulation ("confinement" of photoproducts remaining in the substrate very close to the surface and efficient removal).

Another effect of the photoproduct accumulation at fluences below the threshold may be the enhancement of light absorption with successive laser pulses. This results in an induction effect; that is to say, the desorption signal from freshly deposited films is relatively low, but it increases with successive laser pulses. This effect is most pronounced in the irradiation of films that absorb weakly at the irradiation wavelength (e.g., CH_2Cl_2 and C_6H_{12} at 248 nm),[168] but it is also observed[38,167] for compounds such as C_6H_5Cl, in that their photolysis results in products that are stronger chromophores than the precursor. The observation of incubation even for the simple van der Waals films clearly shows that, in the corresponding phenomenon in polymers,[1,11,170,171] the necessity of chain breakage is of minor importance for its observation. Analytical modeling of the optical changes effected to the substrate with successive laser pulses has been described in ref 171.

Turning now to the formation mechanisms of the photoproducts observed in the ablative regime, in all systems mentioned thus far, these can be fully accounted for by well-known reactions of the radical/fragments produced by the photolysis of the precursor. There is no indication that new reactivity pathways open up in the ablative regime. A few selected examples are summarized in Table 5. For the indicated compounds, thermal decomposition is indicated[160,161] to be minimal due to the strong bonds ($E_{bond} \geq 3$ eV) of the compounds. In the irradiation of C_6H_5Cl films at 248 nm ($\tau_{pulse} = 30$ ns), the suggested radical mechanism (Table 5) is further supported by the fact that changes in the product pattern upon dilution of other compounds (C_6H_{12}, Freon, etc.) in the C_6H_5Cl matrix are found to correlate with the degree of reactivity of C_6H_5 and Cl photofragments toward the added compound.[47,172] The observed product pattern in the irradiation of neat C_6H_5Cl films has been quantitatively modeled by MD simulations.[156,157] However, the modeling relies on reaction rate constants adapted from conventional solution studies. At present, the validity of this (implicit) assumption is unclear.[172,183] Further limitations in MD simulations may result from the necessary scaling of the constants due to computing power restrictions. We have suggested[190] that the study of the influence of deuteration on photoproduct patterns, a well-known methodology in organic kinetic studies, may be particularly useful in addressing such questions.

Importantly, reactions induced in the UV ablation of photolabile systems may be highly exothermic. If these reactions are fast enough to compete with material ejection due to explosive boiling, then the energy release into the system may contribute significantly to material ejection[156,157] (discussed in more

detail in section III.B.2). In the case of van der Waals films, this possibility is indicated in the comparison of the UV ($\lambda = 248$ nm) ablation of $C_6H_5CH_3$ and C_6H_5Cl films. Much more direct evidence has been provided in the 248 nm ablation of films of the highly photoreactive pentafluorophenyl azide (FPA). In the ablation of films of the compound dispersed within Ar, the pentafluorophenylnitrene (FPN) radical is clearly detected[177,180] in the plume, whereas this intermediate is not observed in the ablation of neat FPA films.[169] The difference is ascribed to the enhanced thermal decomposition of the radical in the latter case due to the high temperatures resulting from the high exothermicity of the reactions that take place in the neat films (Table 5). Furthermore, the blackbody radiation spectrum of the plume in the case of the neat film is consistent with a temperature as high as 2900 K. Further studies in this direction are expected to provide detailed information on the "coupling" between thermal and (photo)chemical processes in the UV ablation of photolabile systems.

Despite their importance, ionization processes have not been specifically examined in the UV ablation of simple molecular systems. A number of early works have studied ionization processes for a variety of rather complex organic molecules. Karas and Hillenkamp have delineated different categories of compounds in relation with the observed ions and plausible ionization processes.[195] The various factors that may be involved in ionic desorbate formation in MALDI are discussed in the subsequent articles. In contrast, in the case of van der Waals films, the studied compounds generally lack the functional units that would promote ion formation. As a result, observed ionic desorbates either represent preformed ions of the salts mixed in the substrate[35,36,43,191] or are formed via secondary absorption of photon(s) by the ejected desorbates in the plume.[18,64,139,189] In the former case, it is important that the clusters that are commonly observed in the irradiation of these systems are generally not related to the embedded salts, but instead to the solvated ions (i.e., $M(solvent)_n$ are observed rather than $MX(solvent)_n$, where X = anion). This result supports the suggestion that the clusters are directly ejected from the substrate (since the salts dissociate upon dilution into hydrated ions). Alternatively, the final form of the desorbed species may be dictated by thermodynamic stability factors, as discussed by Knochemuss and Zenobi in this issue. As for the ionization effected by secondary photon absorption in the plume, this has been exploited for the desorption and state-resolved detection of the desorbates[18] in a one-laser experiment (i.e., by the ablating laser pulse) and for analytical purposes.[189] In the irradiation of frozen glycerol films,[64] ion signal is observed at a well-defined threshold, above which it increases linearly with laser fluence. A combination of thermal ionization process (described by the Saha equation[197]) and ionization via a single-photon absorption in the plume was proposed to account for these features.

Studies on ion formation in simple systems exhibiting acid−base reactivity, electron-transfer processes, etc. evidently would help greatly in the elucidation of the ionization processes in MALDI. Mashni and Hess[80] studied ion formation and ejection in the IR irradiation of films of simple organic compounds, and this work could provide the basis for corresponding studies in UV. Such studies may be most useful in addressing the importance of chemical characteristics of the matrix and analyte for desorbate ionization in the UV irradiation, the role that "exciton pooling"[68−71] processes (section II.B.4) are indicated to play, the relative contribution of the processes in the film versus in the plume, the time scale of ion formation versus that of material ejection and plume expansion, etc.

2. Thermal Decomposition Effects

In all previous cases, the compounds are thermally stable, and the attained film temperatures are not high enough to result in any significant decomposition. For thermally labile compounds, however, further chemical modifications via thermal decomposition can be expected. The issue of thermal degradation to the substrate is crucial in the laser-processing/structuring of materials, and thermal decomposition of the desorbates is crucial in analytical applications (laser ablation mass spectrometry and MALDI).

Concerning the extent of thermal degradation to the substrate, this is usually discussed in terms of the thermal diffusion time ($t_{thermal}$, section II.B.2) as compared with the nanosecond laser pulse width. However, as noted in the previous sections, the time scale of material ejection can be considerably longer than the laser pulse width, and so the simple comparison may underestimate somewhat the extent of thermal diffusion.[185] A more detailed description starts from the consideration of the heat conduction problem in the irradiation of the systems. Usually, the enthalpy formulation of the heat equation is employed because of its convenience in dealing with phase changes including melting.[1,187] Written in the frame of reference of the receeding surface (assumed to be along the z-direction), this becomes

$$\frac{\partial H}{\partial t} - v\frac{\partial H}{\partial z} = \frac{\partial}{\partial z}\left(k\frac{\partial T}{\partial z}\right) - \frac{\partial (I\, e^{-\alpha z})}{\partial z}, \qquad H(T) = \rho \int_{T_0}^{T} C(T')\, dT' \quad (14)$$

with the main boundary condition concerning the energy loss at the surface due to evaporation,

$$k\frac{\partial T}{\partial z}\Big|_{z=0} = D\frac{\partial H}{\partial z}\Big|_{z=0} = v(L - H_s + H^V(T_s))$$

Here, v represents the rate of material removal, and the term in the parentheses represents the enthalpy difference between the vapor and the condensed phase (evaluated at the surface temperature, T_s). C is the heat capacity, ρ the density, L the evaporation latent heat, H_s the enthalpy of the substrate at the inteface, and H_s^V the vapor enthalpy, $H_s^V = \rho \int_{T_0}^{T_s} C_P^{(V)}(T')\, dT'$ (all expressed per unit volume). The solution of the equation for the "nonstationary case" relevant to the irradiation with nanosecond pulses has been discussed amply in the literature.[1,187] The

extent of thermal decomposition or any "pseudo-unimolecular" reaction up to time t is then assumed to be given by a time-integrated Arrhenius equation, $\int_0^t A \exp(-E_{act}/RT(t'))\, dt'$ (where A and E_{act} are the corresponding pre-exponential factor and activation energy).[185,186] However, no satisfactory analysis has yet been reported for the case of explosive boiling (though similar to the so-called "volume" models considered in the case of polymer ablation and discussed in the contribution by Bityurin et al. in this issue). Furthermore, the estimation of the extent of thermal decomposition neglects that reaction constants may be significantly affected by the parallel change in the physical state and structure of the substrate. Initial studies[178] on doped polymers indicate that these effects are manifest in unexpected way in the kinetics of photoproduct formation.

It has been even more challenging to account for the thermal stability of the desorbates in the ablation of molecular solids. Evidently, the thermal confinement factor by itself is insufficient to account for the reduced thermal degradation of the ejected desorbates. A number of different suggestions have been advanced to account for this observaion. Early ion, Vertes and Levine[74−76] suggested that the reduced fragmentation of the biopolymers in MALDI is due to a bottleneck in the energy transfer from the matrix to the protein. The suggestion was advanced to reconcile the observed stability of the biopolymers with the very high temperatures necessary for their ejection by a simple thermal desorption/evaporation process. It was suggested that, because of the mismatch between the vibrational frequencies of the matrix and those of the biopolymer, an energy-transfer bottleneck is formed, and the phonons pump readily only the hydrogen bonds between the matrix and the protein, but not the "internal" biopolymer vibrations. A competitive kinetic model[74,76] and computer simulations[77] indicate that the analyte can be, indeed, ejected with an internal temperature much lower than that of the matrix. However, since inter- and intramolecular energy-transfer processes occur efficiently on a picosecond time scale, it is questionable whether irradiation with typical nanosecond pulses is short enough to preclude them. "Bottlenecking" effects appear more likely in the irradiation with picosecond pulses; in fact, strong evidence for such an effect has been indicated in polymers.[196] However, even in the irradiation with nanosecond pulses, the concept of energy bottlenecks may be a significant one, even if their physical origin may not be the one underlined by Vertes and Levine. Indeed, in the case of explosive boiling, the formation of a high number of bubbles within an initially homogeneous medium can introduce barriers of various sorts. The possibility of the fast "exploitation" of the excess energy by the "volatile" matrix in bubble formation/growth contributing to the cooling of the material has already been noted (section II.B.3).

An interesting comparison was early reported by Buck and Hess[26] that in the ablation of neat C_6H_6 films at 248 nm, no naphthalene is formed; significant product is formed instead, presumably via prior decomposition of C−H bond(s), for substrate-mediated heating of the adsorbate layer. Unfortunately, the reported information about the irradiation conditions is insufficient to establish the factors responsible for the observed difference. The use of a metallic substrate may have been responsible for the naphthalene formation in the heating experiment. A more concrete example of thermal decomposition was obtained in the CO_2 laser ablation of frozen aqueous solutions of the tryptophan and tyrosine amino acids.[188] At laser fluences slightly above the ablation threshold, the molecular peak is stronger than that of the fragments formed by the loss of the side chains. With increasing fluence, the molecular and the fragment peaks increase in parallel. However, above a laser fluence about twice the ablation threshold, the fragment signal increases at the expense of the parent molecule peak in a way very similar to that depicted in Figure 16. It was shown that heating of the plume by secondary absorption is insufficient to account for the observed trend. The fragmentation was ascribed to the enhanced degradation of the analyte molecules within the highly heated cavitation bubbles formed in the explosive boiling process (in which case fragmentation precedes any cooling effects due to postdesorption collisions). The study was performed in the IR. Nevertheless, given the similarity of the mechanisms to those described in sections II.B.2 and II.B.3, the findings of the study may be also relevant to UV ablation, though in this case the photoionization/dissociation in the plume, as described above, will probably set in at lower fluences.

A systematic attempt at assessing thermal decomposition in the UV ablation of molecular solids was reported by Vertes and Gijbels.[191] To this end, the ionic and neutral desorbates in the irradiation of phosphonium salts, neat or dissolved in matrices (nicotinic acid, NH_4Cl, 3-nitrobenzyl alcohol, glycerol), at $\lambda = 266$ nm with $\tau_{pulse} \approx 15$ ns were studied. In the irradiation of the neat solids, fragments compatible with thermal decomposition as well as products due to recombination reactions are observed. In contrast, upon dilution of the salts in UV-absorbing matrices, the yield of intact ions is highly increased, and recombination products are greatly reduced (evidently due to the high degree of dilution within the matrix). A detailed characterization of the dependence of the extent of decomposition on irradiation conditions, matrix properties, and analyte concentration was performed. Reduced decomposition is observed for matrices that absorb strongly at the irradiation wavelength (an effect probably sufficiently accounted for by eq 13) and for matrices of a low boiling/sublimation point. On the basis of their results, the authors suggest that triphenylphosphonium salts with polycyclic aromatic substituents can be used as "molecular thermometers", but evidently simpler systems would be preferable. Furthermore, the photochemistry of these systems is not well characterized, and it is not clear to what extent the observed products may also derive from direct photodissociation.

As indicated in section II.C, particular emphasis has been placed on the possibility that the reduced desorbate degradation is largely due to the "plume cooling effect". In fact, this has been the most often

invoked[21,22,30,75,115,116,138,191−193] factor accounting for the "softness" (i.e., low internal energy excitation) of analyte ejection effected in their laser-induced ejection from a matrix. More recently, in view of the MD simulation results (section II.B.2), the rapid evaporation from the clusters (in the plume) has also been suggested as a plausible factor leading to the cooling of the incorporated macromolecules. Yet, in other cases, the importance of the plume cooling has been questioned. For instance, in the UV ablation of tryptophan−glycine and tryptamine (λ = 532 nm with τ_{pulse} = 10 ns at $I = 10^8$ W/cm^2),[140] thermal decomposition of the internal "hot" parent molecule is demonstrated by a high contribution of metastable fragment in the post-ionization spectra. The fragment/parent molecule ratio in ablation is 4 times higher than that for jet-cooled compound.[140] If, instead, postdesorption collisions are promoted by introducing a gas flow, then decomposition is found to be highly reduced. However, the experiment involved absorption by both the adsorbates and the substrate (in this case, the gas-phase collision number may be much lower). Furthermore, the cooling efficiency will depend greatly on the presence, if any, of a matrix, relative concentration, etc.[120−123,133−135,154] Indeed, in the irradiation of analytes within simple inert matrices, the cooling degree is indicated[115,116] to "exceed" that effected via laser ejection of neat compounds into a supersonic jet, as employed in many cases.[117−119] Thus, the importance of plume expansion to reduce internal excitation appears to have much evidence in support, but its determining role remains to be firmly established. Study of bicomponent simple systems such as those used in section II.B.2, in which the analytes have thermally labile/weak bonds, may enable a quantitative assessment to be made of the importance of the various factors for the thermal stability of the desorbates.

In all, the studies on van der Waals films illustrate a number of interesting features about chemical processes and effects in the UV ablation of molecular substrates. These studies provide a basis for understanding the fragmentation/reactivity processes in the UV ablation of more complex molecular substrates. However, evidently many issues remain to be addressed, even in the case of simple compounds. First, it is not clear how reactivity in metastable conditions may be described and how it may differ from that under equilibrium conditions. Though metastable liquids have been studied extensively from a thermodynamic standpoint, very little consideration has been given to their photophysical/chemical properties (e.g., absorption and photolysis cross sections, reactivity, etc.). Furthermore, if vibronic "hot spot" formation occurs,[67,68] the usual concept underlying reaction kinetics in solutions, according to which photofragment "thermalization" occurs very rapidly before any reaction, may not be valid in UV ablation. It would be interesting to examine the applicability of Kasha's rule,[194] which has been shown to underline most photophysics/chemistry in solution studies (de-excitation to the S_1 state is usually ultrafast, and fragmentation yields and reaction patterns are nearly wavelength independent). This is an important point to study, because in polymers, different mechanisms (e.g., photochemical versus thermal) of material ejection are suggested to operate at different wavelengths, depending on the nature of the excited chromophores. Furthermore, thus far, no study of photoproduct formation kinetics has been reported. In the case of polymers, there is evidence that the kinetics of product formation (in the substrate) differs distinctly and in unexpected ways from that at low laser fluences.[178] Such kinetic studies will be definitely much more informative than just the characterization of the ejected products. Unfortunately, addressing these questions via gas-phase diagnostics, even in simple systems, may not be straightforward, since the ejection of some photoproducts within clusters may hinder their quantitative analysis and comparison. Complementary study of the species remaining in the substrate may be much more enlightening.

III. Studies on Liquids

Laser-induced material ejection from liquids has been intensely pursued in its own right. Furthermore, it has provided the basis for understanding laser-induced ablation of more complex systems. In particular, early on it was indicated that the physical mechanisms underlying the "soft" tissue ablation may bear a strong resemblance to that of absorbing liquids. Further strong interest was generated by initial studies showing that laser irradiation of liquid films can have a high technological impact, in particular for the removal of submicrometer particles, laser micromachining, etc.

Laser-induced material ejection from liquids can involve a number of processes, such as evaporation, spallation, photochemical processes, dielectric breakdown, and electrostriction. Herein, we confine description to only some of these processes. In particular, dielectric breakdown and related processes are not discussed, since they have been amply reviewed[197−199] in the literature and they are more of a physical rather than a chemical nature. However, it is noted that laser-induced plasma and breakdown processes may be crucial in various implementations of the phenomenon. Excluding these mechanisms, the liquid-to-vapor transition can be effected by two basic ways, either by boiling (normal boiling or explosive boiling) or by cavitation effected upon application of tensile pressure to the liquid. Finally, the possibility that photochemical processes may induce material ejection has been examined in detail in the case of liquids and this work is discussed in section III. C.

A. Transparent Liquids on Absorbing Surfaces: Liquid Superheating

For a fast enough heating rate such as that attained by an electric current pulse, superheating of liquids well above the saturation point corresponding to their ambient pressure is known to occur.[52,53] In comparison with the conventional techniques, laser irradiation provides the possibility of attaining ultrafast heating rates and studying nucleation phenomena with a high temporal resolution. In this re-

spect, the most well defined case occurs for transparent liquids adjacent to/spread on UV absorbing surfaces (such as polyimide, silicon or metallic film). The system offers the advantage that energy deposition is clearly decoupled from the subsequent phase transformation.

Upon irradiation with a UV pulse, the absorbed energy diffuses from the substrate into the adjacent liquid. Since a short pulse duration implies a small thermal diffusion length, strong overheating of the adjacent liquid layer can be effected even at moderate energy densities far below any damage threshold of the substrate. The transient temperature field established in the liquid adjacent to the absorbing surface is given by eq 7 on the basis of 1-D heat flow[206,207,210] (energy "consumption" for phase change and heat-transfer resistance at the liquid/substrate interface are neglected). The temporal evolution of the interface temperature has been confirmed experimentally by monitoring the reflectance of a semiconductor substrate (e.g., p-Si), which exhibits highly temperature-dependent optical properties.[203,206,207] In particular, the semiconductor layer can be attached on the back surface of the laser-heated metallic substrate.[206,207] In this arrangement, the temperature and the phase change phenomena can be monitored independently (and in parallel) with nanosecond resolution via the optical reflectance, respectively, of the back and of the front side of the system. The development of this technique resolves a main problem in the older conventional studies on superheating of liquids, namely that of accurately knowing the temperature of the vigorously boiling liquid. On the basis of such measurements, it is established that, at sufficiently high laser fluences, peak temperatures above the boiling point of the liquid are attained, in which case bubble formation is expected to occur.

A variety of techniques have been employed to probe bubble nucleation and growth in the superheated liquids adjacent to the absorbing surface. The most direct method has turned out[202−206] to be the temporally resolved monitoring of the reflectance and scattering of an incident probing laser beam (Figure 17). However, the quantification as well as the detection sensitivity of these optical techniques is somewhat limited. To overcome the first limitation, Kim et al.[212] have resorted to interferometric measurements relying on a Michelson-type arrangement to quantify the effective (optical) thickness of the bubble layer. To overcome the second restriction, Yavas et al.[210] have relied on surface plasmon resonance spectroscopy (SPR). The technique is based on the fact that the bubbles represent effective scatterers for the surface plasmons of the metallic substrate, thus resulting in the broadening of their resonance. In the absence of bubble formation or following bubble collapse on the microsecond time scale, only an angular shifting of the resonance curve is observed as a result of the temperature rise in the liquid.

On the basis of these techniques, distinct regimes of the bubble growth have been delineated. In the first stage, separate bubble nuclei (embryos) begin to grow on the surface upon irradiation above a

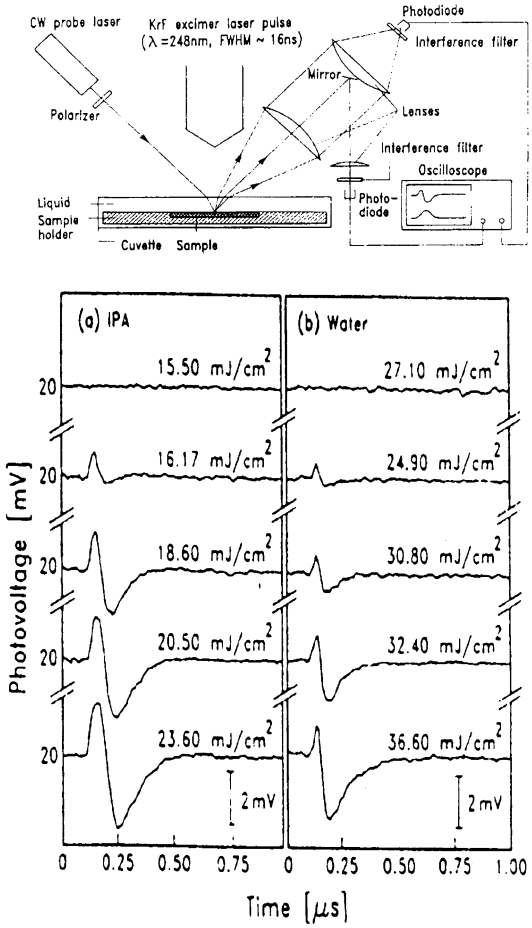

Figure 17. (Top) Experimental setup for the optical reflectance and scattering monitoring of the bubble formation/growth that occurs in the transient laser heating. (Bottom) Transient reflectance in the irradiation of 2-propanol (a) and water films (b) adjacent to a Cr-plated (0.2 μm thick) quartz upon irradiation with an excimer (248 nm) laser pulse. The probe beam has λ = 752 nm, is s-polarized, and is incident at a 7° angle. Reprinted with permission from ref 205. Copyright 1993 The American Physical Society.

liquid-specific threshold fluence. The bubble nuclei formation is evidenced by a characteristic initial increase in the specular reflectance of a probing laser beam incident on the liquid/substrate interface[205] (Figure 17 (bottom)) and by the appearance of a hump in the SPR signal. These changes can be ascribed to the transient change in the dielectric constant, ϵ, of the medium that occurs upon the formation of a foamy layer (corresponding to a thin layer of small bubbles on the metallic surface). Maxwell−Garnett effective medium theory can be employed[205] to calculate ϵ_{eff} of the foam as a function of the fractional volume of the bubbles. A simple ray optics analysis of the three-layer system consisting of liquid, foam, and the metallic substrate satisfactorily accounts for the observed transient increase in the reflectivity.

The exact threshold for embryo formation depends on the sensitivity of the employed probing technique to the bubble size. A particularly sensitive way of monitoring is afforded by SPR, with an indicated detection limit of ~20-nm bubble size. Embryos are found to nucleate for surface temperatures only slightly above the boiling condition ($\Delta T_{\text{surf}} \approx 10$

K).[206,210] The very small overheating necessary for bubble nucleation is due to the heterogeneous nature of the process, with the solid surface providing the nucleation sites. The heterogeneous nature is confirmed by the dependence of the required superheating on the degree of smoothness of the metallic surface. Due to the heterogeneous nature of nucleation, the nucleation rate of bubble formation is modified[52] from that in the homogeneous case (section II. B.2) into

$$J = \frac{N_o^{2/3}(1+\cos\theta)}{2F(\theta)}\left(\frac{3F(\theta)\sigma}{\pi m}\right)^{1/2} \exp\left[-\frac{16\pi F(\theta)\sigma^3}{3k_B T_L(\eta p_{sat} - p_L)^2}\right] \quad (15)$$

where $F(\theta) = {}^1/_4(2 + 3\cos\theta - \cos^3\theta)$. $N_o^{2/3}$ is the number of molecules per unit area at the interface, and θ is the contact angle. As a result of the heterogeneous nature, the degree of penetration effected into the metastable region may be greatly limited.

The embryos are formed during the nanosecond laser pulse, and their initial growth is largely inertia-controlled. The growth of (spherical) bubbles can be estimated from the Rayleigh equation that describes the mechanical energy balance for a growing bubble in an incompressible (i.e., constant density) liquid:[52,53,200,201]

$$R\frac{d^2R}{dt^2} + \frac{3}{2}\left(\frac{dR}{dt}\right)^2 = \frac{1}{\rho_L}\left(P_V - P_L - \frac{2\sigma}{R}\right) \quad (16a)$$

In the early stage, $R(d^2R/dt^2)$ is negligible and bubble growth is inertia controlled, so that the bubble radius as a function of time can be approximated as (contact angle 0°)

$$R = \sqrt{\frac{2(P_V - P_L)}{3\rho_L}}t \qquad \text{with} \qquad P_V - P_L = \frac{\rho_V h_{LV}(T_V - T_{sat}(P_L))}{T_{sat}(P_L)} \quad (16b)$$

where the pressure difference term is approximated using the Clausius−Clapeyron equation. P_V and T_V represent the pressure and temperature inside the bubble, P_L the ambient pressure, $T_{sat}(P_L)$ the saturation temperature corresponding to P_L, ρ the density, and h_{LV} the vaporization heat). The formula yields an upper limit, since it assumes constant superheating of the liquid, a single spherical bubble on a solid surface, and reversible bubble expansion. Thus, the growth rate is estimated[212] to be 10−14 m/s (for H_2O at peak interface temperatures in the range of 425−500 K), whereas experimentally, it is found to be ~3 times lower (0.5−3.6 m/s).[205,206,208,212] At 10 ns following the onset of the excimer laser pulse, the upper limit for the fractional volume of bubbles in the superheated water layer amounts to $f \approx 0.05$−0.1, corresponding to an estimated bubble number density of $\sim 10^{13}$ m^{-2} (~1% mass fraction of vaporization).

Further growth (stage II) of the bubbles can occur only if sufficient heat is supplied from the surface. This growth is reflected by the decrease in the specular reflectance (Figure 17) with the concomitant increase of the scattered light. These optical changes are due to the fact that bubble size (R_{bubble}) grows to a size $\approx \lambda_{probe}/2\pi n$ (where λ_{probe} is the probe beam wavelength and n is the refractive index), and as a result, Mie scattering dominates (in which case the extinction coefficient of the foam layer $C_{ext} = \int N_{bubble}(R_{bubble})2\pi R^2_{effective}\, dR_{bubble}$, with $R^2_{effective} \approx R^2_{bubble}$ for large enough bubbles). Thus, the transition to Mie scattering has been taken to represent the threshold for the bubble growth, distinct from the threshold for bubble nucleation described above. For atmospheric pressure, such growth is observed to occur for peak surface temperatures of ~100 K above the boiling temperature (for H_2O and CH_3OH).[205,208,212] As discussed in section II.B.2, spontaneous growth can occur once the embryonic bubble radius reaches a critical radius, $R_{cr} = 2\sigma/(P_V - P_L)$.[52,53] It is demonstrated that growth is observed when the superheated liquid thickness exceeds the critical radius. Thus, the growth rate in this regime is limited by the speed of heat diffusion from the solid surface into the liquid ($\propto \sqrt{Dt}$). If this condition is met, then both the size and the number density of the bubbles increase for times up to ~150 ns. The bubbles remain confined within the superheated liquid layer, and the bubble size does not exceed the superheated liquid layer thickness.

In the 150−400-ns range (stage III), the effective bubble layer thickness, as monitored via interferometry, increases, but the number density of the bubbles decreases, manifested by recovery of the light-scattering loss.[212] Thus, in this regime, bubbles coalesce, and the bubble layer can be well approximated as a thin vapor film. For high enough fluences, when the film thickness exceeds a certain limit, instabilities set in, resulting in the violent ejection of the overlying liquid layer, which subsequently breaks down into jets. Finally, after 500 ns (stage IV), the size and the number density of the bubbles are reduced, resulting in the decrease of the light scattering in the restoration of the initial width of the surface plasmon resonance. The decay rate of the bubbles is much slower than their growth rate, with their collapse being complete after ~1 μs. This result sharply contrasts the simple ideal bubble dynamics solutions,[201] which predict the collapse time of a bubble to be smaller than the expansion time. Plausibly, the slow decay rate is due to the high density of cavitation bubbles[211] formed at these irradiation conditions. In this case, nonlinear interaction between the bubbles can be expected through the liquid pressure fluctuations that they induce. It is shown that this interaction may result in an increase of the bubble lifetime as compared to that expected from ideal solutions.

The dependence of the phenomenon on external (applied) pressure has been studied.[206,207] For pressures up to ~2.2 MPa, the nucleation of the embryos is found to be nearly insensitive to the pressure, consistent with the fact that this process is domi-

nated by inertial factors. Similarly, the rates for the subsequent bubble growth and collapse (in the Mie scattering regime) are independent of pressure, but the total volume of the bubbles (as measured by the total optical scattering signal) decreases with increasing pressure. This can be ascribed to the fact that, with increasing pressure, the boiling point increases, and thus the corresponding degree of superheating, $T_{surf}(F_{laser}) - T_{boil}$, decreases. At high enough external pressures, bubble formation is inhibited.

Bubble nucleation and formation results in acoustic transients that propagate through the liquid[209,212] with sonic velocity. Below the onset of vaporization threshold, a low-amplitude pressure is generated only via thermal expansion. However, above the threshold, the collective and synchronous expansion of multiple bubbles results in a strong compression pulse. Essentially, the superposition of the pressure wavelets that are produced by the numerous growing bubbles [the pressure generated by a single sphere being $P \propto \rho R^2_{bubble}(d^2R_{bubble}/dt^2)$] results in a pulse that can be approximated as a plane wave. Indeed, the transients have been detected by piezoelectric transducers,[209] by an optical beam deflection technique based on the "mirage effect",[209] and by SPR.[210] Because of differences in their time resolution and integrating nature, these techniques yield somewhat different values, with the more sensitive SPR reporting a ~40-ns width of the acoustic pulse and ~2 MPa peak amplitude. Because the generated pressure is proportional to d^2R_{bubble}/dt^2, the acoustic enhancement in the laser-induced vaporization process is caused by the fast bubble expansion in the growth stage and not by the much slower bubble collapse. This enhanced acoustic excitation is taken advantage of in "steam laser cleaning" and in the liquid-assisted material ablation (section IV).

Most interestingly, even after the bubbles collapse, repeated bubble formation may occur[213] on a longer, microsecond time scale. This secondary bubble formation is due to cavitation at the liquid−solid interface, induced by the reflected acoustic pulses generated by the primary bubble growth. By using a double-laser-pulse experiment and probing different areas of the sample surface, it is shown[213] that an essential requirement for the observation of this "memory effect" is the preceding bubble formation at the liquid−solid interface. With increasing delay time between the two laser pulses, the "memory effect" decays, and eventually no cavitation enhancement is observed. Thus, even upon collapse, the primary bubbles induced by the UV irradiation do not completely disappear but survive for a few hundred microseconds and can serve as embryonic bubbles. The survival rate depends on the nature of the present solutes, with salts (e.g., NaCl) providing a particularly effective stabilization of the embryos. This result is directly related to the issue of the nature and stabilization of microscopic bubbles (nuclei) within liquids, a question that has not yet been satisfactorily resolved.

Liquid superheating can be similarly observed in the case of absorbing particles dispersed within a nonabsorbing solvent for irradiation with short enough pulses ($\tau_p < 10^{-6}$ s).[229] For the case of particle size smaller than their thermal diffusion length, so that they are thermally homogeneous, the fluence for fully developed bubble formation around the particle is

$$F_{laser} = \frac{(T_{boil} - T_0)}{\gamma}\left(\frac{4}{3}R\rho_g C_{p_g} + 4\rho C_p\sqrt{D\tau_{pulse}}\right) + \frac{4}{\gamma}\rho\Lambda\sqrt{D\tau_{pulse}} \quad (17)$$

where T_0 is the initial temperature, R, ρ_g, γ, and C_{p_g} represent the size, density, integral absorption coefficient (such that particle absorption equals $4\pi R^2\gamma$), and heat capacity of the particle, Λ is the specific heat of evaporation, and D is the thermal diffusivity of the solvent. The term within the parentheses gives the fluence necessary for the heated layer to reach the boiling point, and the third term is related to the extra heat required for its vaporization. A further detailed description may be found in ref 230.

The bubble formation around individual microparticles (melanosomes) heated by a 30-ps laser pulse has been visualized by time-resolved optical microscopy. Bubbles are observed as early as 0.5 ns afterward, expanding to a few micrometers on 0.1−1-μs[215] time scale. Collapse of the bubbles formed close to the free surface of the colloidal solution generates hydrodynamic flow, which can result in significant material ejection in addition to any evaporative losses.[229] The bubble formation in the superheating of colloids has also been exploited to set up a novel optical switch.[216] The scheme relies on the fact that the bubbles coalesce into a large one with a large refractive index change from the surrounding medium.

The bubble formation results in a sharp acoustic transient,[215] as detected by piezoelectric measurements and optically, whereas below the bubble formation threshold, the detected pressure is much weaker and due to the thermoelastic expansion of the particles. Furthermore, the use of time-resolved degenerate four-wave mixing has shown a large transient change of the refractive index of colloidal suspensions of carbon irradiated with nanosecond pulses.[221,222] The amplitude oscillates on a time scale that is much shorter than the laser pulse width. This behavior has been associated with the acoustic wave generated in the fluid "coherently" by the explosive boiling around the heated particles. Furthermore, this pressure generation may be responsible for the "giant" photoacoustic effect observed in the irradiation of carbon colloids,[217] though other explanations, such as stable gas formation[217] and/or formation of microplasmas, had been advanced earlier. The bubble formation around the heated particles has been treated theoretically. In particular, a recent analytical study stresses the importance of the pressure, besides the thermal factor, for bubble formation/growth.[223] A dependence of the bubble dynamics (growth rate and size) on the laser pulse width is predicted, even for times much shorter than the thermal relaxation time. MD simulations of the damage effected to the absorbing particle itself at higher fluences have also been reported.[224]

Absorbing particle suspensions have also been employed to effect laser ejection and ionization of macromolecules for mass spectroscopic examination. In fact, it was the method employed by Tanaka et al.[3] in one of the first publications demonstrating the potential of laser irradiation to effect "soft ejection" of macromolecules in the gas phase. To this end, the biopolymers are dissolved in glycerol suspensions of cobalt nanoparticles (30 nm in diameter) acting as chromophores. The term SALDI, for surface-assisted laser desorption/ionization, has been introduced[218] to differentiate this technique from MALDI. The advantages of this approach for analytical purposes include (a) the lack of matrix-related interfering peaks in the mass spectra and (b) the nearly constant value of the particle suspension absorption over a large wavelength range accessible by a variety of lasers, thereby overcoming the limitation of restricted wavelength range absorption of matrices. The influence of the particle size and nature on the ejection efficiency of macromolecular analyte ions has been studied[218−220] and has been largely explained by the different degree of overheating attained for different particle sizes. Ejection of ions as high as ~30 kDa has been demonstrated, but there seems to be a limitation for higher masses. It is likely that this limitation is related mainly to the ionization step rather than the ejection process. The present evidence suggests that the ionization process is mediated by the liquid and not by the particles.

In all, the studies on superheating of liquids adjacent to laser-absorbing substrates has provided detailed information on the kinetics of nucleation phase change phenomena that would not have been amenable through the conventional heating methods. The use of even shorter laser pulses will provide the possibility of addressing in more detail the initial embryo formation and thus the validity of several tenets of the classical thermodynamic theory of metastability. Furthermore, the method provides a convenient experimental approach to study in detail properties of the superheated liquids, particularly their photophysical and chemical properties (thus providing a basis for understanding processes in other systems, e.g., van der Waals solids, section II.B.2), and in addition a convenient means of producing "controllably" a high-density ensemble of structures (i.e., bubbles) on the submicrometer/nanometer level, with plausible applications in nanotechnology.

B. Absorbing Solutions and Liquids

1. Photoinert Systems: Photomechanical Mechanism of Material Ejection

Material ejection of absorbing liquids and solutions has also been studied by techniques similar to those described in section III.A [Here the presentation is limited only to the studies of irradiation of the free surface of the solutions. A large number of studies, e.g.,[226,235,236] employing immersed optical fibers or irradiation of tissues within solutions, are more of a medical interest and are discussed by Vogel and Venugopalan in this issue]. For instance, time-resolved transmission of a probing beam propagating parallel to the free (irradiated) surface of the liquid and laser-flash photography (probing can be conveniently performed in the visible range, where the solutions are transparent) have been employed to probe processes within the irradiated liquids. Usually, aqueous solutions with dissolved (photostable) chromophores such as Orange G at 532 nm ($\tau_{pulse} \approx$ 25 ns, $\alpha = 50-150$ cm^{-1}),[231,232] K_2CrO_4 at 355 and 248 nm ($\tau_{pulse} \approx$ 25 ns, $\alpha = 1 \times 10^2-1.7 \times 10^3$ cm^{-1}),[227,228,233,234] NaCl solutions at 193 nm,[214] etc. have been studied (Figure 18). A noticeable drop in the transmission through the solution of the probing beam is observed above a specific fluence of the UV

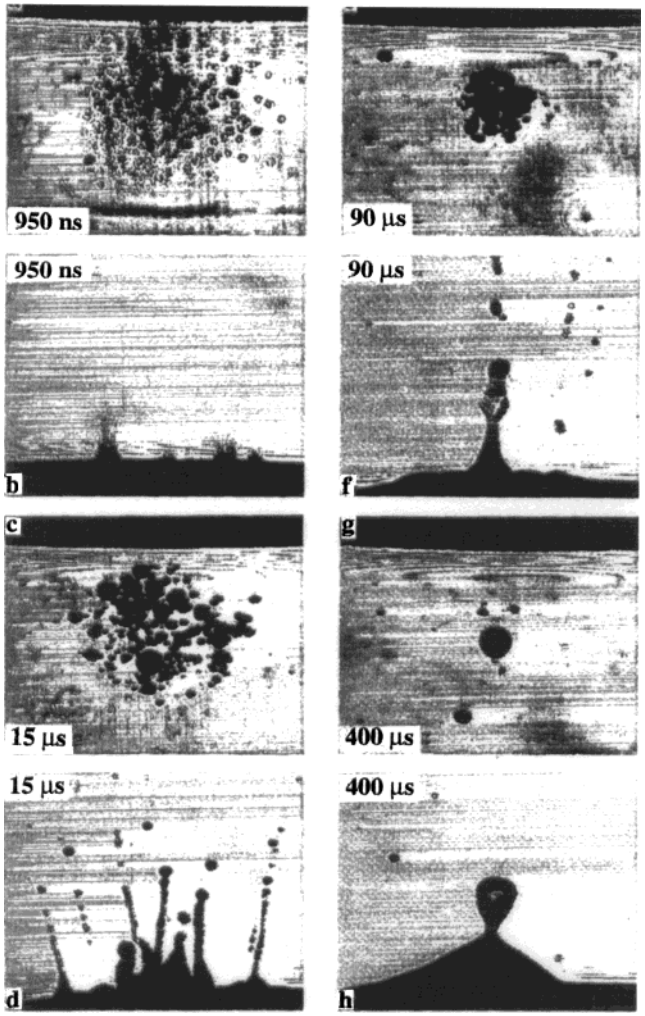

Figure 18. Sequence of images within the liquid (1st and 3rd row) and above its free surface (2nd and 4th row) obtained by laser flash photography in the 248-nm ablation of aqueous K_2CrO_4 solution ($\alpha = 55$ cm^{-1}). For the photographs in the left column, $F_{laser} = 1.2$ J/cm^2, and for those in the right column, $F_{laser} = 1.85$ J/cm^2 (estimated average temperature increase in the irradiated volume of 15 and 26 K, respectively). Photograph a shows the initiation and growth of cavitation bubbles in the surface millimeter layer. The black and white stripe at the bottom of the photograph is due to the refractive index change induced by the propagating bipolar pressure wave. Photograph c at 15 μs shows the fusion of bubbles into larger ones (~100−150 μm in diameter), while other bubbles have collapsed (seen as empty spaces between the bubbles close to the surface). Reprinted with permission from ref 227. Copyright 1995 American Institute of Physics.

beam.[227,228,232−234] Flash photography at various time delays relative to the ablating laser pulse demonstrates the drop to be due to the scattering of the probing light by bubbles growing within the bulk of the liquid. Importantly, by either technique, bubble formation at depths well below the optical penetration depth is demonstrated (e.g., in the 355-nm irradiation of aqueous K_2CrO_4, $\alpha = 55\ cm^{-1}$, maximal bubble concentration is observed at twice the optical penetration depth, decreasing to zero only at twice this length).[227,228] The bubbles grow rapidly over the first microsecond, with the ones close to the surface rupturing and resulting in material ejection, while further material ejection occurs in a second stage following the expansion, coalescence, and collapse of bubbles (Figure 18).

The threshold for material ejection is more accurately determined from a change in the acoustic transients generated during laser irradiation (Figure 19). The measurement relies on the fact that, without

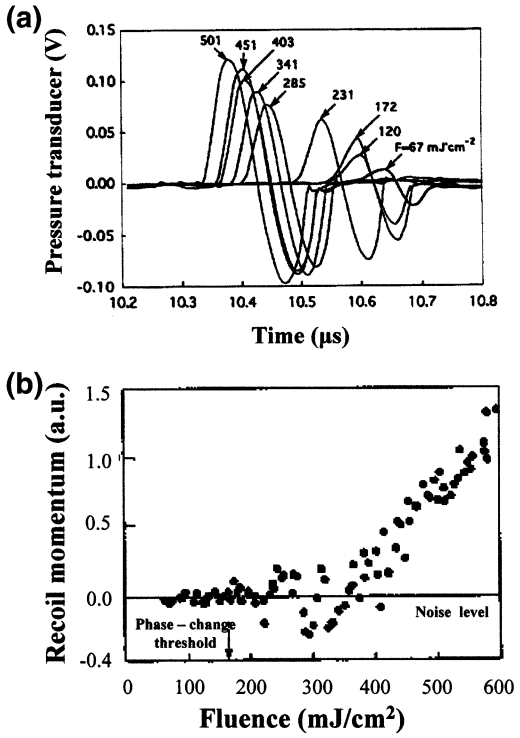

Figure 19. (a) Temporal shape of the acoustic pulses measured by a broadband piezoelectric transducer in the 248-nm irradiation of K_2CrO_4 solutions ($\alpha = 5.5 \times 10^2\ cm^{-1}$) for the indicated excimer laser fluences. Reprinted with permission from ref 233. Copyright 1998 Elsevier Science B.V. (b) F_{laser} dependence of the integrated signal of the acoustic pulses. Above a specific fluence (ablation threshold), the integrated signal deviates from zero as a result of the recoil momentum of the ejected plume. Reprinted with permission from ref 234. Copyright 1998 Springer-Verlag.

mass ejection, the generated pressure pulse in the medium is bipolar (vide infra) and the time-integrated pressure is zero, whereas with material ejection, the positive component of the pressure pulse exceeds the negative one due to the recoil momentum. On the basis of such measurements, the threshold for material ejection is indicated[233,234] to be somewhat higher than the threshold for cavity formation. At any rate, the temperature at the ablation threshold is estimated (assuming a one-photon process) to be well below the solvent boiling point. The absorbed energy is about 1 order of magnitude lower than the specific enthalpy of vaporization. Thermal explosion around superheated micro-inhomogeneities cannot be invoked to account for material ejection in these systems. In the case of the homogeneous aqueous solutions, the average distance between chromophores (at least for reasonable concentrations) is in the range of a few nanometers, and thermal diffusion smooths out any thermal heterogeneities within the typical nanosecond laser pulse width. Furthermore, the employed solutes (NaCl, K_2CrO_4, etc.) have been demonstrated to be photochemically stable, even after extensive irradiation. Thus, photochemical processes such as those considered in section III.B.2 cannot be responsible in the present case. Given the very small thermal diffusion length into water ($\sim 0.1\ \mu m$ for $t \approx 1\ \mu s$), temperature changes below the optical penetration depth can be neglected (at least for moderate laser fluences), and thus, they cannot be responsible for bubble formation at these depths. Bubble formation and the effected material ejection have to be ascribed to a photomechanical mechanism, i.e., to the effect of stress-wave generation and propagation in the bulk of the liquid at ambient temperature.

The photomechanical mechanism and its consequences are described in detail in the article in this issue by Paltauf and Dyer; thus, only a brief description is provided here. This mechanism relies on the fact that the rapid laser-induced thermal expansion causes a pressure rise, given by the product of the Grüneisen coefficient Γ and the absorbed energy density:[225]

$$\Delta P = \Gamma \alpha F_{laser}\left(\frac{1 - e^{-\theta}}{\theta}\right) = \frac{\beta}{\rho \kappa_T c_V} \alpha F_{laser}\left(\frac{1 - e^{-\theta}}{\theta}\right) \quad (18)$$

where β is the thermal expansion coefficient, c_s the speed of sound, C_V the heat capacity at constant volume, and κ_T the isothermal compressibility, and $\theta = \tau_{pulse}/t_{acoustic}$, where $t_{acoustic}$ is the time required for an acoustic wave to traverse the irradiated volume. The factor in the parentheses corrects for the reduction in the stress amplitude due to the wave propagating out of the irradiated volume during the laser pulse (assumed to have a rectangular time profile). The stress entails a radially propagating cylindrical wave, which can be neglected for laser beam diameters substantially wider than the light penetration depth, and two plane waves counter-propagating along the laser beam axis (one toward the surface and the other into the sample). The plane wave that travels toward the free surface (liquid/air surface) suffers a change of its amplitude sign upon reflection from it, due to the acoustic impedance ρc_s (ρ is the density and c_s the speed of sound) of the irradiated medium being higher than that of air. Physically, the thermal expansion directed into the medium generates a compression wave, whereas the outward expansion generates negative stress (rarefaction wave).

The faster the heating, the higher the magnitude of the stress in the medium, with the ultimate

efficiency of stress generation attained for heating times much faster than the time required for stress to propagate through the irradiated volume. This is usually expressed as $\alpha c_s \tau_{pulse} \ll 1$ (α is the absorption coefficient, c_s the speed of sound, and τ_{pulse} the laser pulse duration), where the dimensionless parameter represents the degree of temporal confinement of the laser-induced stress in the irradiated volume. For typical excimer nanosecond pulses, this condition is satisfied for aqueous solutions for $\alpha \leq 10^3$ cm^{-1}.

The generated bipolar pressure wave propagates into the depth of the medium without significant attenuation. If the pressure of the tensile component is lower than the saturation pressure of the liquid at a given temperature, the liquid is in a thermally metastable state under tension, and the vapor-cavity nucleation is initiated. For amplitudes of the tensile stress exceeding the critical value balancing the surface tension, cavity growth occurs, and the continuity of the liquid is broken. Ablation can therefore be interpreted in terms of a mechanical "rupture" of the liquid surface effected by large tensile stress. The threshold value of the tensile pressure for ablation from aqueous solutions is found[227,231−234] to be approximately 1.8−3.6 MPa (the exact value strongly depending on the existing nucleation sites—trapped gas bubbles—in the liquid). Rupture of the bubbles grown close to the liquid surface produces a plume of vapor and microdroplets. The collapse of the initial crater and of the large bubbles formed by coalescence of smaller ones in the depth of the irradiated volume results in a complex hydrodynamic flow entailing further ejection of material in the form of liquid streams (jets) (Figure 18).

Ablation creates sufficiently high recoil stress amplitudes that convert into so-called "weak shock waves" upon propagation into the (acoustic nonlinear) medium. Low-amplitude (not exceeding several bars) acoustic waves propagate at the speed of sound (1.5 km/s), but higher amplitudes propagate at supersonic velocities that make the front of the pressure wave steeper. This evolution is well monitored by flash photography.[227,228] In a medium with acoustic nonlinearity, these shock waves develop after propagation over a characteristic distance, L_{sh}:

$$L_{sh} \approx \rho {c_s}^3 \tau_{ac} / 2\pi\epsilon P \tag{19}$$

where ρ is the medium density, c_s is the speed of sound, τ_{ac} is the duration of a transient stress wave, and P is the pressure amplitude. The formation of these weak shocks is important for the optimization of the various implementations of UV ablation, as they propagate through the substrate and may cause mechanical deformations[178] at regions relatively far away from the irradiation spot (e.g., injuries in tissues, delaminations in painted artworks, etc.).

For irradiation at very high fluences, superheating will occur in parallel, and material ejection arises from the combination of explosive boiling and mechanical rupture. In this case, material ejection is indicated to occur in three distinct stages.[233,234] During the nanosecond laser pulse irradiation, no significant surface deformation or plume ejection is observed, despite the high surface temperature rise to the superheat limit. This delay can be related to the time necessary for bubble growth. However, afterward a dense vapor-cavity zone is formed in the subsurface region due to the explosive nucleation, accompanied by violent plume ejection. Thus, explosive vaporization is the dominant material ejection mechanism in the early stage. The vapor-plume ejection is maintained for a few microseconds. The surface depression that is caused by the recoil momentum of the ejected material activates subsequently hydrodynamic motion, which results in upward flow and bulk liquid ejection. Thus, the final stage is dominated by large-scale surface deformations under the influence of gravity and liquid inertia acquired by the impact of the ejected mass. This long-term hydrodynamic motion is not observed in the case of the spallation-induced material ejection at lower fluences. In that case, no significant surface deformation is observed after $\sim$20 μs.

2. Photolabile Liquids: Photochemical Mechanism of Material Ejection

In the previous studies, the absorbing analytes as well as the solvents are photochemically inert. In the irradiation of photolabile organic compounds, a "photochemical mechanism" may also contribute to material ejection. This mechanism was advanced[11] already in the very first studies on the UV ablation of polymers in order to account for the "clean" etching effected in this case. This result was suggested to be related to the fact that UV light absorption results in bond dissociations and the fragments or the small gaseous photoproducts they form were considered to expand (requiring a larger volume than the initial macromolecular structure), thereby causing a pressure rise and ejection of the material. Accordingly, ablation was suggested to occur above a certain fluence, at which the bond dissociation rate exceeds the electronic energy relaxation time or the recombination rate of the produced radicals so as to achieve a critical number of species (fragments and/or products) (the need to consider rates is introduced in order to account for the observation that for long enough laser pulses, volume ejection is not observed):

$$\rho(t,x) = \int_0^t \left[\frac{q\sigma_{abs} N I_{laser}(t',x)}{h\nu} - R(t',x) \right] dt' \geq \rho_{cr} \tag{20}$$

where q is the quantum yield, σ_{abs} the absorption cross section, N the number density of the chromophores, R the rate of any "loss" mechanism, and ρ_{cr} the critical number of radicals/photoproducts that must be formed to induce material ejection. Since most of the incident energy is used in bond dissociations, this hypothesis seems to directly account for the observed "clean" etching (i.e., little thermal dissipation and degradation, e.g., melting to the surrounding area). It is clear that the validity of such a mechanism would be of profound importance for the optimization of the implementations of UV ablation. However, despite the large number of studies, it has proven difficult to obtain conclusive evidence for this mechanism.

In the case of complex systems, it is very difficult to delineate between the various contributing mechanisms (i.e., between photochemically induced reactions and thermal decomposition of the weaker bonds). To address the contribution of photochemical mechanism in simpler systems, Srinivasan and Ghosh examined photoproduct formation in the 248-nm ablation of liquid C_6H_6.[241] A number of different species (naphthalene, biphenyl, carbon) were detected in the post-irradiation analysis of the samples. On the basis of this result, a "pure" photochemical mechanism was suggested for the ablation of this system. However, since reactivity may occur/continue well after material ejection, product formation does not constitute sufficient evidence to establish the photochemical nature of ejection. Furthermore, similar products may be formed by different mechanisms. For instance, in the 193-nm irradiation of liquid benzene at fluences higher than ~10 mJ/cm^2, products similar to those reported by Srinivasan and Ghosh were observed.[242] However, in this case, they are indicated to derive from the thermal decomposition of the compound due to the much higher temperatures attained (the absorption coefficient of the compound at this wavelength being orders of magnitude higher than that at 248 nm). In fact, most of these products are observed[253,254] even in the laser-induced breakdown of the aromatic liquids, though their formation in this case is mediated via free electrons, and no electronically excited states are detected.

Fukumura, Masuhara, and co-workers have reported several comparative studies on the KrF excimer laser (248 nm)-induced material ejection from organic photolabile liquids, namely neat samples of C_6H_6 and its derivatives (C_6H_5X and $C_6H_5CH_2X$, where X = CH_3, Cl), as well as solutions of these compounds in nonabsorbing solvents (alkanes and chloroalkanes). The threshold for material ejection has been established[243−246] by photoacoustic spectroscopy. The first sharp change in the generated photoacoustic signal as a function of laser fluence (Figure 20) is verified by shadowgraphic detection[243−246] of the ejected plume to correspond to the onset of ablation (the second breakpoint in the figure may be related to the enhanced scattering of the incident light by the plume). Most importantly, the determined ablation thresholds of the neat benzene derivatives and of their highly concentrated solutions (0.6−1 M, $\alpha \approx 250$ cm^{-1}) do not correlate with the boiling points of the liquids (Table 6). Accordingly,

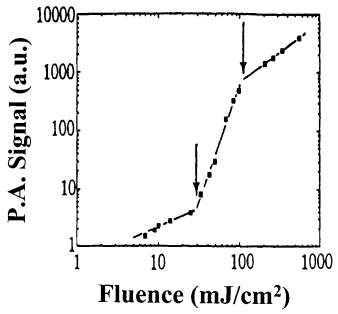

Figure 20. Photoacoustic signal amplitude as a function of the laser fluence in the irradiation of benzyl chloride at λ = 248 nm. Reprinted with permission from ref 243. Copyright 1994 American Chemical Society.

Table 6. Laser Ablation Thresholds (λ = 248 nm, $\tau_{pulse} \approx$ 30 ns) of Aromatic Compounds (at Ambient Conditions)[a] (Reprinted with permission from ref 252. Copyright 1996 American Chemical Society.)

liquid	F_{thr} (mJ/cm^2)	α (cm^{-1})	T_{thr} (K)	bp (K)
benzene	100	2100	410	353
chlorobenzene	60	1900	370	405
toluene	35	2400	350	383
benzyl alcohol	60	~1900[b]	~350	478
benzyl chloride	30	~2200[b]	~340	452

[a] F_{thr}, threshold laser fluence; α, absorption coefficient; T_{thr}, estimated surface temperature at threshold ($T_{thr} = F_{thr}/\rho C_P$, where ρ is density and C_P specific heat); bp, boiling point.

the authors relate the 248-nm-induced material ejection from these systems to the photochemical activity (β-bond cleavage efficiency) of the compounds: $C_6H_5CH_3$ with a high quantum photodissociation efficiency having the lowest threshold, and the photochemically inactive C_6H_6 having the highest.

$$C_6H_5CH_2X \xrightarrow{h\nu} C_6H_5CH_2 + X \qquad (21)$$

The suggested radical formation has been confirmed by time-resolved luminescence and absorption spectroscopies.[246] An absorption band around 320 nm, which can be ascribed to benzyl radical, is observed for all examined systems. Chain reactions of these radicals are likely responsible for the photoproducts observed by Srinivasan and Ghosh.[241] Time-resolved absorbance of the incident UV light is found to be nearly constant during the laser pulse. It is thus suggested that one-photon absorption occurs mainly by chromophores, which subsequently undergo efficient fragmentation. The radical concentration is estimated to be ~0.05 M at the threshold for all neat liquids and ~0.006 M for the highly concentrated solutions. In fact, it is somewhat smaller for alkylbenzene derivatives and somewhat higher for the benzyl compounds (the difference ascribed to the different viscosity of the solvents). This indicates that a critical number of species/fragments must be produced for material ejection to occur. The authors suggest that the small radicals (H, Cl, CH_3) produced by reaction 21 form gaseous products that induce a volume increase (estimated to be ~20%), leading to material ejection. The time necessary for the formation of these products may be responsible for the delayed material ejection in the UV laser irradiation of these liquids. Indeed, at the threshold, material ejection (plume development) was detectable by laser shadowgraphy nearly 100−500 ns after the laser pulse (for ambient pressure), and only at very high fluences is ejection observed to be initiated during the laser pulse.

In contrast, observations differ significantly for low-concentration solutions (0.06−0.1 M, $\alpha \approx 25$ cm^{-1}) of the aromatic compounds. In this case, the ablation thresholds are about twice the ones for the high-concentration solutions.[248] This difference could be presumed to be simply due to the lower absorption coefficient of these solutions. However, this cannot

be the only factor, since the ablation threshold of the dilute solutions is found to scale with the boiling point of the solvent, whereas no such correlation is found at high solute concentrations. Furthermore, the delay in the jet-ejection onset with respect to the ablating laser pulse, as established by laser shadowgraphy, is shown[245] to be related to the absorbed energy density, ranging from ~2 μs close to the threshold down to a few tens of nanoseconds at much higher fluences. Similar dependences of the jet-ejection onset times on absorbed energy are observed for each solvent independently of the employed absorbing solute. Thus, ejection dynamics appears to be regulated by the solvent and not by the solutes. In parallel, the luminescence spectra of the solutes are found[245−247] to become unstructured and broader with increasing delay time between pump and probing beams and with increasing pump fluence. These spectral changes are consistent with those expected for highly vibrationally excited/heated molecules. The spectral broadening precedes the onset of material ejection, thereby providing strong evidence that the liquid is heated prior to the jet development. Material ejection is indicated to initiate at the ambient boiling temperatures of the solvents (i.e., regular boiling), taking on the character of the explosive boiling at higher fluences (the exact estimation of the attained temperatures depends on the extent of multiphoton processes that take place in the irradiation of these systems, as described in section III.C).

On the basis of the previous results, the authors[245] suggest the mechanism of material ejection from the solutions of the benzene derivatives to switch from a photochemical to a thermal one with decreasing concentration of the photolabile solute. Evidently, it is assumed that the amount of radicals and of volatile products that is formed with decreasing photolabile solute concentration becomes insufficient to result in material ejection, and as a result, a thermal mechanism takes over. Though this is a very attractive delineation of mechanisms, it must be noted that the photomechanical mechanism described in section III.B has not been considered in detail. Given the strong evidence for the importance of the laser-induced stress to effect "cold" ablation of solutions, the argument that estimated temperatures at threshold are lower than the boiling point (Table 6) is inconclusive for a photochemical mechanism. It is plausible that a combined contribution of the two mechanisms is involved. Examination of the laser-induced stresses and cavity formation in the irradiation of these systems would be useful in addressing this point further.

Insight into the role of photochemical processes in laser-induced material ejection has recently been provided by MD simulations[157] (in fact, performed for van der Waals films). These simulations have shown that the energy liberated by exothermic reactions can contribute to reaching the critical energy for material ejection (E_{cr} in eq 6). Additionally, the formation of photoproducts with weaker intermolecular interactions lowers the cohesive energy of the system, thereby facilitating further material ejection. In the framework of nucleation theory, it may be considered that "volatile" photoproducts serve as nuclei to promote heterogeneous bubble formation and growth (i.e., enhanced J in eq 15). In view of these results, it is important to examine in the photolabile organic liquids whether material ejection is due to photoproduct-induced volume expansion (i.e., as usually presumed by simple photochemical models) or to the energy released by exothermic reactions resulting in explosive boiling (e.g., as suggested by the MD simulations[157]).

It is interesting that, in the two cases that the same compound has been studied in both liquid and solid phases, discrepancies are noted in relation with the observed products. The naphthalene and biphenyl species observed[241] by Srinivasan and Ghosh in the 248-nm ablation of liquid C_6H_6 have not been detected[26] in the corresponding study on condensed C_6H_6 films. On the basis of this result, Buck and Hess questioned the validity of the suggestion of Shrinivasan and Ghosh[241] for the photochemical nature of UV ablation of C_6H_6 (section III.C.). In the ablation of condensed $C_6H_5CH_3$ films, no products have been detected[47] (at least for moderate fluences above the threshold), thus indicating a very low photolysis efficiency of condensed $C_6H_5CH_3$.[47] This sharply contrasts with the efficient radical formation detected in the irradiation of the liquid.[245,252] Several plausible reasons for these discrepancies can be advanced, but there is no direct experimental evidence. A systematic comparison of photoproduct formation according to the phase of the substrate is evidently required in order to get further insight into the chemical processes in UV ablation. This comparative study is also needed to assess the extent to which results on photochemical processes in liquids are extrapolable to the ablation of polymers and tissues. [In the case of polymers, an initial study has reported a number of interesting differences in the material ejection dynamics according to the state of the substrate.[255]]

Studies on the femtosecond-induced material ejection from the above photolabile liquids have also been reported. Hatanaka et al. have relied[249,252] on time-resolved absorption spectroscopy to study processes in the irradiation of aromatic liquids with femtosecond pulses (248 nm, ~300 fs). In the irradiation of $C_6H_5CH_2Cl$ liquid at low laser fluences (<15 mJ/cm^2), an absorption band ascribable to the benzyl radical is already intense 10 ps after the pump pulse, suggesting a very fast predissociation of benzyl chloride upon a one-photon excitation. Upon irradiation at higher pump laser intensities, a significant drop in the transmittance is additionally observed at times >1 ns. High-resolution surface-scattering imaging[250] reveals the liquid surface to remain nearly flat in the first nanosecond, while enhanced surface roughness is indicated after this time. Assuming similar detection limits, the ablation threshold is indicated to be nearly equal for the nanosecond and femtosecond laser pulses. This sharply contrasts with the predictions of photomechanical models and of molecular dynamics simulations[30] for a decrease of the threshold upon irradiation with femtosecond pulses. The authors suggest that the invariability of the threshold in the $C_6H_5CH_2Cl$ system indicates the

operation of a photochemical mechanism similar to that suggested in the nanosecond case.[242]

On the other hand, in the corresponding femtosecond irradiation of liquid toluene, the ablation threshold is reported[251] to be lower than that of $C_6H_5CH_2Cl$, whereas the opposite trend is found in the corresponding nanosecond examination of the two compounds.[242] Furthermore, the benzyl radical in the femtosecond irradiation of $C_6H_5CH_3$ liquid could not be detected, even at the highest examined fluences, whereas the radical is efficiently produced in the corresponding nanosecond process. To account for this difference, the benzyl radical in the case of toluene is suggested to be formed via a secondary photon absorption by the triplet state. This process is likely in the irradiation with nanosecond pulses but, of course, not in the case of femtosecond pulses. Concerning ablation of toluene, it is suggested that ablation with femtosecond pulses must be photothermal in nature. However, clearly, there are many aspects that must be examined before even a basis for understanding femtosecond-induced material ejection can be formulated.

C. Optical Processes in the Irradiation at High Irradiances

Evidently, optical processes constitute the first step preceding any of the material ejection processes described in the previous sections. The reason for placing this section last is the limited information on the issue. Changes in the optical properties of liquids upon superheating can be expected, since their density decreases[52,53] with increasing degree of superheating. The consequent change in intermolecular interactions can affect strongly the electronic states. However, as the following studies indicate, there are additional, dynamic processes that become significant in the irradiation at high fluences.

Upon superheating at high energy densities ($\geq$600 J/cm^3 for α in the range of 825−11 500 cm^{-1}), the surface reflectivity of aqueous K_2CrO_4 solutions is observed to decrease sharply in the later part of the incident nanosecond laser pulse (pulse "truncation") ($\lambda = 248$ nm).[238] Pump−probe experiments employing two different wavelengths indicate that this decrease is not due to scattering of the incident light by the ejected plume. Thus, the pulse truncation must be ascribed to a sharp decrease of the refractive index of the liquid in the later part of the incident laser pulse. Nikiforov et al.[238] suggest that the decrease reflects the highly reduced density of the overheated H_2O solvent. On the other hand, the 193-nm absorption coefficient of superheated H_2O is indicated[237] to be nearly 5 orders of magnitude larger than the room-temperature absorption value. In these experiments, a Q-switched Er:YAG laser is employed to heat H_2O, while the absorption at 193 nm is probed 300 ns afterward. The increase has been ascribed to the blue-shifting of the UV absorption spectrum[239] of the overheated liquid due to the disruption of the hydrogen bond network of H_2O. In contrast, Longtin and Tien[240] ascribe the optical changes that are induced in the irradiation of H_2O at 266 nm ($I = 1.0 \times 10^{10}$−2.0×10^{10} W/cm^2) to the ejected electrons and the OH radicals formed by the photoionization and the photodissociation of H_2O. The hydrated electron absorbs strongly throughout the near-IR, visible, and UV regions (a 7−10 orders of magnitude increase of the absorption coefficient). Longtin and Tien suggested that these optical changes can be taken advantage of in applications by coupling irradiation at 266 nm with wavelengths in the visible (e.g., 532 nm).

Fukumura, Masuhara, and co-workers have reported particularly detailed studies on the issue of electronic excitation processes in the irradiation at high UV laser irradiances. Time-resolved absorption and luminescence spectroscopies have been used to probe the dynamics of electronic excitation and de-excitation in the ablation process. In the irradiation of organic chromophores in nonabsorbing solvents (Table 5), they note[245,247,248] that, for some of the employed chromophores (biphenyl or phenanthrene), the internal conversion from the excited S_1 state has a very low quantum yield to account for the indicated efficient heat generation. Furthermore, the total fluorescence intensity as a function of laser fluence saturates close to the threshold, indicating that a new channel of the S_1 state deactivation opens up. In parallel, in the irradiation of the low-concentration solutions, the time-resolved absorbance is found to increase during the excitation pulse.[245] A plausible explanation was advanced on the basis of "a cyclic mutiphotonic absorption process". According to this, the absorbing solutes and/or the benzyl radicals produced by the photolysis of the photolabile solutes absorb further photons to higher electronic states. Alternatively, higher electronic states may be formed via annihilation of S_1 excited molecules. Deactivation of these A*(S_n) states occurs extremely fast ($\sim$picosecond) and provides a way to rapidly convert the absorbed energy into heat. Following deactivation, the recovered A*(S_1) can participate in subsequent excitation/de-excitation cycles.

$$\begin{aligned} A + h\nu &\rightarrow A^*(S_1) \\ A^*(S_1) + h\nu &\rightarrow A^*(S_n) \rightarrow A^*(S_1) + \text{heat} \\ A^*(S_1) + A^*(S_1) &\rightarrow A^*(S_n) \rightarrow A^*(S_1) + \text{heat} \end{aligned} \quad (22)$$

Their results appear to be analogous to those reported in the irradiation of van der Waals films,[68−71] and also closely related to the previous changes in optical properties noted upon superheating of aqueous solutions.[237−239] Indeed, the group has demonstrated that similar annihilation processes may be most important also in the ablation of doped polymers.

Despite their limited number, these studies are most important because they clearly illustrate that photophysical properties of highly heated liquids may differ significantly from those under equilibrium conditions, and they demonstrate the importance of taking into account these changes for the quantitative understanding of the processes in the laser-induced material ejection processes. To this end, further studies must establish the exact conditions under which these processes become important.

IV. Applications

In this section, applications of the ablation of molecular solids and liquids are presented. To avoid extensive overlap with other articles in this issue and other reviews, the discussion highlights a few specific directions, rather than trying to provide an exhaustive list of the many different applications (described in detail in refs 1, 5−7).

A. Cryogenic Films-Based Techniques

Cryogenic films are finding increasing use in both analytical and material-processing applications. In the first case, laser-induced material ejection from frozen aqueous solutions has been always of interest because of the widespread occurrence of H_2O in the environment, in tissues, etc. However, the transparency of H_2O in the visible and UV regions has limited work on the ablation of frozen aqueous solutions. On the other hand, the high absorptivity of H_2O in the IR and the recent availability of convenient and reliable lasers in this spectral range have resulted in renewed interest in these systems. Besides studies on the potential of MALDI,[43,106,107,256−258] the IR-induced material ejection has been exploited for the characterization and monitoring of processes in ices in relationship with atmospheric studies.[36,259,260]

The ablation of frozen solvent/biopolymer systems has also been demonstrated as a convenient technique for the ejection and subsequent deposition of novel microstructure formation, as discussed by Chrisey et al. in this issue. Leone[19,22,112,113,261] first advanced the potential of using laser-ablated beams to study collisional and reaction dynamics of hyperthermal species. Harrison and Polanyi[262] presented a theoretical analysis of the feasibility of using crossed ablated beams to this end. The use of laser-ablated beams for such studies can meet a significant need, since except for seeded beams and photolytic sources, there are no other convenient ways to produce high-flux jets of hyperthermal neutral molecules/atoms. An extra advantage of the use of ablated beams accrues from the capability to vary the desorbate translational energy conveniently via the laser irradiation parameters (laser fluence, forward or backward irradiation, etc.). Experimentally, this potential has been exploited to study the dependence of the etching process of Si on this parameter. Hyperthermal Cl_2 (E_{kin} up to ∼6 eV) is shown[112] to etch Si >30 times more efficiently than thermal Cl_2. For practical applications, etching may be further enhanced by using higher fluences to increase the Cl fragment concentration and/or by applying an external electric field to enhance ionic formation in the ejected plume.[162] Enhanced oxidation of Si is also demonstrated by ablated hyperthermal O_3 beams.[279,280]

The advantages of high-flux beams of radical/reactive species produced in the UV ablation of photolabile cryogenic films can be particularly useful for the processing of substrates. The use of laser-ejected reactive plumes for this purpose presents versatility and can complement plasma techniques. The beams of high-purity reactive fragments that are produced in the UV ablation of FPA/Ar condensed films (Table 5) have been used for the chemical surface modification of aromatic polyester, alkylthiol, poly(ethylene terephthalate), etc.[281] The treatment results in the fluorination of the polymer surface, which thus becomes hydrophobic and chemically inert.[281] Silylation of polymer surfaces has been effected with the plume produced in the ablation of frozen silanes.[265] Surface nitridation of carbon and silicon substrates is effected by using the reactive nitrogen plume produced in the ablation of N_2 films.[274−276]

Irradiation of frozen systems can also be used for the deposition of new materials, thereby widening the choice of target materials that can be used for pulsed laser deposition. SiC and CN films have been prepared, respectively, by ablation of CH_4 on Si and co-ablation of frozen CH_4/N_2 targets.[276] Diamond-like carbon films have been deposited by ablation of frozen CH_4 and CO_2 on graphitic carbon,[275] acetone,[271,272] or acetylene.[270] Ablation of these compounds results in the efficient production of CH_x species, which are known to play an important role in diamond synthesis. Amorphous diamond-like films of a high electrical resistivity (>10^5 Ω·m) with a ∼40% sp^3 fraction are produced. Some debris is observed (for deposition at $T_{dep} \approx 200$ °C), probably due to droplets ejected from the frozen target (related to the mechanisms discussed in section II.B.2). Deposition at higher substrate temperatures ($T_{dep} \approx 300$ °C) results in the vaporization/disintegration of these droplets and in the formation of a very high quality film. No films could be produced in the irradiation of CH_3OH films, probably because the abundant oxygen radicals (detected optically in the plume) react with the deposit. Pulsed laser deposition has been used extensively for a number of larger organic molecules (i.e., not cryogenic films) with excellent results. For instance, thin films of pentacene deposited by ablation at 248 nm exhibit reduced surface roughness and increased electrical conductivity as compared to films grown by conventional thermal evaporation.[285] Liquid crystal mixtures have also been transferred to a target while retaining the original composition.[277] Novel electroluminescence molecules were ablated and deposited for electroluminescence device preparation.[278] In this case, because of the photolabile nature of the end groups of the molecules, the fluence must be carefully optimized to avoid photodecomposition. Deposition methods and mechanisms are discussed in further detail in the article by Chrisey et al. in this issue.

B. Liquid-Based Applications

1. "Steam Laser Cleaning" Technique

The studies on laser-induced superheating of liquids presented in section III.A have largely been motivated by the potential of so-called "steam laser removal" of submicrometer particulates from surfaces. Due to the ever-decreasing device size, cleaning micrometer and submicrometer particles from surfaces has become a strong need in lithography,

microelectronics, telecommunications, etc. Particulates of this size adhere with relatively strong force, van der Waals force being the dominant one for submicrometer particles [in which case the force is proportional to $AR_{particle}/8\pi z^2$, where z represents the separation between the particle and the surface, and A is a constant in the range of a few (1−10) electronvolts, depending on the nature of particle/substrate material(s)], whereas electrostatic force becomes important for larger ones.[202,287] Because the adhesion force is proportional to the particle radius, whereas the cleaning force is usually proportional to the surface area or volume [i.e., inertial force $m(d^2x/dt^2) \propto R^3(d^2x/dt^2)$], the acceleration necessary to effect ejection scales as R^{-2}. As a result, conventional removal techniques such as ultrasonic, plasma cleaning, etc. become ineffective for micrometer and submicrometer particles.

By comparison to conventional techniques, laser irradiation has been shown to have high potential as a solution to this problem.[202] Laser-induced removal of the contaminants can be effected via either direct absorption of the laser light by the particles and/or the substrate ("dry laser cleaning") or the prior application of a liquid film ("steam cleaning"). The particle removal can be followed by either optical microscopic examination or the scattering via the particles of an incident probing laser beam. Usually, "steam cleaning" is effected with strongly absorbing substrates and liquid films that are transparent at the incident laser wavelength, though the feasibility of CO_2 laser radiation in combination with (absorbing) water films has also been examined.[295] Typically, water mixed with 10−20% alcohol (to improve substrate wetting) is applied in a few tenths to several micrometers thickness (the optimal film thickness has not thus far been specified, though evidence suggests that this parameter may be important for the efficiency of the technique). A range of different particulates, such as those of Au, SiO_2, Al_2O_3, Fe_2O_3, Si, polystyrene, debris, etc., are demonstrated to be efficiently removed from substrates such as Au, Mo, Si wafers and membranes, polyimide photoresist films, polymers, etc. (Figure 21) with 248-nm excimer-laser radiation.[287−289,295,296] The important result of these studies is that the laser cleaning efficiencies are much higher than those in dry cleaning. This permits the use of lower laser fluences, which is particularly important for heat-sensitive substrates or for particles that can melt. It is noted also that the steam-laser technique differs distinctly from the usual liquid-removal/dissolution methods, since the applied liquid film is nearly completely evaporated upon laser heating and thus its penetration in the substrate is minimized.

The process has been studied for well-characterized spherical polymer and silica particles of different diameters (∼ tens of micrometers to 100 nm) on Si (λ = 532 nm, $\tau_{pulse} \approx 7$ ns) (Figure 21). The dependence of the cleaning efficiency on the number of laser shots, N_{laser}, can be approximated by $H(N_{laser}) \approx 1 - (1 - \eta)^{N_{laser}}$, where η represents the cleaning efficiency for a single pulse (the formula assumes identical isolated particles). In practice, deviations

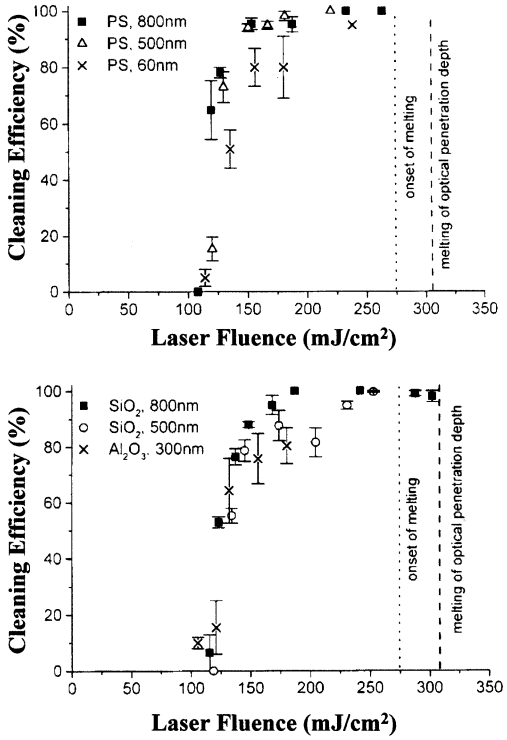

Figure 21. Laser steam cleaning efficiency as a function of laser fluence (λ = 248 nm) for polystyrene spheres of various sizes and for SiO_2 and Al_2O_3 particles on Si substrate (20 cleaning steps have been applied). A film consisting of 90% H_2O and 10% 2-propanol is applied in a well-controlled (200−400 nm) thickness. The results clearly indicate a material and size-independent removal threshold and a steep increase of the removal efficiency with increasing laser fluence. Reprinted with permission from ref 288. Copyright 2000 Springer-Verlag.

are usually observed and may be ascribed to the different cleaning threshold fluences for particles of different sizes, to the surface roughness of the substrate, etc. Applying typically 10−20 pulses, efficiencies from 10−50% up to 40−90% are observed until finally they saturate with a higher number of pulses. At least for submicrometer particles, a sharp, well-defined threshold for removal is demonstrated[287] which is independent of the particle shape and material, though for larger particles, removal appears[289,290] to require lower laser fluences. The particle removal threshold is shown to correlate with the onset of vaporization.[287−290] Thus, the particulate detachment is related not to the high pressure associated with the critical conditions of the liquid but to the high-amplitude pressure wave which is generated by the fast-growing bubbles (section III.A). For micrometer-sized particles, the acoustic transients result in large enough accelerations (10^8−10^9 m/s^2) to effect the detachment of the particles, which are subsequently carried away by the ejected high-speed jet stream. Theoretical models of the removal process have been reported,[291,292] but several experimental observations remain to be accounted for in a satisfactory way. At any rate, the induced temperature and acoustic transients are short enough that no damage or deterioration is induced to the relatively robust solid substrates. For shorter laser pulses (30 ps, λ = 583 nm), an even lower threshold is

indicated.[293] The decrease in the threshold has been tentatively related to the lower conduction heat losses in the metallic/Si wafer, and thus more efficient heating of the liquid.[293]

The use of "steam laser cleaning" has also been examined in relation with the removal of coatings. Oxide coatings from metallic and semiconductor substrates can be removed, with the removal efficiency increased further via electrochemical potential application.[294] This enhancement appears to result from an increase in the absorptivity of the coating. Organic coatings can also be removed from a variety of substrates, including painted artworks. In this case, however, the use of liquid on the highly sensitive organic/painted surfaces may have deleterious side effects, and we have advocated the potential of the "dry cleaning" process, instead.[10,85,86]

2. Liquid-Assisted Material Processing and Nanostructure Formation

A different application concerns the laser irradiation of absorbing solutions for the etching/structuring of transparent or hard-to-process substrates such as silica,[263,264,268] calcium fluoride,[268] fluoropolymer films,[267] etc. To this end, a thin layer of strongly absorbing solution is spread on the material to be processed, and irradiation is performed through the transparent substrate (laser-induced backside wet etching, LIBWE).[267,268,283] It is suggested that the liquid is highly overheated via cyclic multiphotonic processes (section III.C). The highly heated vapor of high presure that is formed close to the interface attacks the softened surface of the substrate and results in material removal.[267,268] The importance of the liquid overheating has been directly shown recently for the case of a (transparent) liquid layer applied on an absorbing substrate.[269] A substantial reduction (by 20−40%) of the ablation threshold and augmentation of the ablation efficiency of the substrate were observed at fluences at which liquid explosive vaporization is initiated. The rapid subsequent cooling prevents damage to the bulk. The method overcomes most drawbacks of alternative laser-processing schemes of such materials, presents the advantages of simplicity and of one-step processing in ambient conditions, and may thus be useful for mass production/processing.

There is an increasing number of reports on novel material formation and, in particular, formation of nanostructures via the laser heating of absorbing surfaces immersed within liquids or of appropriately prepared absorbing solutions/colloids. Various forms of carbon, including amorphous diamonds films, have been deposited from simple aromatic compounds (benzene, toluene, cyclohexane, etc.) at a laser-heated solid−liquid interface.[282,284] Cr_2O_3 has been deposited in the irradiation of aqueous CrO_3. Au[298] and Ag[296,299,300] nanoparticles have been prepared via ablation of corresponding targets in water by a Cu vapor laser (10−20 J/cm^2). The metal nanoparticles obtained upon solvent evaporation are disk-shaped, with a 20−60-nm diameter. The laser-prepared Ag colloids have been shown to be useful for surface-enhanced Raman spectroscopy (SERS), and in fact their activity is comparable or even superior to that of chemically prepared systems.[299,300] The approach overcomes the problems of particle contamination and of limited stability that are encountered in the use of chemically prepared colloids. Furthermore, the colloids can be prepared in the presence of solutes and can be used directly for the SERS examination.[299,300] The reduction of cytochrome *c* by such colloids has also been examined.[301] Cu particles have been prepared by ablation of CuO powder within 2-propanol at 1064 and 532 nm.[302] Most interestingly, the colloids obtained in the 1064-nm irradiation are stable under aerobic conditions even without the use of protective agents, whereas the corresponding colloids prepared by chemical approaches are highly unstable toward oxidation. The difference has been tentatively ascribed to the somewhat higher size and more perfect spherical shape of the particles produced by the laser method. Dispersed micrometer-sized powders of aromatic hydrocarbons and phthalocyanines in poor solvents are fragmented upon excimer laser irradiation, and as a result the initially turbid solutions become transparent ones, composed of ∼100-nm particles.[303]

A phenomenological model of the growth of the nanostructures has been described,[297,298] but the fundamental mechanisms of their formation remain to be elucidated. It appears likely that the very fast vaporization of the liquid adjacent to the absorbing units plays a critical role in the process.[282−284] The very high transient pressures, temperatures, and vapor densities attained certainly affect crucially the decomposition/reaction processes and the kinetics of aggregation for the formation of the clusters. The subsequent fast cooling of the bubble products may be responsible for the formation of the indicated novel metastable forms. At any rate, despite the present mechanistic uncertainties, several advantages of laser ablation over other techniques for nanostructure preparation are clear: a chemically "clean" preparation (i.e., reduced byproduct formation, simpler starting materials, no need for catalyst, etc.), the possibility of producing material forms that may not be attainable by milder preparation methods, and a high degree of control over the size and properties of the produced structures via appropriate selection of irradiation parameters (wavelength, fluence, repetition rate, etc.). The degree of control afforded by the laser method has been indicated in a number of cases. Particle size is generally observed to decrease with increasing number of laser pulses.[297,298,304] Control over the average particle size and size distribution via laser wavelength has also been indicated for Ag nanoparticle formation in H_2O (for instance, irradiation at 1064 nm results in particles of ∼30 nm mean size, whereas at 355 nm, their mean diameter decreases to ∼10 nm).[304] These effects seem to be related to the extent of fragmentation of the nanoparticles induced by self-absorption (i.e., absorption of the incident laser light). Further control has been obtained by employing solutes[298,305] which may coat or react with the surface of the clusters, thereby limiting their agglomeration.

The previous examples clearly indicate the potential of irradiation of liquids/solutions at high laser irradiances for highly innovative processing and/or material production schemes that may turn out to be of very high and widespread impact in various fields and, in particular, in nanotechnology.

V. Acknowledgments

We thank Dr. Akira Yabe and Dr. Hiroyuki Niino (NIMC) for help and many suggestions in the first stages of the preparation of this manuscript. The work was supported in part by the Ultraviolet Laser Facility operating at F.O.R.T.H. under the Improving Human Potential (IHP)-Access to Research Infrastructures program (contract no. HPRI-CT-1999-00074), by the Training and Mobility of Researchers (TMR) program of the European Union (project no. ERBFMRX-CT98-0188), and by the PENED program (project no. 99E D 6) of the General Secretariat of Reseach and Technology—Ministry of Development (Greece).

VI. References

(1) Bäuerle, D. *Laser Processing and Chemistry*; Springer-Verlag: Berlin, 2000.
(2) Karas, M.; Hillenkamp, F. *Anal. Chem.* **1988**, *60*, 2299.
(3) Tanaka, K.; Waki, H.; Ido, Y.; Akita, S.; Yoshida, Y.; Yoshida, T. *Rapid Commun. Mass Spectrom.* **1988**, *2*, 151.
(4) Hillenkamp, F.; Karas, M. *Int. J. Mass Spectrom.* **2000**, *200*, 71.
(5) Boyd, I. A. *Photochemical Processing of Electronic Materials*; Academic Press: London, 1992.
(6) Miller, J. C., Haglund, R. F., Jr., Eds. *Laser Ablation and Desorption*; Experimental Methods in the Physical Sciences 30; Academic Press: San Diego, CA, 1998.
(7) Azema, A. G., Laude, L. D., Eds. *Excimer Lasers*; Kluwer Academic Publishers: Dordrecht, The Netherlands, 1994; p 447.
(8) Tam, A. C.; Leung, W. P.; Zapka, W.; Ziemlich, W. *J. Appl. Phys.* **1992**, *71*, 3515.
(9) Chrisey, D. B.; Hubler, G. K. *Pulsed Laser Deposition of thin films*; Wiley-Interscience: New York, 1994.
(10) Georgiou, S.; Zafiropulos, V.; Anglos, D.; Balas, C.; Tornari, V.; Fotakis, C. *Appl. Surf. Sci.* **1998**, *127*−*129*, 738.
(11) Srinivasan, R.; Braren, B. *Chem. Rev.* **1989**, *89*, 1303.
(12) Zhou, X.-L.; Zhu, X.-Y.; White, J. M. *Surf. Sci. Rep.* **1991**, *13*, 73.
(13) Domen, K.; Chuang, T. J. *Phys. Rev. Lett.* **1987**, *59*, 1484.
(14) Domen, K.; Chuang, T. J. *J. Chem. Phys.* **1989**, *90*, 3318.
(15) Domen, K.; Chuang, T. J. *J. Chem. Phys.* **1989**, *90*, 3332.
(16) Chuang, T. J.; Domen, K. *J. Vac. Sci. Technol.* **1987**, *A5*, 473.
(17) Kutzner, J.; Lindeke, G.; Welge, K. H.; Feldman, D. *J. Chem. Phys.* **1989**, *90*, 548.
(18) Natzle, W. C.; Padowitz, D.; Sibener, S. J. *J. Chem. Phys.* **1988**, *88*, 7975.
(19) Cousins, L. M.; Leone, S. R. *J. Mater. Res.* **1988**, *3*, 1158.
(20) Cousins, L. M.; Leone, S. R. *Chem. Phys. Lett.* **1989**, *155*, 162.
(21) Cousins, L. M.; Levis, R. J.; Leone, S. R. *J. Phys. Chem.* **1989**, *93*, 5325.
(22) Cousins, L. M.; Levis, R. J.; Leone, S. R. *J. Chem. Phys.* **1989**, *91*, 573.
(23) Nishi, N.; Shinohara, H.; Okuyama, T. *J. Chem. Phys.* **1984**, *80*, 3898.
(24) Tabares, F. L.; March, E. P.; Bash, G. A.; Cowin, J. P. *J. Chem. Phys.* **1986**, *86*, 738.
(25) Braun, R.; Hess, P. *J. Chem. Phys.* **1993**, *99*, 8330.
(26) Buck, M.; Hess, P. *Appl. Surf. Sci.* **1989**, *43*, 358.
(27) Cho, C.-C.; Polanyi, J. C.; Stanners, C. D. *J. Phys. Chem.* **1988**, *92*, 6859.
(28) Zhigilei, L. V.; Kodali, P. B. S.; Garrison, B. J. *J. Phys. Chem. B* **1997**, *101*, 2028.
(29) Zhigilei, L. V.; Kodali, P. B. S.; Garrison, B. J. *J. Phys. Chem. B* **1998**, *102*, 2845.
(30) Zhigilei, L. V.; Garrison, B. J. *J. Appl. Phys.* **2000**, *88*, 1281.
(31) Märk, T. D.; Foltin, M.; Kolibar, M.; Lezius, M.; Schreiber, P. *Phys. Scr. T* **1994**, *53*, 43.
(32) Haskin, S. M.; John, P. *J. Phys. Chem. B* **1999**, *103*, 4566.
(33) Srinivasan, R. *Appl. Phys. A* **1993**, *56*, 417.
(34) Handschuh, M.; Nettesheim, S.; Zenobi, R. *Appl. Surf. Sci.* **1999**, *137*, 125.
(35) Han, C. C.; Han Y.-L. W.; Chen, Y. C. *Int. J. Mass Spectrom.* **1999**, *189*, 157.
(36) Focsa, C.; Destombes, J. L. *Chem. Phys. Lett.* **2001**, *347*, 390.
(37) Georgiou, S.; Koubenakis, A.; Kontoleta P.; Syrrou, M. *Laser Chem.* **1997**, *17*, 73.
(38) Georgiou, S.; Koubenakis, A.; Lassithiotaki, M.; Labrakis, J. *J. Chem. Phys.* **1998**, *109*, 8591.
(39) Koubenakis, A.; Elimioti T.; Georgiou, S. *Appl. Phys. A: Mater. Sci. Process.* **1999**, *69*, 637.
(40) Yingling, Y. G.; Zhigilei, L. V.; Garrison, B. J.; Koubenakis, A.; Labrakis, J.; Georgiou, S. *Appl. Phys. Lett.* **2001**, *78*, 1631.
(41) Koubenakis, A.; Labrakis, J.; Georgiou, S. *Chem. Phys. Lett.* **2001**, *346*, 54.
(42) Duncan, M. A.; Knight, A. M.; Negishi, Y.; Nagao, S.; Nakamura, Y.; Kato, A.; Nakajima, A.; Kaya, K. *Chem. Phys. Lett.* **1999**, *309*, 49.
(43) Baltz-Knorr, M. L.; Scriver, K. E.; Haglund, R. F. *Appl. Surf. Sci.* **2002**, *197*−*198*, 110.
(44) Godovac-Zimmermann, J.; Brown, I. R. *Mass Spectrom. Rev.* **2001**, *20*, 1 and references therein.
(45) Sadeghi, M.; Wu, X.; Vertes, A. *J. Phys. Chem. A* **2001**, *105*, 2578.
(46) Robin, M. B. *Higher Excited States of Polyatomic Molecules*; Academic Press: New York, 1974; (a) Vol. I, pp 155−178; (b) Vol. II, pp 230−232.
(47) Koubenakis, A. UV Laser Ablation of Molecular Cryogenic Films. Ph.D. Thesis, University of Crete, Heraklion, 2002.
(48) Kelly, R.; Miotello, A. *Phys. Rev. E* **1999**, *60*, 2616.
(49) Miotello, A.; Kelly, R. *Appl. Phys. Lett.* **1995**, *67*, 3535.
(50) Kelly, R.; Miotello, A. *Appl. Surf. Sci.* **1996**, *96*−*98*, 205.
(51) Knight, C. J. *AIAA J.* **1982**, *20*, 519.
(52) Debenedetti, P. *Metastable Liquids: Concepts and Principles*; Princeton University Press: Princeton, NJ, 1996.
(53) Skripov, V. P. *Metastable Liquids*; John Wiley & Sons Inc.: New York, 1974.
(54) Skripov, V. P.; Pavlov, P. A. *Sov. Technol. Rev. B: Therm. Phys.* **1989**, *2*, 171.
(55) aus der Wiesche, S.; Rembe, C.; Hofer, E. P. *Heat Mass Transfer* **1999**, *35*, 25.
(56) Batanov, V.; Fedorov, V. B. *JETP Lett.* **1973**, *17*, 247.
(57) Martynyuk, M. M. *Sov. Phys. Technol. Phys.* **1974**, *19*, 793.
(58) Martynyuk, M. M. *Combust. Explos. Shock Waves* **1977**, *13*, 178.
(59) Porteous, W.; Blander M. *AIChE J.* **1975**, *21* (3), 560.
(60) Ready, J. F. *Effects of High-Power Laser Radiation*; Academic Press: Orlando, 1971; p 433.
(61) Oxtoby, D. W. *Appl. Phys. B* **1994**, *58*, 267.
(62) Shen, V. K.; Debenedetti, P. G. *J. Chem. Phys.* **1999**, *111*, 3581.
(63) Schilling, G.; Ernst, W. E.; Schwentner, N. *Appl. Phys. B* **1994**, *58*, 267.
(64) Wu, P. K.; Ringeisen, B. R.; Bubb, D. M.; Auyeung, R. C. Y.; Horwitz, J.; Houser, E. J.; Piqué, A.; McGill, R. A.; Chrisey, D. B. *J. Appl. Phys.* **2001**, *90*, 3623.
(65) Westmacott, G.; Ens, W.; Hillenkamp, F.; Dreisewerd, K.; Schürenberg, M. *Int. J. Mass Spectrom. Ion Processes* **2002**, *221*, 67.
(66) Dreisewerd, K.; Schürenberg, M.; Karas, M.; Hillenkamp, F. *Int. J. Mass Spectrom. Ion Processes* **1994**, *141*, 127.
(67) Fain, B.; Lin, S. H. *J. Chem. Phys.* **1989**, *91*, 2726.
(68) Logan, D.; Wight, C. A.; Apkarian, V. A. *Chem. Phys.* **1997**, *217*, 99.
(69) Ehring, J. H.; Sundqvist, B. U. R. *J. Mass Spectrom.* **1995**, *30*, 1303.
(70) Ehring, J. H.; Sundqvist, B. U. R. *Appl. Surf. Sci.* **1996**, *96*−*98*, 577.
(71) Knochenmuss, R.; Vertes, A. *J. Phys. Chem. B* **2000**, *104*, 8406.
(72) Allwood, D. A.; Dyer, P. E.; Dreyfus, R. W. *Rapid Commun. Mass Spectrom.* **1997**, *11*, 499.
(73) Karas, M.; Gluckmann, M.; Schfer, J. *J. Mass Spectrom.* **2000**, *35*, 1.
(74) Vertes, A.; Levine, R. D. *Chem. Phys. Lett.* **1990**, *171*, 284.
(75) Vertes, A.; Gijbels, R. *Scanning Microsc.* **1991**, *5*, 317.
(76) Vertes, A.; Gijbels R.; Levine, R. D. *Rapid Commun. Mass Spectrom.* **1990**, *4*, 228.
(77) Bencsura, A.; Navale, V.; Sadeghi, M.; Vertes, A. *Rapid Commun. Mass Spectrom.* **1997**, *11*, 679.
(78) Dutkiewicz, Ł.; Johnson, R. E.; Vertes, A.; Pędrys, R. *J. Phys. Chem. A* **1999**, *103*, 2925.
(79) Iwaki, L. K.; Deàk, J. C.; Dlott, D. D. *Chem. Phys. Lett.* **1998**, *293*, 405.
(80) Mashni, M.; Hess, P. *Appl. Phys. B* **1982** *29*, 205.
(81) Antonov, V. S.; Lethokov, V. S.; Matveyets, Y. A.; Shibanov, A. N. *Laser Chem.* **1982**, *1*, 37.
(82) Chekalin, S. V.; Golovlev, V. V.; Kozlov, A. A.; Matveyets, Y. A.; Yartsev, A. P.; Lethokov, V. S. *Phys. Chem.* **1988**, 6855.
(83) Demirev, P.; Westman, A.; Rimann, C. T.; Hakansson, P.; Barofsky, D.; Sundqvist, B. U. R.; Chen, Y. D.; Seibt, W.; Siegbahn, K. *Rapid Commun. Mass Spectrom.* **1992**, *6*, 187.
(84) Dreisewerd, K.; Schürenberg, M.; Karas, M.; Hillenkamp, F. *Int. J. Mass Spectrom. Ion Processes* **1996**, *154*, 171.

(85) Lassithiotaki, M.; Athanassiou, A.; Anglos, D.; Georgiou, S.; Fotakis, C. *Appl. Phys. A* **1999**, *69*, 363.
(86) Athanassiou, A.; Andreou, E.; Anglos, D.; Georgiou, S.; Fotakis, C. *Appl. Phys. A* **1999**, *86*, 285.
(87) Arnolds, H.; Rehbein, C.; Roberts, G.; Levis, R. J.; King, D. A. *J. Phys. Chem. B* **2000**, *104*, 3375.
(88) Guo, H.; Saalfrank, P.; Seideman, T. *Prog. Surf. Sci.* **1999**, *62*, 239.
(89) Niino, H.; Sato, T.; Yabe, A. *Proc. SPIE* **2001**, *4274*, 232.
(90) Niino, H.; Sato, T.; Narazaki, A.; Kawaguchi, Y.; Yabe, A. *Appl. Surf. Sci.* **2002**, in press 7978.
(91) Okoshi, M.; Higuchi, S.; Hanabusa, M. *Appl. Surf. Sci.* **2000**, *154*, 376.
(92) Preuss, S.; Späth, M.; Zhang, Y.; Stuke, M. *Appl. Phys. Lett.* **1993**, *62*, 3049.
(93) Baudach, S.; Krüger, J.; Kautek, W. *Rev. Laser Eng.* **2001**, *29*, 705.
(94) Hosokawa, Y.; Yashiro, M.; Asahi, T.; Masuhara, H. *J. Photochem. Photobiol. A* **2001**, *142*, 197.
(95) Maechling, C. R.; Clemett, S. J.; Engelke, F.; Zare, R. N. *J. Chem. Phys.* **1996**, *104*, 8768.
(96) Handschuh, M.; Nettesheim, S.; Zenobi, R. *J. Chem. Phys.* **1997**, *107*, 2603.
(97) Handschuh, M.; Nettesheim, S.; Zenobi, R. *J. Chem. Phys.* **1998**, *108*, 6548.
(98) Carslaw, H. S.; Jaeger, J. C. *Conduction of Heat in Solids*; Oxford University Press: Oxford, 1959.
(99) Karaiskou, A.; Papazoglou, D.; Kafetzopoulos, D.; Zergioti, I.; Fotakis, C. *Appl. Surf. Sci.*, in press.
(100) Ellegaard, O.; Schou, J. *J. Appl. Phys.* **1998**, *83*, 1078.
(101) Jette, A. N.; Benson, R. C. *J. Appl. Phys.* **1994**, *75*, 3130.
(102) Dou, Y.; Zhigilei, L. V.; Winograd, N.; Garrison, B. J. *J. Phys. Chem. A* **2001**, *105*, 2748.
(103) Dou, Y.; Zhigilei, L. V.; Postwa, Z.; Winograd, M.; Garrison, B. J. *Nucl. Instrum. Methods Phys. Res. B* **2001**, *180*, 105.
(104) Young, D.; Auyeung, R. C. Y.; Piqué, A.; Chrisey, D. B.; Dlott, D. D. *Appl. Surf. Sci.* **2002**, *197*−*198*, 181.
(105) Young, D.; Auyeung, R. C. Y.; Piqué, A.; Chrisey, D. B.; Dlott, D. D. *Appl. Phys. Lett.* **2001**, *78*, 3169.
(106) Nelson R. W.; Rainbow, M. J.; Lohr, D. E.; Williams, P. *Science* **1989**, *246*, 1585.
(107) Williams, P. *Int. J. Mass Spectrom. Ion Processes* **1994**, *131*, 335.
(108) Amster, I. J.; Speir, J. P. *Anal. Chem.* **1992**, *64*, 1041.
(109) Koulikov, S. G.; Dlott, D. D. *J. Photochem. Photobiol. A: Chem.* **2001**, *145*, 183.
(110) Herminghaus, S.; Leiderer, P. *Appl. Phys. Lett.* **1991**, *58*, 352.
(111) Comsa, G.; David, R. *Surf. Sci. Rep.* **1985**, *5*, 145.
(112) Campos, F. X.; Weaver, G. C.; Waltman, C. J.; Leone, S. R. *J. Vac. Sci. Technol.* **1992**, *B10*, 2217.
(113) Campos, F. X.; Waltman, C. J.; Leone, S. R. *Chem. Phys. Lett.* **1993**, *201*, 399.
(114) Kools, J. C. J.; Baller, T. S.; De Zwart, S. T.; Dieleman, J. *J. Appl. Phys.* **1992**, *71*, 4547.
(115) Elokhin, V. A.; Krutchinsky, A. N.; Ryabov, S. E. *Chem. Phys. Lett.* **1990**, *70*, 193.
(116) Zhang, J.-Y.; Nagra, D. S.; Li, L. *Anal. Chem.* **1993**, *65*, 2812.
(117) de Vries M. S.; Hunziker H. E. *J. Photochem. Photobiol. A: Chem.* **1997**, *106*, 31.
(118) Heinrich, E. N.; Hunziker, E.; de Vries, M. S. *Anal. Chem.* **1999**, *71*, 1674.
(119) Jones, A. C.; Dale, M. J.; Keenan, G. A.; Langridge-Smith, P. R. R. *Chem. Phys. Lett.* **1994**, *219*, 174.
(120) Kelly, R.; Dreyfus, R. W. *Surf. Sci.* **1988**, *198*, 263.
(121) Kelly, R. *J. Chem. Phys.* **1990**, *92*, 5047.
(122) Sibold, D.; Urbassek, H. M. *Phys. Rev. A* **1991**, *43*, 6722.
(123) Sibold, D.; Urbassek, H. M. *J. Appl. Phys.* **1993**, *73*, 8544.
(124) Anisimov, S. I.; Bäuerle, D.; Luk'yanchuk, B. S. *Phys. Rev. B* **1993**, *48*, 12076.
(125) Anisimov, S. I.; Luk'yanchuk, B. S.; Luches, A. *Appl. Surf. Sci.* **1996**, *96*−*98*, 24.
(126) Kelly, R. *Phys. Rev. A* **1992**, *46*, 860.
(127) Kelly, R.; Dreyfus, R. W. *Nucl. Instrum. Methods B* **1988**, *32*, 341.
(128) Kelly R.; Miotello, A. *Appl. Phys. B* **1993**, *57*, 145.
(129) Kelly, R.; Miotello, A. *Nucl. Instrum. Methods B* **1997**, *122*, 374.
(130) NoorBatcha, I.; Lucchese, R. R. *Phys. Rev. B* **1987**, *36*, 4978.
(131) NoorBatcha, I.; Lucchese, R. R.; Zeiri, Y. *J. Chem. Phys.* **1987**, *86*, 5816.
(132) NoorBatcha, I.; Lucchese, R. R.; Zeiri, Y. *J. Chem. Phys.* **1988**, *89*, 5251.
(133) Urbassek, H. M.; Sibold, D. *Phys. Rev. Lett.* **1993**, *70*, 1886.
(134) Dreyfus, R. W.; Kelly, R.; Walkup, R. E. *Appl. Phys. Lett.* **1986**, *49*, 1478.
(135) Itina, T. E.; Patrone, L.; Marine, W.; Autric, M. *Appl. Phys. A* **1999**, *69*, S59.
(136) Vertes, A. *Microbeam Anal.* **1991**, *1991*, 25.
(137) Vertes, A.; Irinyi, G.; Gibjels, R. *Anal. Chem.* **1993**, *65*, 2389.
(138) Zhigilei, L. V.; Garrison, B. J. *Appl. Phys. Lett.* **1997**, *71*, 551.
(139) Elam, J. W.; Levy, D. H. *J. Chem. Phys.* **1997**, *106*, 10368.
(140) Elam, J. W.; Levy, D. H. *J. Phys. Chem.* **1998**, *102*, 8113.
(141) Georgiou, S.; Kosmidis, C.; Koubenakis, A.; Jia, W.; Ledinhgam, K. W. D. *Phys. Chem. Chem. Phys.* **1999**, *1*, 5339.
(142) Leboeuf, J. N.; Chen, K. R.; Liu, C. L.; Wood, R. F.; Geohegan, D. B.; Puretzky, A. A.; Donato, J. M. *Mater. Sci. Eng. B* **1997**, *47*, 70.
(143) Chen, K. R.; Leboeuf, J. N.; Wood, R. F.; Geohegan, D. B.; Donato, J. M.; Liu, C. L.; Puretzky, A. A. *Phys. Rev. Lett.* **1995**, *75*, 4706.
(144) Wood, R. F.; Chen, K. R.; Leboeuf, J. N.; Puretzky, A. A.; Geohegan, D. B. *Phys. Rev. Lett.* **1997**, *79*, 1571.
(145) Chen, K. R.; Leboeuf, J. N.; Wood, R. F.; Geohegan, D. B.; Donato, J. M.; Liu, C. L.; Puretzky, A. A. *J. Vac. Sci. Technol. A* **1996**, *14*, 1111.
(146) Puretzky, A. A.; Geohegan, D. B.; Itina, T. E.; Marine, W.; Autric, M. *Appl. Surf. Sci.* **1998**, *171*, 127.
(147) Huth-Fehre, T.; Becker, C. H. *Rapid Commun. Mass Spectrom.* **1991**, *5*, 378.
(148) Beavis, R. C.; Chait, B. T. *Chem. Phys. Lett.* **1991**, *181*, 479.
(149) Westman, A.; Demirev, P.; Huth-Fehre, T.; Bielawski, J.; Sundqvist, B. U. R. *Int. J. Mass Spectrom. Ion Processes* **1994**, *130*, 107.
(150) Zhang, W.; Chait, B. T. *Int. J. Mass Spectrom. Ion Processes* **1997**, *160*, 259.
(151) Fournier, I.; Beavis, R. C.; Blais, J. C.; Tabet, J. C.; Bolabch, G. *Int. J. Mass Spectrom. Ion Processes* **1997**, *169/170*, 19.
(152) Pan, Y.; Cotter, R. J. *Org. Mass. Spectrom.* **1992**, *27*, 3.
(153) Puretzky, A. A.; Geohegan, D. B.; Hurst, G. B.; Buchanan, M. V.; Luk'yanchuk, B. *Phys. Rev. Lett.* **1999**, *83*, 444.
(154) Itina, T. E.; Tokarev, V. N.; Marine, W.; Autric, M. *J. Chem. Phys.* **1997**, *106*, 8905.
(155) Garrison, B. J.; Srinivasan, R. *J. Appl. Phys.* **1985**, *57*, 2909.
(156) Yingling Y. G.; Zhigilei L. V.; Garrison B. J. *Nucl. Instrum. Methods B* **2001**, *180*, 171.
(157) Yingling Y. G.; Zhigilei L. V.; Garrison B. J. *J. Photochem. Photobiol. A* **2001**, *145*, 173.
(158) Sekine, S.; Ichimura, S.; Shimizu, H.; Hashizume, H. *Jpn. J. Appl. Phys.* **1994**, *33*, L387.
(159) Lippert, T.; Yabe, A.; Wokaun, A. *Adv. Mater.* **1997**, *9*, 105.
(160) Weaver, G. C.; Leone, S. R. *Surf. Sci.* **1995**, *328*, 197.
(161) Weaver, G. C.; Leone, S. R. *J. Phys. Chem.* **1996**, *100*, 4188.
(162) Ventzek, P. L. G.; Suzuki, M.; Date, H.; Sakai, Y.; Tagashira, H.; Kitamori, K. *J. Appl. Phys.* **1996**, *80*, 1146.
(163) Kukreja, L. M.; Hess, P. *Appl. Phys. Lett.* **1993**, *62*, 105.
(164) Georgiou, S.; Koubenakis, A.; Kontoleta, P.; Syrrou, M. *Chem. Phys. Lett.* **1997**, *270*, 491.
(165) Yingling, Y. G.; Garrison, B. J. *Chem. Phys. Lett.* **2002**, *364*, 237.
(166) Nishiguchi, T.; Morikawa, Y.; Miyamoto, M.; Nonaka, H.; Ichimura, S. *Jpn. J. Appl. Phys.* **2000**, *39*, L1200.
(167) Georgiou, S.; Koubenakis, A.; Labrakis, J.; Lassithiotaki, M. *Appl. Surf. Sci.* **1998**, *127*−*129*, 122.
(168) Georgiou, S.; Koubenakis, A.; Kontoleta, P.; Syrrou, M. *Chem. Phys. Lett.* **1996**, *260*, 166.
(169) Niino, H.; Sato, T.; Yabe, A. *Appl. Phys. A* **1999**, *69*, 145.
(170) Srinivasan, R.; Braren, B.; Casey, K. G. *J. Appl. Phys.* **1990**, *68*, 1842.
(171) Dyer, P. E.; Karnakis, D. M. *Appl. Phys. A* **1994**, *59*, 275.
(172) Koubenakis, A.; Labrakis, J.; Georgiou, S. *J. Chem. Soc., Faraday Trans.* **1998**, *94*, 3427.
(173) Fournier, I.; Tabet, J. C.; Bolbach, G. *Int. J. Mass Spectrom.* **2002**, *219*, 515.
(174) Krajnovich, D. J.; Vazquez, J. E. *J. Appl. Phys.* **1993**, *73*, 3001.
(175) Hare, D. E.; Franken, J.; Dlott, D. D. *J. Appl. Phys.* **1995**, *77*, 5950.
(176) Bubb, D. M.; Wu, P. K.; Horwitz, J. S.; Callahan, J. H.; Galicia, M.; Vertes, A.; McGill, R. A.; Houser, E. J.; Ringeisen, B. R.; Chrisey, D. B. *J. Appl. Phys.* **2002**, *91*, 2055.
(177) Niino, H.; Sato, T.; Yabe, A. *Appl. Phys. A* **1999**, *69*, 605.
(178) Athanassiou, A.; Andreou, E.; Bonarou, A.; Tornari, V.; Anglos, D.; Georgiou, S.; Fotakis, C. *Appl. Surf. Sci.* **2002**, *197*−*198*, 757.
(179) Athanassiou, A.; Andreou, E.; Fragouli, D.; Anglos, D.; Georgiou, S.; Fotakis, C. *J. Photochem. Photobiol. A: Chem.* **2001**, *145*, 229.
(180) Niino, H.; Koga, Y.; Yabe, A. *J. Photochem. Photobiol. A: Chem.* **1997**, *106*, 9.
(181) Pimentel, G. C. *Formation and Trapping of Free Radicals*; Academic Press Inc.: New York, 1960.
(182) Song, Y.; Garder, P.; Conrad, H.; Bradshaw, A. M.; White, J. M. *Surf. Sci.* **1991**, *248*, L279.
(183) Siskin, M.; Katritzky, A. R.*Chem. Rev.* **2001**, *101*, 825.
(184) Kawasaki, M.; Sato, H.; Nishi, N. *J. Appl. Phys.* **1989**, *65*, 792.
(185) Venugopalan, V.; Nishioka, N. S.; Mikic, B. B. *Trans. ASME J. Biomech. Eng.* **1994**, *116*, 62.
(186) Venugopalan, V.; Nishioka, N. S.; Mikic, B. B. *Biophys. J.* **1995**, *69*, 1259.
(187) Bityurin, N.; Arnold, N.; Luk'yanchuk, B.; Bauerle, D. *Appl. Surf. Sci. Phys.* **1998**, *127*−*129*, 164.
(188) Belov, M. E.; Alimpiev, S. S.; Mlynsky, V. V.; Nikiforov, S. M.; Derrick, P. J. *Rapid Commun. Mass Spectrom.* **1995**, *9*, 1431.

(189) Dotter, R. N.; Smith, C. H.; Young, M. K.; Kelly, P. B.; Jones, A. D.; Mc Cauley, E. M.; Chang, D. P. Y *Anal. Chem.* **1996**, *68*, 2319.
(190) Koubenakis, A.; Venturini, J.; Georgiou, S. *Appl. Surf. Sci.* **2002**, *197−198*, 77.
(191) Claereboudt, J.; Claeys, M.; Geise, H.; Gijbels, R.; Vertes, A. *J. Am. Soc. Mass Spectrom.* **1993**, *4*, 798.
(192) Levis, J. *Annu. Rev. Phys. Chem.* **1994**, *45*, 4830.
(193) Johnson, R. E. *Int. J. Mass Spectrom. Ion Processes* **1994**, *139*, 25.
(194) Turro, N. J. *Modern Molecular Photochemistry;* University Science Books: Mill Valley, CA, 1991.
(195) Ehring, H.; Karas, M.; Hillenkamp, F. *Org. Mass Spectrom.* **1992**, *27*, 472.
(196) Wen, X.; Tolbert, W. A.; Dlott, D. D. *J. Chem. Phys.* **1993**, *99*, 4140.
(197) Root, R. G. *Laser-Induced Plasmas and Applications*; Marcel Dekker: New York, 1989; p 69.
(198) Krokhin, O. N. Generation of high-temperature vapors and plasmas by laser radiation. In *Laser Handbook*; Arecchi, F. T., Schulz-DuBois, E. O., Eds.; North-Holland Publishing Co.: Amsterdam, 1972; p 1371.
(199) Venugopalan, V.; Guerra, A.; Nahen, K.; Vogel, A. *Phys. Rev. Lett.* **2000**, *88*, 078103.
(200) Blander, M.; Katz, J. L. *AIChE J.* **1975**, *21*, 833.
(201) Brennen, C. E. *Cavitation and Bubble Dynamics*; Oxford University Press: New York, 1995.
(202) Tam, A. C.; Leung, W. P.; Zapka, W.; Ziemlich W. *J. Appl. Phys.* **1992**, *71*, 3515.
(203) Leung, P. T.; Do, N.; Klees, L.; Leung, W. P.; Tong, F.; Lam, L.; Zapka, W.; Tam, A. C. *J. Appl. Phys.* **1992**, *72*, 2256.
(204) Do, N.; Klees, L.; Tam, A. C.; Leung, P. T.; Leung, W. P. *J. Appl. Phys.* **1993**, *74*, 1534.
(205) Yavas, O.; Leiderer, P.; Park, H. K.; Grigoropoulos, C. P.; Poon, C. C.; Leung, W. P.; Do, N.; Tam, A. C. *Phys. Rev. Lett.* **1993**, *70*, 1830.
(206) Park, H. K.; Grigoropoulos, C. P.; Poon, C. C.; Tam, A. C. *Appl. Phys. Lett.* **1996**, *68*, 596.
(207) Park, H. K.; Zang, X.; Grigoropoulos, C. P.; Poon, C. C.; Tam, A. C. *ASME Trans. J. Heat Transfer* **1995**, *118*, 702.
(208) Schilling, A.; Yavas, O.; Bischof, J.; Boneberg, J.; Leiderer, P. *Appl. Phys. Lett.* **1996**, *69*, 4159.
(209) Park, H. K.; Kim, D.; Grigoropoulos, C. P.; Tam, A. C. *J. Appl. Phys.* **1996**, *80*, 4072.
(210) Yavas, O.; Schilling, A.; Bischof, J.; Boneberg, J.; Leiderer, P. *Appl. Phys. A* **1997**, *64*, 331.
(211) Strauss, M.; Kaufman, Y.; Sapir, M.; Amendt, P. A.; London, R. A.; Clinsky, M. E. *J. Appl. Phys.* **2002**, *91*, 4720.
(212) Kim, D.; Park, H. K.; Grigoropoulos, C. P. *Int. J. Heat Mass Transfer* **2001**, *44*, 3843.
(213) Yavas, O.; Leiderer, P.; Park, H. K.; Grigoropoulos, C. P.; Poon, C. C.; Tam, A. C. *Phys. Rev. Lett.* **1994**, *72*, 2021.
(214) Turovets, I.; Palanker, D.; Lewis, A. *J. Photochem. Photobiol.* **1994**, *60*, 412.
(215) Lin, C. P.; Kelly, M. W. *Appl. Phys. Lett.* **1998**, *72*, 2800.
(216) Lawson, C. M.; Euliss, G. W.; Michael, R. R. *Appl. Phys. Lett.* **1991**, *58*, 2195.
(217) Chen, H.; Diebold, G. *Science* **1995**, *270*, 963.
(218) Sunner, J.; Dratz, E.; Yu-Chie, C. *Anal. Chem.* **1995**, *67*, 4335.
(219) Dale, M. J.; Knochenmuss, R.; Zenobi, R. *Rapid Commun. Mass Spectrom.* **1997**, *11*, 136.
(220) Schürenberg, M.; Dreisewed, K.; Hillenkamp, F. *Anal. Chem.* **1999**, *71*, 221.
(221) McEwan, K. J.; Madden, P. A. *J. Chem. Phys.* **1992**, *97*, 8748.
(222) Lowen, H.; Madden, P. A. *J. Chem. Phys.* **1992**, *97*, 8760.
(223) Sun, J. M.; Gerstman, B. S.; Li, B. *J. Appl. Phys.* **2000**, *88*, 2352.
(224) Zhigilei, L. V.; Garisson, B. J. *Appl. Surf. Sci.* **1998**, *127*, 142.
(225) Gusev, V. E.; Karabutov, A. A. *Laser Optoacoustics*; American Institute of Physics: New York, 1993; p 271.
(226) Jansen, E. D.; van Leeuwen, T. G.; Motamedi, M.; Borst, C., Welch, A. J. *J. Appl. Phys.* **1995**, *78*, 564.
(227) Oraevsky, A. A.; Jacques, S. L.; Tittel, F. K. *J. Appl. Phys.* **1995**, *78*, 1281
(228) Oraevsky, A. A.; Jacques, S. L.; Esenaliev, R. O.; Tittel, F. K. *Lasers Surg. Med.* **1996**, *18*, 231.
(229) Esenaliev, R. O.; Karabutov, A. A.; Podymova, N. B.; Letokhov, V. S. *Appl. Phys. B* **1994**, *59*, 73.
(230) Thompson, C. R.; Gerstman, B. S.; Jacques, S. L.; Rogers, M. E. *Bull. Math. Biol.* **1996**, *58*, 513.
(231) Paltauf, G.; Schmidt-Kloiber, H. *Appl. Phys. A* **1996**, *62*, 303.
(232) Paltauf, G.; Schmidt-Kloiber, H. *J. Appl. Phys.* **1997**, *82*, 1525.
(233) Kim, D.; Grigoropoulos, C. P. *Appl. Surf. Sci.* **1998**, *127−129*, 53.
(234) Kim, D.; Ye, M.; Grigoropoulos, C. P. *Appl. Phys. A* **1998**, *67*, 169.
(235) Siano, S.; Pini, R.; Salimbeni, R.; Vannini, M. *Appl. Phys. B* **1996**, *62*, 503.
(236) Frenz, M.; Könz, F.; Pratisto, H.; Weber, H. P.; Silenok, A. S.; Konov, V. I. *J. Appl. Phys.* **1998**, *84*, 5905.
(237) Staveteig P. T.; Walsh J. T. *Appl. Opt.* **1996**, *35*, 3392.
(238) Nikiforov, S. M.; Alimpiev, S. S.; George, M. W.; Sartakov, B. G.; Simanovsky, Y. O. *Opt. Commun.* **2000**, *182*, 17.
(239) Hale, G. M.; Querry, M. R.; Rusk, A. N.; Williams D. *J. Opt. Soc. Am.* **1972**, *62*, 1103.
(240) Longtin, P.; Tien C.-L. *Int. J. Heat Mass Transfer* **1997**, *40*, 951.
(241) Srinivasan, R.; Ghosh, A. P. *Chem. Phys. Lett.* **1988**, *143*, 546.
(242) Katoh, R.; Yokoi, H.; Usuba, S.; Kakudate, Y.; Fujiwara, S. *Chem. Phys. Lett.* **1998**, *291*, 305.
(243) Tsuboi, Y.; Hatanaka, K.; Fukumura, H.; Masuhara, H. *J. Phys. Chem.* **1994**, *98*, 11237.
(244) Tsuboi, Y.; Fukumura, H.; Masuhara, H. *Appl. Phys. Lett.* **1994**, *64*, 2745.
(245) Hatanaka, K.; Kawao, N.; Tsuboi, Y.; Fukumura, H.; Masuhara, H. *J. Appl. Phys.* **1997**, *82*, 5799.
(246) Tsuboi, Y.; Hatanaka, K.; Fukumura, H.; Masuhara, H. *J. Phys. Chem. A* **1998**, *102*, 1661.
(247) Hirai, A.; Tsuboi, Y.; Itoh, K.; Ichioka, Y. *Rev. Sci. Instrum.* **1996**, *67*, 3222.
(248) Tsuboi, Y.; Fukumura, H.; Masuhara, H. *J. Phys. Chem.* **1995**, *99*, 10305.
(249) Hatanaka, K.; Itoh, T.; Asahi, T.; Ichinose, N.; Kawanishi, S.; Sasuga, T.; Fukumura, H.; Masuhara, H. *Chem. Phys. Lett.* **1999**, *300*, 727.
(250) Hatanaka, K.; Itoh, T.; Asahi, T.; Ichinose, N.; Kawanishi, S.; Sasuga, T.; Fukumura, H.; Masuhara, H. *Appl. Phys. Lett.* **1998**, *73*, 3498.
(251) Hatanaka, K.; Itoh, T.; Asabi, T.; Ichinose, N.; Kawanishi, S.; Sasuga, T.; Fukumura, H.; Masuhara, H. *J. Phys. Chem. A* **1999**, *103*, 11257.
(252) Hatanaka, K.; Tsuboi, Y.; Fukumura, H.; Masuhara, H. *J. Phys. Chem. A* **2002**, *106*, 3049.
(253) Toyota, K.; Nakashima, S.; Okada, T. *Chem. Phys. Lett.* **2000**, *323*, 323.
(254) Toyota, K.; Tanaka, T.; Nishiwaki, S.; Nakashima, S.; Okada, T. *J. Photochem. Photobiol. A: Chem.* **2001**, *141*, 9.
(255) Hopp, B.; Smausz, T.; Wittmann, T.; Ignacz, F. *Appl. Phys. A* **2000**, *71*, 315.
(256) Berkenkamp, S.; Karas, M.; Hillenkamp, F. *Proc. Natl. Acad. Sci. U.S.A.* **1996**, *93*, 7003.
(257) Schieltz, D. M.; Chou, C. W.; Luo, C. W.; Thomas, R. M.; Williams, P. *Rapid Comm. in Mass Spectrom.* **1992**, *6*, 631.
(258) Sheffer, J. D.; Murray, K. K. *J. Mass Spectrom.* **2000**, *35*, 95.
(259) Livingston, F. E.; Smith, J. A.; George, S. M. *Anal. Chem.* **2000**, *72*, 5596.
(260) Livingston, F. E.; George, S. M. *J. Phys. Chem. A* **2001**, *105*, 5155.
(261) Levis, R. J.; Waltman, C. J.; Cousins, L. M.; Copeland, R. G.; Leone, S. R. *J. Vac. Sci. Technol.* **1990**, *A8*, 3118.
(262) Harrison, I.; Polanyi, J. C. *Z. Phys. D: Atoms, Molecules Clusters* **1988**, *10*, 383.
(263) Wang, J.; Niino, H.; Yabe, A. *Appl. Phys. A* **1999**, *68*, 111.
(264) Wang, J.; Niino, H.; Yabe, A. *Appl. Phys. A* **1999**, *69*, S271.
(265) Drinek, V.; Niino, H.; Pola, J.; Yabe, A. *Appl. Phys. A* **2001**, *73*, 527.
(266) Yasui, Y.; Niino, H.; Kawaguchi, Y.; Yabe, A. *Appl. Surf. Sci.* **2002**, *186*, 552.
(267) Wang, J.; Niino, H.; Yabe, A. *Jpn. J. Appl. Phys.* **1999**, *38*, L761.
(268) Wang, J.; Niino, H.; Yabe, A. *Appl. Surf. Sci.* **2000**, *154−155*, 571.
(269) Kim, D.; Lee, H. *J. Appl. Phys.* **2001**, *89*, 5703.
(270) Hanabusa, M.; Tsujihara, K. *J. Appl. Phys.* **1995**, *78*, 4267.
(271) Okoshi, M.; Higuchi, S.; Hanabusa, M. *J. Appl. Phys.* **1999**, *86*, 1768.
(272) Okoshi, M.; Higuchi, S.; Hanabusa, M. *Jpn. J. Appl. Phys.* **2001**, *40*, 4926.
(273) Hiroshima, Y.; Ishiguro, T.; Esaki, K. *Jpn. J. Appl. Phys.* **1997**, *36*, 798.
(274) Hiroshima, Y.; Ishiguro, T.; Esaki, K. *Jpn. J. Appl. Phys.* **1997**, *36*, 2267.
(275) Ishiguro, T.; Esaki, K.; Hiroshima, Y. *Appl. Surf. Sci.* **1998**, *127−129*, 553.
(276) Ishiguro, T.; Shoji, T.; Inada, H. *Appl. Phys.* **1999**, *A69*, S149.
(277) Allwood, D. A.; Dyer, P. E.; Gonzalo, J.; Snelling, H. V.; Hird, M. *Chem. Phys. Lett.* **1999**, *301*, 91.
(278) Farrar, S. R.; Contoret, A. E. A.; O'Neil, M.; Nicholls, J. E.; Eastwood, A. J.; Richards, G. J.; Vlachos, P.; Helly, S. M. *Appl. Surf. Sci.* **2002**, *186*, 435.
(279) Nishiguchi, T.; Morikawa, Y.; Miyamoto, M.; Nonaka, H.; Ichimura, S. *Appl. Phys. Lett.* **2001**, *79*, 382.
(280) Nishiguchi, T.; Morikawa, Y.; Miyamoto, M.; Nonaka, H.; Ichimura, S. *Jpn. J. Appl. Phys.* **2001**, *40*, L897.
(281) Niino, H.; Yabe, A. *Appl. Surf. Sci.* **1996**, *96−98*, 572.
(282) Simakin, V.; Voronov, V. V.; Shafeev, G. A.; Brayner, R.; Bozon-Verduraz, F. *Chem. Phys. Lett.* **2001**, *348*, 182.
(283) Böhme, R.; Braun, A.; Zimmer, K. *Appl. Surf. Sci.* **2001**, *186*, 276.

(284) Simakin, A. V.; Shafeev, G. A.; Loubnin E. N. *Appl. Surf. Sci.* **2000**, *154−155*, 405.
(285) Salih, A. J.; Lau, S. P.; Marshall, J. M.; Maud, J. M.; Bowen, W. R.; Hilal, N.; Lovitt, R. W.; Williams, P. M. *Appl. Phys. Lett.* **1996**, *69*, 2231.
(286) Rong, F.-X. *Appl. Phys. Lett.* **1995**, *67*, 1022.
(287) Arnold, N. *Appl. Surf. Sci.* **2002**, *197−198*, 904.
(288) Mosbacher, M.; Dobler, V.; Boneberg, J.; Leiderer, P. *Appl. Phys. A* **2000**, *70*, 669.
(289) Tam, A. C.; Park, H. K.; Grigoropoulos, C. P. *Appl. Surf. Sci.* **1998**, *127−129*, 721.
(290) She, M.; Kim, D.; Grigoropoulos, C. P. *J. Appl. Phys.* **1999**, *86*, 6519.
(291) Lu, Y. F.; Zhang, Y.; Wan, Y. H.; Song, W. D. *Appl. Surf. Sci.* **1999**, *138−139*, 140.
(292) Wu, X.; Sacher, E.; Meunier, M. *J. Appl. Phys.* **2000**, *87*, 3618.
(293) Mosbacher, M.; Chaoui, N.; Siegel, J.; Dobler, V.; Solis, J.; Boneberg, J.; Afonso, C. N.; Leiderer, P. *Appl. Phys. A* **1999**, *69*, 331.
(294) Pasquet, P.; del Coso, R.; Boneberg, J.; Leiderer, P.; Oltra, R.; Boquillon, J. P. *Appl. Phys. A* **1999**, *69*, S727.
(295) Héroux, J. B.; Boughaba, S.; Ressejak, I.; Meunier, M. *J. Appl. Phys.* **1996**, *79*, 2857.
(296) Lee, Y. P.; Lu, Y. F.; Chan, D. S. H.; Low, T. S.; Zhou, M. S. *Jpn. J. Appl. Phys.* **1998**, *37*, 2524.
(297) Mafuné, F.; Kohno, J.-y.; Takeda, Y.; Kondow, T.; Sawabe, H. *J. Phys. Chem. B* **2000**, *104*, 9111.
(298) Mafuné, F.; Kohno, J.-y.; Takeda, Y.; Kondow, T.; Sawabe, H. *J. Phys. Chem. B* **2001**, *105*, 5114.
(299) Procházka, M.; Vlčkova, B.; Stěpánek, J.; Srnovà, I.; Mal'y, P. *J. Mol. Struct.* **1997**, *410−411*, 213.
(300) Srnovà, I.; Procházka, M.; Vlčkova, B.; Stepanek, J.; Mal'y, P. *Langmuir* **1998**, *14*, 4666.
(301) Sibbald, M. S.; Chumanov, G.; Cotton, T. M. *J. Phys. Chem.* **1996**, *100*, 4672.
(302) Yeh, M.-S.; Yang, Y.-S.; Lee, Y.-P.; Lee, H.-F.; Yeh, Y.-H.; Yeh, C.-S. *J. Phys. Chem. B* **1999**, *103*, 6851.
(303) Tamaki, Y.; Asahi, T.; Masuhara, H. *Appl. Surf. Sci.* **2000**, *168*, 85.
(304) Tsuji, T.; Iryo, K.; Watanabe, N.; Tsuji, M. *Appl. Surf. Sci.* **2002**, *202*, 80.
(305) Bae, C. H.; Nam, S. H.; Park, S. M. *Appl. Surf. Sci.* **2002**, *197−198*, 628.

CR010429O